MONTE CARLO SIMULATION
OF
AQUEOUS DILUTE SOLUTIONS OF POLYHYDRIC ALCOHOLS

by

Arnys Clifton Lilly, Jr.

Dissertation submitted to the Faculty of the
Virginia Polytechnic Institute and State University
in partial fulfillment of the requirements for the degree of

DOCTOR OF PHILOSOPHY

in

Physics

APPROVED:

J. C. Schug

L. D. Roper

C. D. Williams

R. Zallen

R. K. P. Zia

May, 1989

Blacksburg, Virginia

Monte Carlo Simulation of Aqueous Dilute Solutions of Polyhydric Alcohols

by

Arnys Clifton Lilly, Jr.

Committee Chairman: John C. Schug, Ph.D.
Physics

(ABSTRACT)

In order to investigate the details of hydrogen bonding and solution molecular conformation of complex alcohols in water, isobaric-isothermal Monte Carlo simulations were carried out on several systems. The solutes investigated were ethanol, ethylene glycol, 1,2-propylene glycol, 1,3-propylene glycol and glycerol. In addition, propane, which does not hydrogen bond but does form water hydrates, was simulated in aqueous solution. The complex alcohol-water systems are very nonideal in their behavior as a function of solute concentration down to very dilute solutions. The water model employed was TIP4P water[1] and the intermolecular potentials employed are of the Jorgensen type[2] in which the interactions between the molecules are represented by interaction sites usually located on nuclei. The interactions are represented by a sum of Coulomb and Lennard-Jones terms between all intermolecular pairs of sites. Intramolecular rotations in the solute are modeled by torsional

potential energy functions taken from ethanol, 1-propanol and 2-propanol for C-O and C-C bond rotations. Quasi-component pair correlation functions were used to analyze the hydrogen bonding. Hydrogen bonds were classified as proton acceptor and proton donor bonds by analyzing the nearest neighbor pair correlation function between hydroxyl oxygen and hydrogen and between solvent-water hydrogen and oxygen.

The results obtained for partial molar heats of solution are more negative than the experimental values by 3.0 to 14 kcal/mol. In solution, all solutes reached a contracted molecular geometry with the OH groups generally on one side of the molecule. There is a tendency for the solute OH groups to hydrogen bond with water, with more proton acceptor bonds than proton donor bonds. The water-solute binding energies correlate with experimental measurements of the water-binding properties of the solute.

1. Jorgensen, W.L. et al, J. Chem. Phys., 79, 926 (1983).
2. Jorgensen, W.L., J. Phys Chem., 87, 5304 (1983).

Acknowledgements

I would like to acknowledge the guidance and support of my advisor, Dr. John Schug. I have always respected his ability, and value him as a friend. Also, thanks go to my committee of distinguished physicists at Virginia Tech for their support and advice; Dr. Richard Zallen, Dr. David Roper, Dr. Clayton Williams, Dr. Royce Zia, and to Dr. Sam Bowen, who is now at Argonne National Laboratory. Dr. Tom Gilmer was always interested in how I was doing and has been very helpful in many areas of administration. I wish him well in his retirement. I cannot thank enough for all of the assistance and advice she gave me; it was invaluable.

The support of , Vice President of Research and Development, Philip Morris USA, was always there in good times and bad, and I shall never forget it. and have been equally supportive. Encouragement was graciously given by many of my Philip Morris colleagues; , , , , , , , , and . The late was always there with good advice and encouragement and I will never forget him. I thank for the use of his molecular conformation data.

was invaluable with his knowledge of computer systems and programming skills. He is also a close friend. Thanks to for his help with graphical techniques, and to for

reproducing the thesis. Discussions of many thermodynamic topics with

are greatly appreciated.

always had a kind word or a compliment, and I appreciate her interest in science. Thanks,

.

organized and typed the manuscript. Her support and encouragement through long hours of work was without peer.

Finally, I thank my wife, , and my children, , , , and 's husband , for their outstanding support during the past two years.

Dedication

This dissertation is dedicated to my parents; my mother, , and my late father, , who valued education above all things, and to my lovely wife, , whose love and understanding are responsible for any success that I have had in science.

TABLE OF CONTENTS

List of Figures

List of Tables

I. INTRODUCTION

1. General

Polyhydric alcohols, in particular glycerol, propylene glycol and ethylene glycol, are economically important, being widely used as humectant systems, antifreezes and emulsifiers in many industrial applications throughout the world. Aqueous solutions of these compounds, particularly glycerol (1,2,3-propanetriol), exhibit nonideal densities, activities, heats of solution, freezing points, and internal pressures. These effects in dilute solutions have been attributed by many to be the result of hydrogen bonding between the polyhydric alcohol's hydroxyl (OH) groups and water, and hydrogen bonding between the alcohols themselves at high concentrations. Even though hydrogen bonding has been established by many investigators in these systems, experiments that directly show the details of the bonding and the effects of molecular conformation in solution are missing from the literature. Very few experimental techniques outside of neutron diffraction have the resolving power to study the details of the glycol-water interaction in dilute solution. Ultrasonic propagation, NMR, Raman scattering, dielectric spectroscopy, heat capacity, and classical solution chemistry have verified strong hydrogen bonding properties. The details of the water-OH interactions in these systems are still unknown.

It is the intent of this study to develop better understanding of the hydrogen bonding details, the solute-solvent interactions, and the reasons for the nonideal behavior in these

systems. To accomplish the objective, a statistical mechanics simulation procedure for N molecules is employed using isobaric-isothermal (NPT-ensemble) Monte Carlo simulation. This technique has proven to be a powerful tool in recent investigations of the structure and properties of pure liquids and dilute solutions.

2. Properties of Monohydric and Polyhydric Alcohols

As was just discussed, aqueous solutions of polyhydric alcohols, particularly glycerol, $C_3H_5(OH)_3$, are nonideal. When water and glycerol are mixed there is a rise in temperature and a contraction of the solution volume. Bosart and Snoddy,[1] Minor and Dalton[2] and the International Critical Tables[3] have tables of the density of glycerol-water solutions over ranges of temperature and concentration. Figure 1 shows the 25°C data compiled by Bosart and Snoddy.[1] The nonideality (i.e., nonlinear dependence on concentration) is clearly demonstrated in Figure 1 and also in Figure 2 through 5. Figure 2 shows the contraction of glycerol-water solutions as a function of the concentration of glycerol as measured by Gerlach.[4] In Figure 3 the negative heat of solution (ΔH) of glycerol-water mixtures is shown as a function of glycerol concentration. Glycerol has a negative heat of solution of 6.3kJ/mol solute[3] at infinite dilution in water. Figure 4 shows the freezing points of glycerol-water solutions as a function of glycerol concentration.[6]

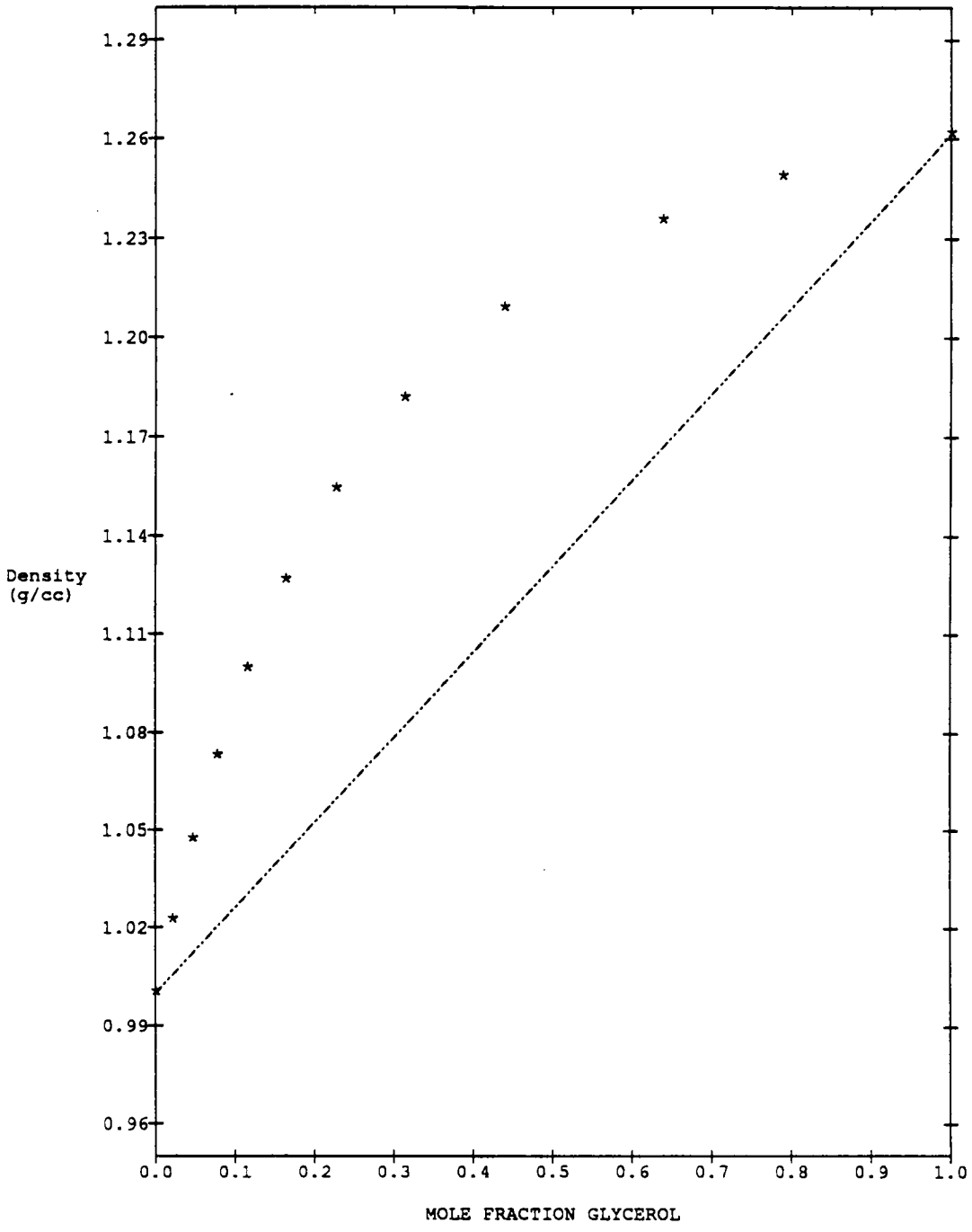

Figure 1. The density of glycerol-water solutions at 25°C versus mole fraction of glycerol.[1] The stars represent the actual density and the line represents an ideal solution.

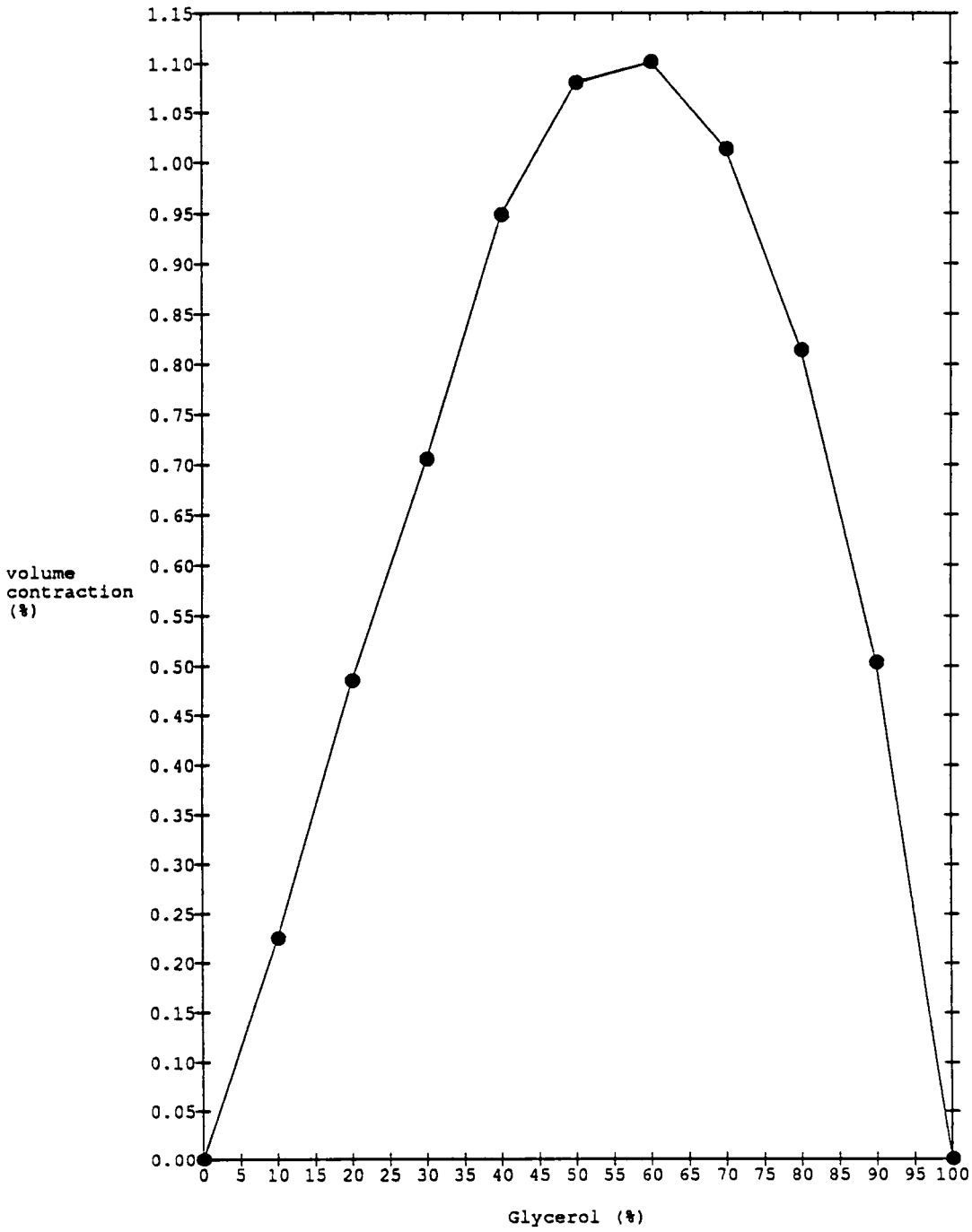

Figure 2. Volumetric contraction of glycerol-water solutions versus glycerol concentration in weight percent.

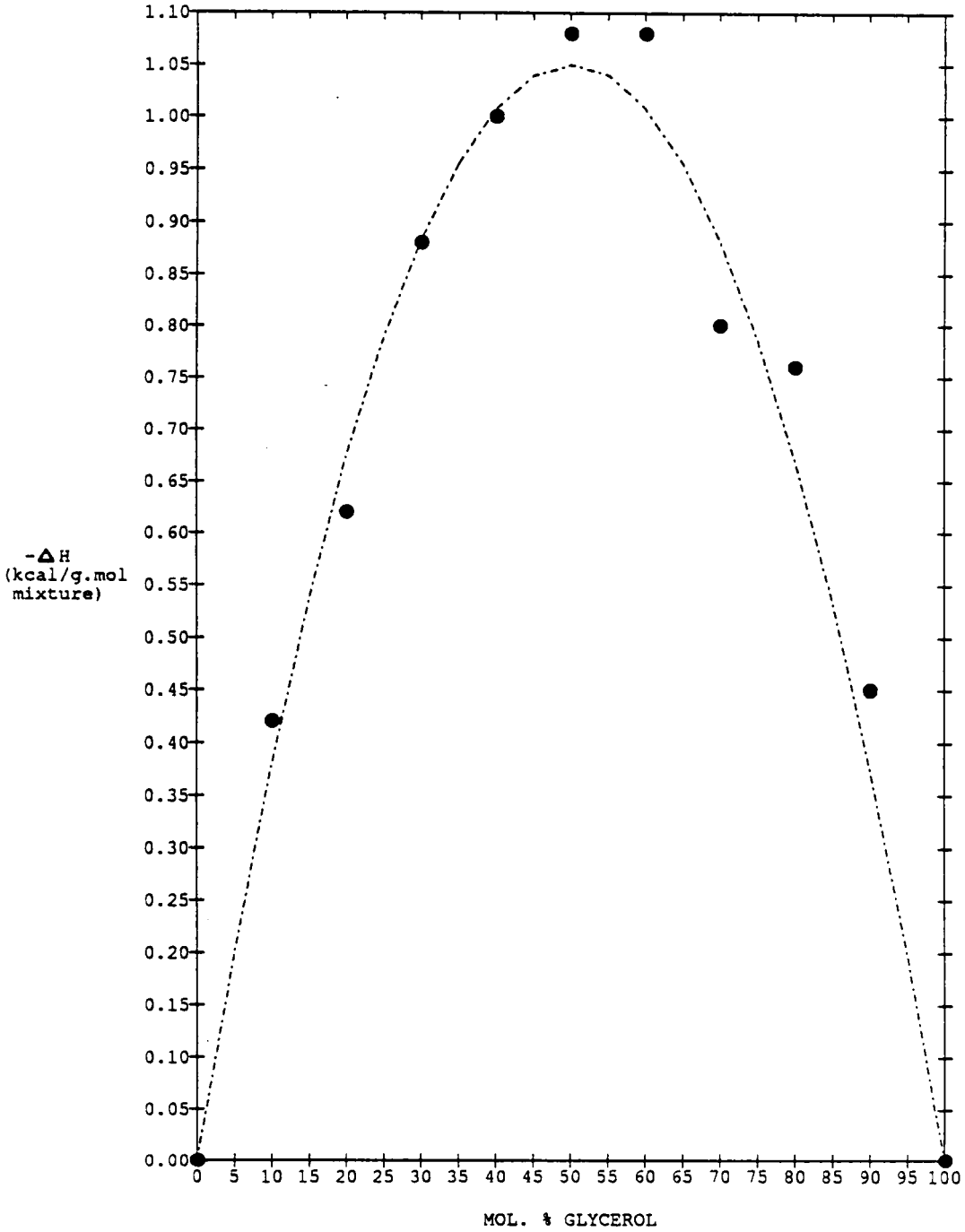

Figure 3. Negative heat of solution of glycerol-water mixtures as a function of mole fraction glycerol[3]. The dotted line is a parabolic fit to the data (solid circles). The fitted line was used to derive the partial molar heat of solution of glycerol.

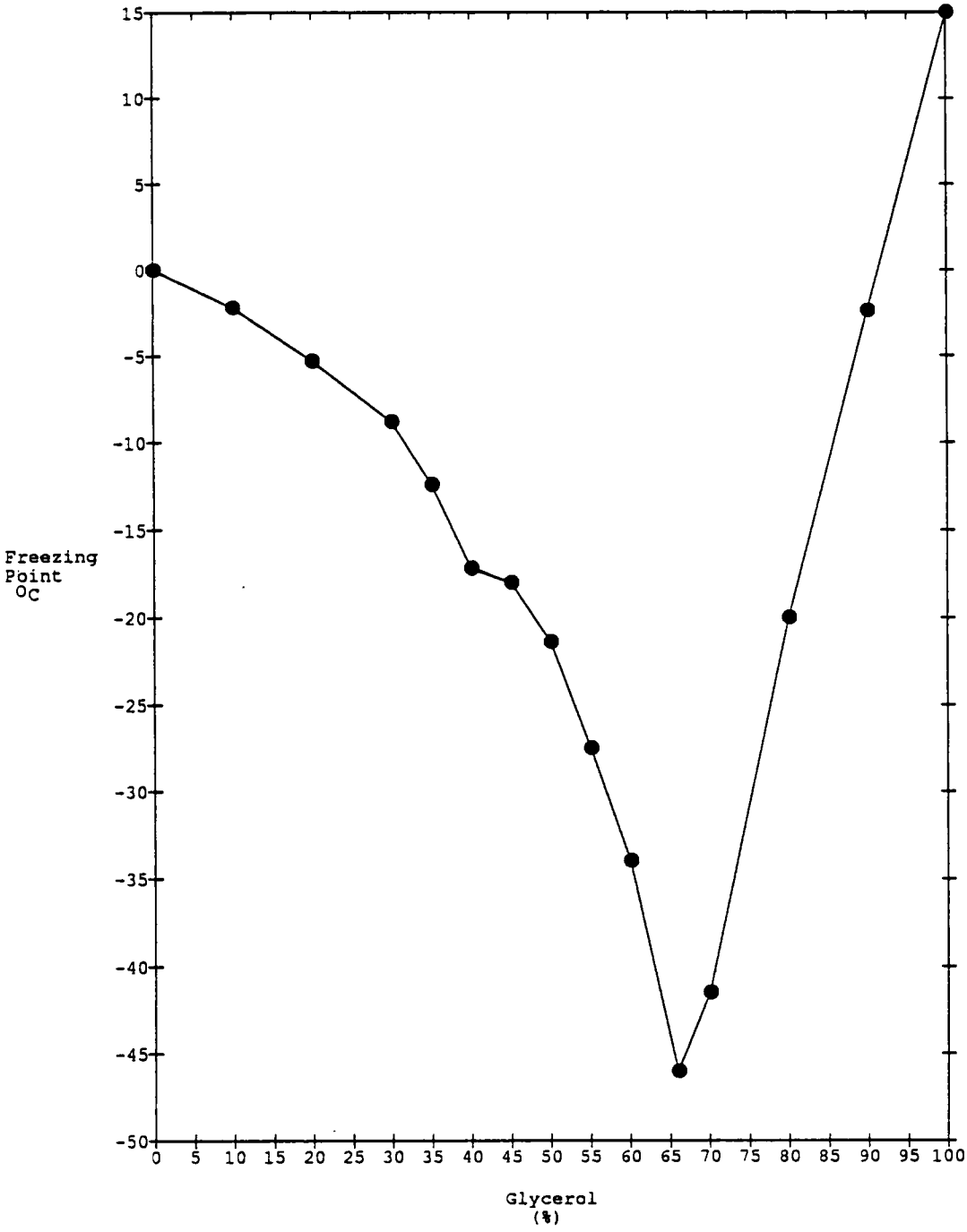

Figure 4. Freezing points of glycerol-water solutions as a function of glycerol concentration in weight percent.[6]

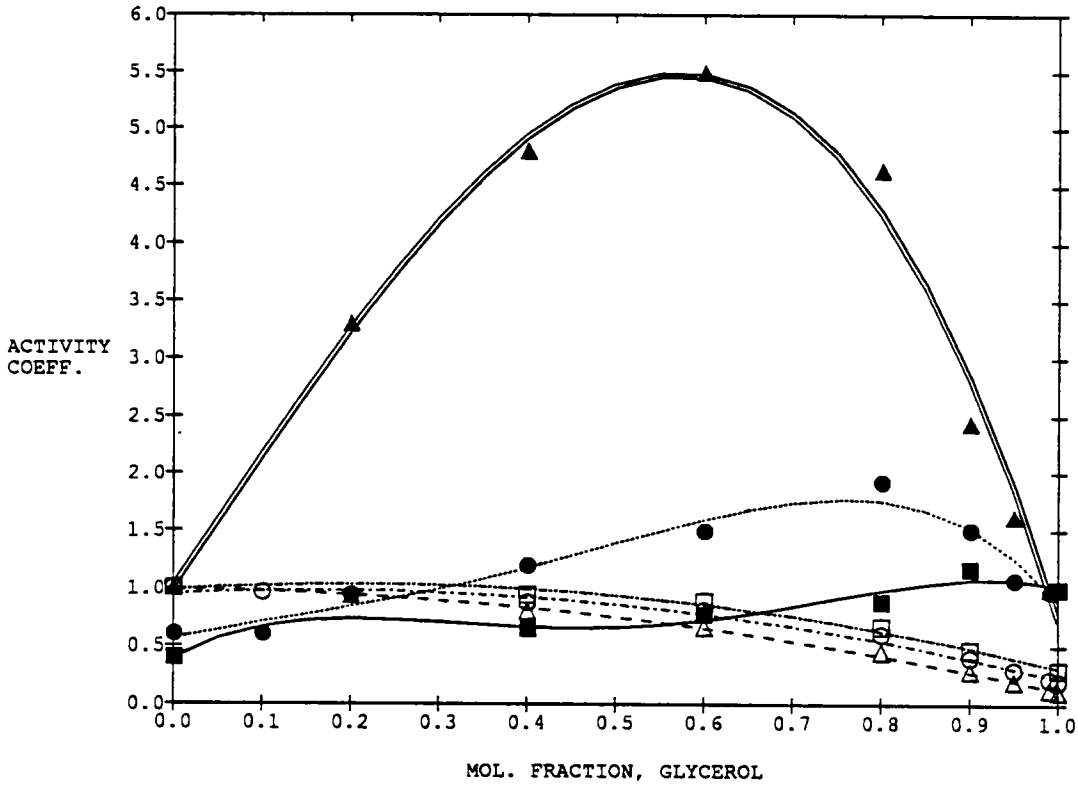

Figure 5. Activity coefficients of glycerol and water in glycerol-water solutions as a function of glycerol concentration at several constant pressures.

Another physical quantity which exhibits strong nonlinearity with composition in glycerol-water systems is the glycerol activity (in an ideal system the ratio of glycerol vapor over the solution to glycerol vapor over the pure liquid at constant temperature and pressure). Ladyn[5] measured the vapor-phase equilibrium activity coefficients of glycerol-water solutions as a function of glycerol content, temperature and pressure. These data are shown in Figure 5; note the strong peaking of the low temperature (low pressure) glycerol activity coefficients in the 50-60 mol percent glycerol region. Rajagopalan and Verma[10] have interpreted ultrasonic absorption and reflection data in terms of the presence of two types of hydrogen bonded complexes in aqueous mixtures of glycerol. One type is glycerol·1 H_2O; the other is glycerol·6 H_2O.

Solomon,[11] in his studies of the OH Raman stretching band in glycerol, and Burnett and Roeder,[12] in their ^{13}C NMR study of molecular reorientation in glycerol, suggested an intramolecularly bonded six-membered ring as a possible conformation of glycerol in the pure liquid. The ring is made by the three carbons, the terminal oxygens and one of the terminal hydrogens. Champeney et al.[7] and Garawi et al.[8] have recently carried out extensive neutron diffraction measurements on liquid perdeuterated glycerol at 193°K and 296°K. In the pure liquid the diffraction results are interpreted in terms of an elongated (linear) molecular geometry as shown in Figure 6. They also both show short-range and long-range correlation due to molecular packing effects. Very recently, Root and Stillinger,[9] using the

neutron diffraction results as a base, constructed a model for liquid glycerol and carried out a molecular dynamics calculation. Of the thirteen conformational isomers found for glycerol, the lowest energy geometry is an elongated structure having weak intramolecular hydrogen bonding. This structure is very similar to the starting conformation in this work. In the glycerol crystal, Root and Stillinger[9] also arrive at an elongated structure lying 1.2 kcal/mol above the previous structure in energy. In this geometry the glycerol molecule has the three backbone carbons and the two terminal oxygens almost coplanar and in the shape of a "W". This conformation is ideal for forming strong glycerol-glycerol hydrogen bonds in the pure liquid or solid.

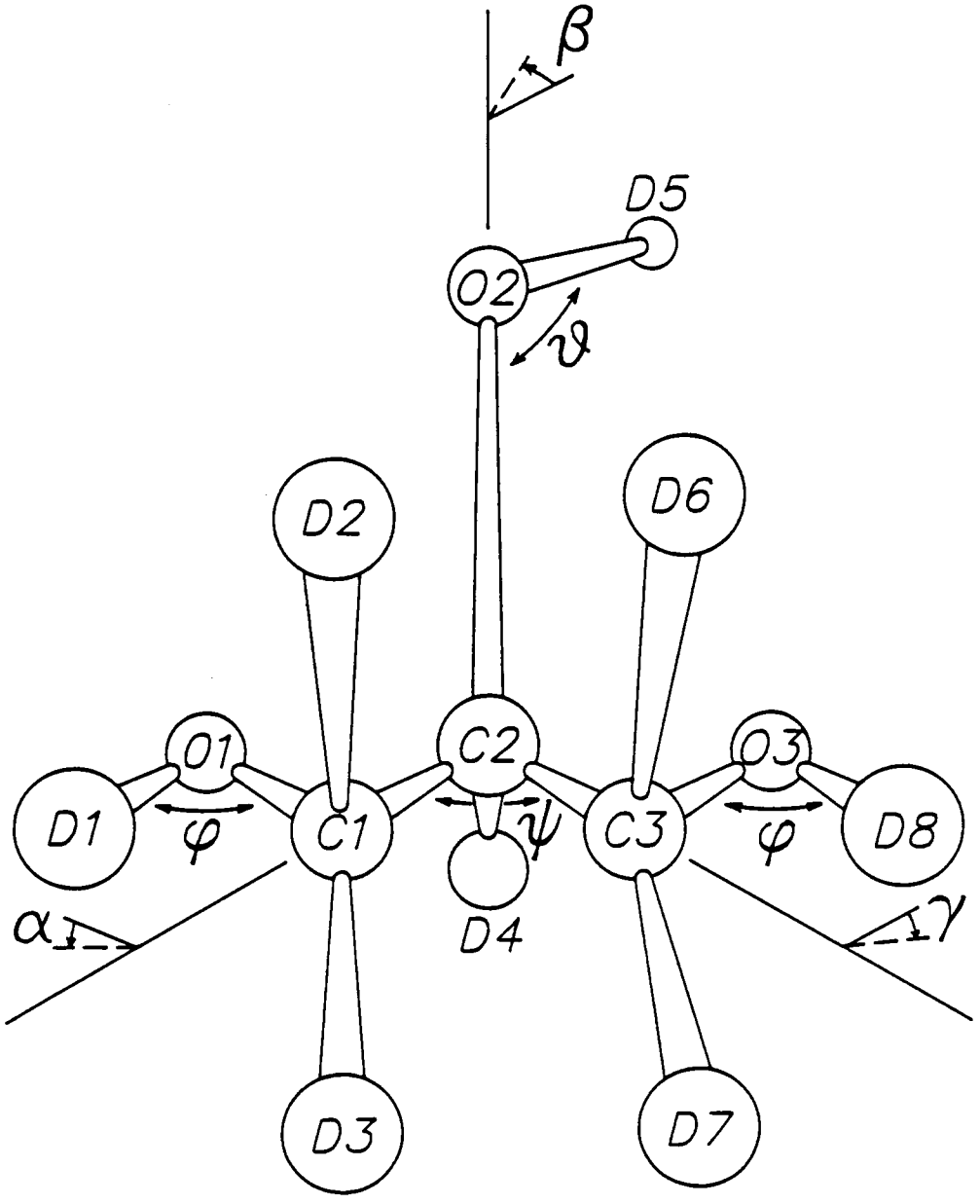

Figure 6. Neutron diffraction structure of perdeuterated glycerol molecules in the pure liquid.[8] The angles are $\alpha = 28.6^{\circ}$, $\beta = 34.1^{\circ}$, $\gamma = -20.6^{\circ}$, $\theta = 112.8^{\circ}$, $\varphi = 109.3^{\circ}$, and $\psi = 112.3^{\circ}$.

Murthy and Subrahmanyam[13] found the densities of pure ethylene glycol and glycerol at 25°C to be 1.1101 g/cm^3 and 1.25835 g/cm^3, respectively. They also measured the excess molar heat capacities at constant pressure and volume from ultrasonic velocity, density and specific heat measurements. Their results pointed to ethylene glycol and glycerol as water hydrogen bond structure breakers at low solute concentrations. In other words, the addition of ethylene glycol or glycerol to water results in a disruption of the water hydrogen bonded network. The same authors[14] also found that propylene glycol acted as a water structure breaker at low solute concentrations.

Srivastava and Tripathi[15] evaluated excess internal pressure in binary mixtures of water and t-butanol, n-propanol, ethylene glycol, and glycerol at 25°C. They found that the intermolecular interaction is stronger with water + monohydric alcohols than with water + polyhydric alcohols. Chidichimo et al.[16] did NMR measurements on the conformation of ethylene glycol in a D_2O solution and found only a **gauche** conformation with the value of the OC-CO dihedral angle at 72°C. Schwartz and Colville[17] used proton NMR to measure chemical shifts in aqueous mixtures of ethylene glycol, 1,2-propylene glycol and glycerol as a function of mole fraction at 0°C and 25°C. In glycerol, the nonequivalence of the CHOH and the CH_2OH was shown at 0°C but not at 25°C, indicating a strong temperature dependence of proton exchange. The methylene peaks showed anomalous temperature dependence which was attributed to intramolecular hydrogen-bonding.

Pimentel and McClellen[18] concluded that the formation of hydrogen bonds results in the decrease of the molar volume due to a shortening of interatomic distances. Jeffrey and Takagi[19] also discussed the bond distance criteria of 1.85 $\mathring{A}$ approach distance for selecting linear hydrogen bonds. Terasawa et al.[20] studied partial molar volumes of several glycols in water at 25°C. The partial molar volume of ethanol in water at infinite dilution is 55.1 ml/mol and for ethylene glycol is 55.6 ml/mol. Huot et al.[21] argued that ethylene glycol has some weak hydrophobic properties at low concentrations in water. Ethylene glycol in water exhibits smaller volume than in the neat liquid. These workers confirmed that in dilute aqueous solution ethylene glycol exists in the **gauche** conformation. Intramolecular hydrogen-bonding would reduce ethylene glycol-water hydrogen bonding and increase the hydrophobicity of ethylene glycol.

Generally, the properties of the monohydric and polyhydric alcohols may be summed up as follows. All of the polyhydric alcohols exhibit nonideal properties in aqueous solution, with glycerol being very nonideal; the molecules' adjacent OH groups tend to be in a **gauche** conformation in water at high dilution; most tend to be water hydrogen-bond breakers at low concentrations; ethylene glycol tends to be weakly hydrophobic in aqueous solution; and finally, there is little known about the details of hydrogen bonding and molecular conformation in dilute aqueous solutions of these molecules.

3. NPT-Ensemble Monte Carlo Simulation

Although the ideas were developed years ago, recent developments in computer storage and calculating speed and in the understanding of intermolecular potential functions have made Monte Carlo and Molecular Dynamics powerful tools in the simulation of molecular many-body systems. In this work, equilibrium properties of systems undergoing volume changes at standard temperature and pressure are under investigation. For these reasons, the isobaric-isothermal (NPT) ensemble Monte Carlo technique is used. The Monte Carlo method for obtaining the equation of state of a system of interacting particles was formulated by Metropolis et al.[22] The NPT-ensemble Monte Carlo technique was discussed in detail by Wood and Parker,[23,26] McDonald[24] and Ben-Naim,[25] and the following description closely follows what they have published.

A system of N particles at temperature T and pressure p has the following configurational Gibbs free energy:

$$G(N,p,T) = -\beta^{-1} \ln \Delta \qquad (1)$$

with $\beta = (kT)^{-1}$ and with

$$\Delta = \Lambda \ (2\pi m\beta/h^2)^{3N/2} \ (1/N!) \int_0^\infty dv \ \exp \ (-\beta pv) \int_v d\underline{r}^N \ \exp \ (-\beta\Phi(\underline{r}^N)) \quad (2)$$

where Λ is a multiplicative factor and Φ is the total potential energy of a configuration denoted by $\underline{r}^N$.

The NPT-ensemble average of a function $f(\underline{r}^N, v)$ is given by

$$\langle f(\underline{r}^N, v)\rangle = \frac{\int_0^\infty dv \ \exp \ (-\beta pv) \int_v d\underline{r}^N \ f \ (r^N, v) \ \exp \ (-\beta\Phi(\underline{r}^N))}{\int_0^\infty dv \ \exp \ (-\beta pv) \int_v d\underline{r}^N \ \exp \ (-\beta\Phi \ (\underline{r}^N))} \quad (3)$$

In a calculation using the Monte Carlo technique with periodic boundary conditions, the particles are always confined to a cube of side L. Therefore introducing scaled coordinates

$$\underline{\alpha}_i = L^{-1}\underline{r}_i \quad (4)$$

Equation (3) can be written

$$\langle f([L\underline{\alpha}]^N, v)\rangle = \frac{\int_0^\infty dv \exp(-\beta p v) v^N \int_\omega d\underline{\alpha}^N f([L\underline{\alpha}]^N, v) \exp(-\beta\Phi([L\underline{\alpha}]^N, L))}{\int_0^\infty dv \exp(-\beta p v) v^N \int_\omega d\underline{\alpha}^N \exp(-\beta\Phi([L\underline{\alpha}]^N, L))}, \tag{5}$$

where ω is the unit 3N-cube. Expression (5) represents an average in the (3N + 1)-dimensional space of $\{v, \underline{\alpha}_1 \ldots\ldots \underline{\alpha}_N\}$ with a probability density proportional to the pseudo-Boltzmann weight factor -

$$\exp[-\beta p v - \beta\Phi([L\underline{\alpha}]^N, L) + N \ln v] \tag{6}$$

Trial configurations are generated according to rules

$$\underline{\alpha}_i \rightarrow \underline{\alpha}_i \pm \lambda R^{\underline{\alpha}} \tag{7}$$

$$L \rightarrow L \pm \mu R^L \tag{8}$$

Particle i is chosen randomly as are R^{α} and R^{L}, λ is a displacement parameter and μ is a volume change parameter. If the total potential energy of the new configuration is Φ'' and the new volume is v", and Φ', v′ are the previous best values, then the quantity

$$W = (\Phi'' - \Phi') + p(v'' - v') - N\beta^{-1} \ln (v''/v') \qquad (9)$$

is calculated and the new configuration replaces the previous configuration with a probability P given by

$$P = 1, \text{ if } W \leq 0$$

$$P = \exp(-\beta W), \text{ if } W > 0 \qquad (10)$$

This procedure is repeated to build up a chain of configurations which are distributed in phase space with a probability density proportional to the pseudo-Boltzmann weight factor (Equation 6). A configuration is recounted if the trial configuration is rejected. This procedure allows calculations of the molar internal energy E_i and the molar volume V_m from the mean values of Φ and v.

Specific heat and compressibility may be obtained from the mean-square fluctuations in (Φ + pv) and v.

NPT-ensemble simulations have been carried out by W. L. Jorgensen and colleagues[27-41] on pure systems and these have been used to generate a set of intermolecular potential functions suitable for computer simulations on organic fluids. Jorgensen and his group have treated pure liquid hydrocarbons, liquid water, liquid amides, liquid alcohols, and aqueous solutions of hydrocarbons, amides, carboxylate ions and ammonium ions. In addition, they computed absolute free energies of binding of the methane dimer in water,[39] simulated the hexanol-water interface[40] and created from their work OPLS (optimized potentials for liquid simulations) potential functions for proteins.[41]

Mehrotra and Beveridge[42] have simulated the properties of an aqueous solution of formaldehyde (HCOH) using an NVT-ensemble technique. In this work they developed the concept of quasi-component distribution functions enabling them to investigate the hydration shells around the solute molecule. Rossky and Karplus[43] carried out a very detailed analysis using molecular dynamics techniques of the solvation of a dipeptide in water. They investigated hydrogen bonding around polar groups and also the organization of water around nonpolar groups. They found that nonpolar groups decrease translational and rotational freedom of water molecules. The water molecules were structured by nonpolar solutes into 1,2, and 5-membered species. Rossky and Karplus[43] found water-water hydrogen bonds of energy -5.25 kcal/mol and defined hydrogen bonding of water to the solute at

energies beginning at -3.0 kcal/mol. Alagona and Tani[44,45] used an NVT-ensemble simulation of ethanol in water to determine that an average of two water molecules are hydrogen bonded to ethanol through the OH group. In this calculation they kept the ethanol molecule fixed in a **trans** conformation in the solution.

4. **Simulations of Liquid Water**

Water is, of course, one of the liquids in which the properties have to be simulated accurately in order to make progress in understanding solutions. A number of intermolecular potentials have been developed for water: ST2,[47] Bernal-Fowler (BF),[46] SPC,[48] TIPS2,[30] TIP3P,[30] and TIP4P[27]. In general, the numbers in the potential designation refer to the number of interaction sites in the molecules. These sites can be the centers for Lennard-Jones terms or the charge centers. Also, the **ab initio** quantum intermolecular interaction function developed by Matsuoka, Clementi and Yoshimine[49] has been employed by many researchers. Jorgensen et al.[30] have carried out an extensive comparison of a number of simple potential functions for simulating liquid water by using an NPT-ensemble Monte Carlo method at 25°C and 1.0 atmosphere. In general, only the BF (Bernal-Fowler) potential was not in reasonable accord with experimental data, giving an 18% overestimate of the density and poor structural results. The TIP4P potential gives a density without correction for molecules beyond the potential cutoff in exact agreement with experiment for water at 25°C and 1.0 atmosphere, which is attractive for NPT simulations of aqueous solutions. Overall, the

SPC, ST2, TIPS2 and TIP4P models give reasonable structural and thermodynamic descriptions of liquid water.

Recently, the TIP4P model potential has been used to examine properties such as dielectric relaxation,[50] the liquid-vapor interface,[51-53] the ice-water interface,[54] the high pressure properties of water[50] and the structure of expanded water at high temperatures.[55]

The TIP4P potential model[30] is a 4-site water model. Water molecules are represented by four interaction sites, three on the nuclei and one on a point M located on the HOH bisector 0.15 $\mathring{A}$ from oxygen toward the hydrogens. The potential is represented by Lennard-Jones terms plus Coulomb terms as shown below. The Lennard-Jones terms are centered on the oxygen atom while the hydrogens and point M are charge centers.

$$\Phi_{ab} = \sum_{i}^{a} \sum_{j}^{b} (q_i q_j \, r_{ij}^{-1} + A_{ij} \, r_{ij}^{-12} - C_{ij} \, r_{ij}^{-6}) \qquad (11)$$

The summations i,j are over all sites for molecule a and molecule b, respectively. The 4-site parameters, where A_{oo} and C_{oo} are the Lennard-Jones parameters for oxygen, are A_{oo} = 600,000 kcal $\mathring{A}^{12}$ mol^{-1} = 2510400 kJ $\mathring{A}^{12}$ mol^{-1}, C_{oo} = 610 kcal $\mathring{A}^{6}$ mol^{-1} = 2552 kJ $\mathring{A}^{6}$ mol^{-1},

q_M = -1.04e and q_H = 0.52e. The OH bond length (0.9572 Å) and HOH angle (104.52°) are fixed.

Jorgensen et al.[30] obtained for the density of water 0.999 g/cm^3 (expt. 0.997) at 25°C and 1 atmosphere, for the internal energy -10.07 kcal/mol (expt. 9.92) and for the heat of evaporation 10.66 kcal/mol (expt. 10.51). The agreements with experimental C_p, isothermal compressibility, and thermal expansion are not nearly so good. However, internal degrees of freedom of the water molecule are left out of the model, and the quantities are calculated from fluctuations of the internal energy and density so that extremely long runs are needed to obtain reasonable results. This work employed the TIP4P potential for water because of the good results on first order thermodynamic quantities and structural features.

5. Objective of This Study

The intent of this study is to use NPT-ensemble Monte Carlo simulation to study low concentrations of ethylene glycol, 1,2-propylene glycol, 1,3-propylene glycol and glycerol in TIP4P water. In addition, ethanol (with a single OH-group) and propane, a hydrocarbon molecule with hydrate-forming properties, will be simulated in water in order to obtain results on solutes containing from zero to three OH-groups.

The objective is to use the internal energy and density to give confidence in the accuracy of the simulations while using solute-water binding energy, molecular pair interaction energy distribution,

total radial distribution functions (RDF), primary RDF and secondary RDF (primary plus secondary equal total) to extract the details of hydrogen bonding and water structure near both the hydrophilic and hydrophobic regions of each molecule. In addition, the gas phase ground state energy molecular conformation will be used to start the calculation, and the best available models of the potential for torsional motion (rotation about a bond axis) in the molecules will be incorporated so as to study the effect of solvent-solute interaction on molecular conformation in water solution. At all times the intent will be to use results from available literature to provide assurance of the correctness of the model calculations.

II. COMPUTATIONAL PROCEDURES

1. NPT Monte Carlo Simulation

As was previously discussed, the NPT ensemble Monte Carlo was chosen for this work because of the need to calculate equilibrium properties at atmospheric pressure and also because volume changes take place in the system. To carry out the intended analysis, several systems were simulated. First, TIP4P water[27] properties were calculated with 108 and 125 molecules at 25°C and one atmosphere. Next, mixtures of one solute molecule and 108 water molecules were simulated. The solutes selected were propane (a C_3- hydrocarbon), ethanol (a simple monohydric alcohol), ethylene glycol, 1,2-propylene glycol and 1,3-propylene glycol (polyhydric alcohols with two OH groups) and glycerol, a complex polyhydric alcohol with three OH groups. The idea was to span the range of solute interactions with water from full hydrophobic to slightly hydrophobic, and finally to strongly hydrophilic solutes. Figure 7 shows simple two-dimensional representations of the solute molecules employed in this work.

SOLUTE MOLECULES

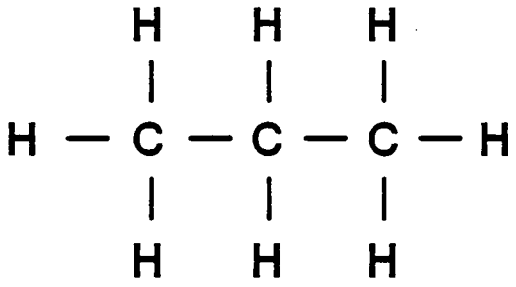

PROPANE

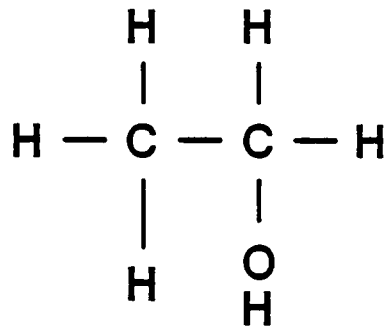

ETHANOL

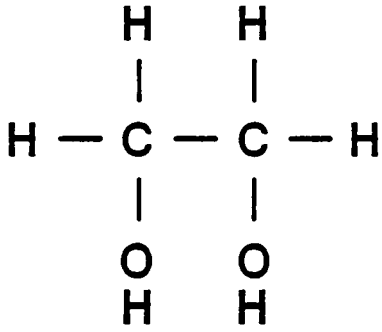

ETHYLENE GLYCOL

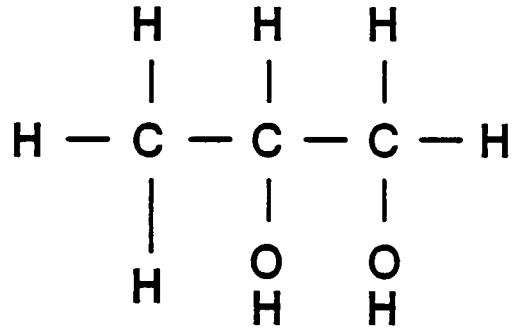

1, 2 PROPYLENE GLYCOL

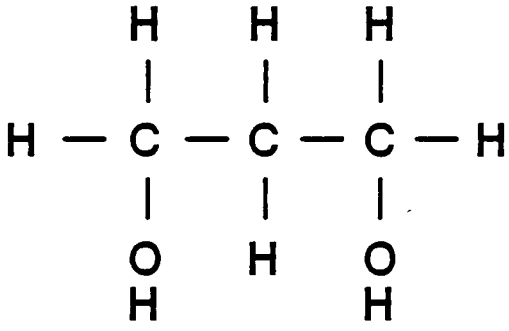

1,3 PROPYLENE GLYCOL

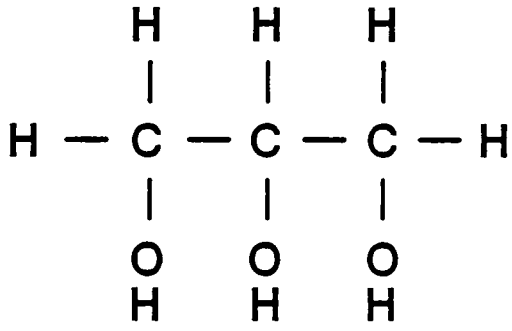

GLYCEROL

Figure 7. Schematic representations of the solute molecules employed in these simulations.

The Monte Carlo scheme employed was the one generally in standard use by workers in the field. First, periodic boundary conditions were employed with the minimum image convention.[22,23] The basic cube containing 108 water molecules plus one solute molecule is surrounded by periodic images of itself which contain the same number of molecules in the same relative positions. Each molecular pair interaction is calculated using the image that gives the smallest separation (this is the "minimum" image convention). This means that all contributions to the system potential energy arise from interactions between pairs of molecules separated by a distance of less than one-half the box edge. Interactions from particles separated by greater distances can be obtained by integration over a uniform density or by saving configurations and making the correction off-line. Metropolis sampling was employed in general, and in the case of water-solute mixtures an Owicki-Scheraga[56,57] weighting factor was used so as to preferentially sample position variations of those water molecules in the vicinity of the solute molecule. This was done to ensure that more configurations are sampled in the region near the solute where solvent-solute interactions are to be investigated. New configurations were generated by moving randomly selected molecules in three Cartesian directions; the water molecules were also rotated about a randomly chosen axis while the solute molecules were translated only. Changes in the dihedral angles were attempted every 110 moves and the solute molecule was translated every 210 configurations. Volume changes were attempted every 600

configurations by scaling all of the molecular positions. Following Gao and Jorgensen,[40] acceptance rates of 40-50% for new configurations were sought. The maximum ranges used for translation and rotation were ± 0.15 Å and $\pm 15^{\circ}$ for water molecules, ± 0.15 Å for translation of the solute molecules and ± 50 Å^3 for volume changes. The dihedral angle changes for the solute molecules were restricted to $\pm 15^{\circ}$.

Spherical cutoffs were used to truncate the interatomic interactions at a distance of 7.5 Å. Configurations were saved every 5×10^4 configurations and used to calculate the potential energy contributions from solvent molecules beyond the cutoff distance. An example of the cumulative percent error correction to the energy in the glycerol-water system is shown in Figure 8. This curve is averaged over the 40 configurations saved and shows the maximum error to be less than 2.0%. For all runs the first 1×10^6 configurations were discarded in equilibrating the system and averaging was carried out on the next 4×10^6 configurations (except for propane-water in which 2×10^6 configurations were used). Wood control functions[23] were calculated every 5000 configurations for the energy and every 100 volume changes for the density. Cumulative averages were calculated from Wood functions. Binding energy distributions and pair interaction energy distributions for both water-water and solute-water were continuously averaged over all configurations of the system. In addition, solute atom-solvent atom pair correlation functions centered on each atom on the solute molecule (except for the carbons on the molecular backbone) were compiled and continuously averaged over all

system configurations. This was done by the method described by Wood and Parker[23] in which the r_{ij}'s for every configuration are divided into a number of bins in equal intervals, and a continuous count of the number in each bin is maintained. Step by step summation of the bin number averaged over all of the configurations gives the cumulative pair correlation distribution function. This gives the average number of molecules or atoms inside a sphere of radius r, excluding the reference molecule or atom at the center. Differentiation of this cumulative distribution function gives the pair correlation function. With suitable radial normalization, the integral over the first peak in the appropriate nearest-neighbor pair correlation function can give the number of atoms of a particular type that are the nearest neighbors of the central atom. This is how hydrogen bond numbers are derived from oxygen-hydrogen pair correlation functions, for example.

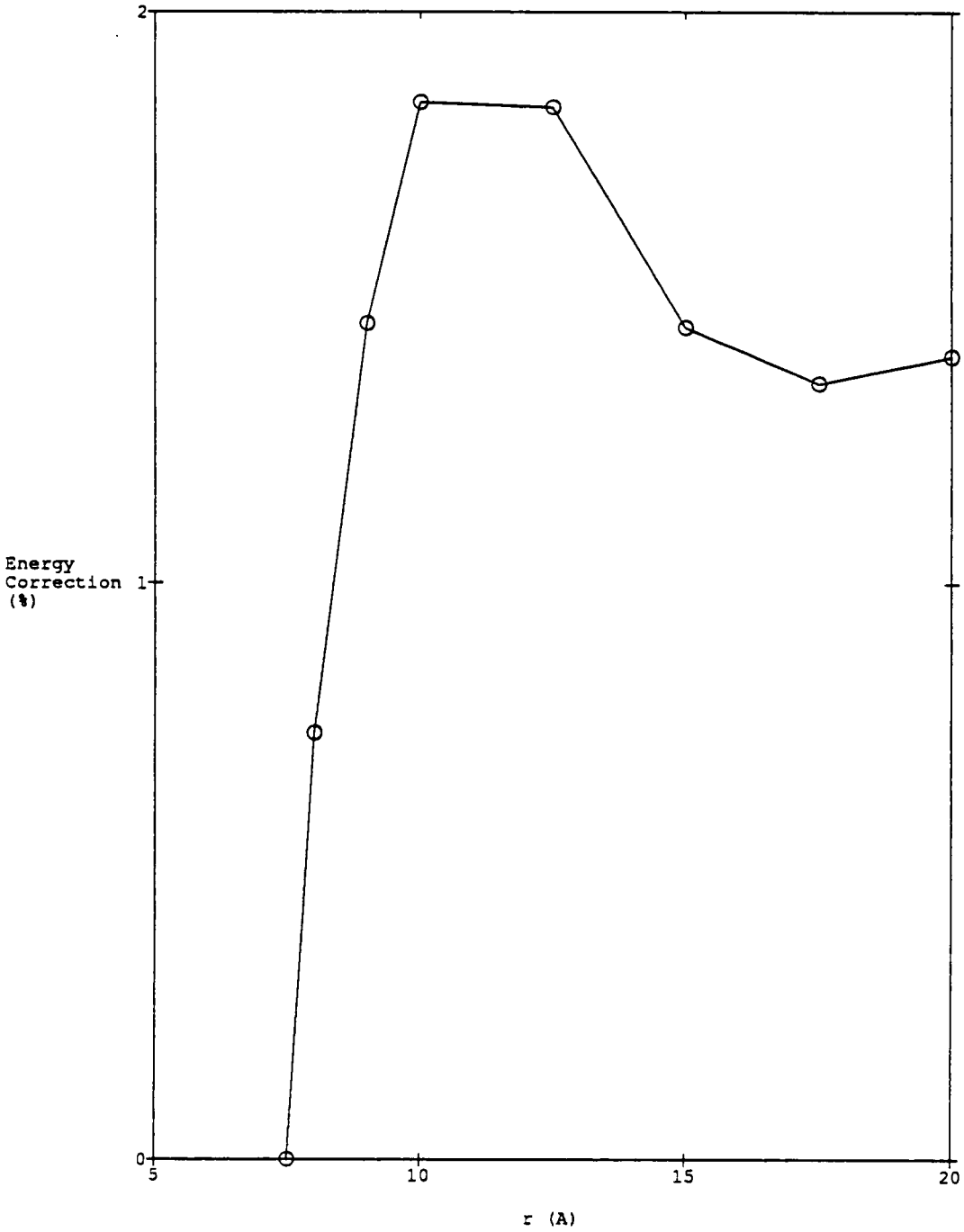

Figure 8. Cumulative error in total energy for solvent molecules beyond the system cutoff from the solute (glycerol). The curve was calculated from saved configurations of the system.

Total pair correlation functions g(OO), g(HO), g(OH), and g(HH) were calculated along with primary (nearest neighbor) and secondary (next nearest neighbor) pair correlation functions following Mehrotra and Beveridge.[42] All functions were averaged over all system configurations. The simulations were run on several computers including the IBM 3090, Gould 9500, Multiflow 200/14 and Sun 4. Most of the work was carried out on the Multiflow, and the time for 3×10^6 configurations ranged from 24 hours on the Multiflow to 176 hours on the Sun 4.

2. Intermolecular Potential Functions

Intermolecular potential functions have to be formulated for each problem. Jorgensen and co-workers have formulated potential functions for simple alcohols,[38] hydrocarbons[29,33] and liquid amides[34] with the goal that combinations of these functions can be transportable to more complex molecules. In general, the intermolecular potential functions are in the form of simple Lennard-Jones plus Coulomb terms as was given in Equation (11) for TIP4P water. Standard combining rules[27] are used for the Lennard-Jones coefficients so that $A_{ij} = (A_{ii} \cdot A_{jj})^{1/2}$ and $C_{ij} = (C_{ii} \cdot C_{jj})^{1/2}$. A and C can also be expressed in terms of Lennard-Jones σ's and ε's as $A_{ii} = 4\varepsilon_i\sigma_i^{12}$ and $C_{ii} = 4\varepsilon_i\sigma_i^{6}$. The Lennard-Jones σ and ε are defined in Figure 9.

Lennard - Jones Potential

$$U_{L.J}(R) = 4\epsilon[(\sigma/R)^{12} - (\sigma/R)^{6}]$$

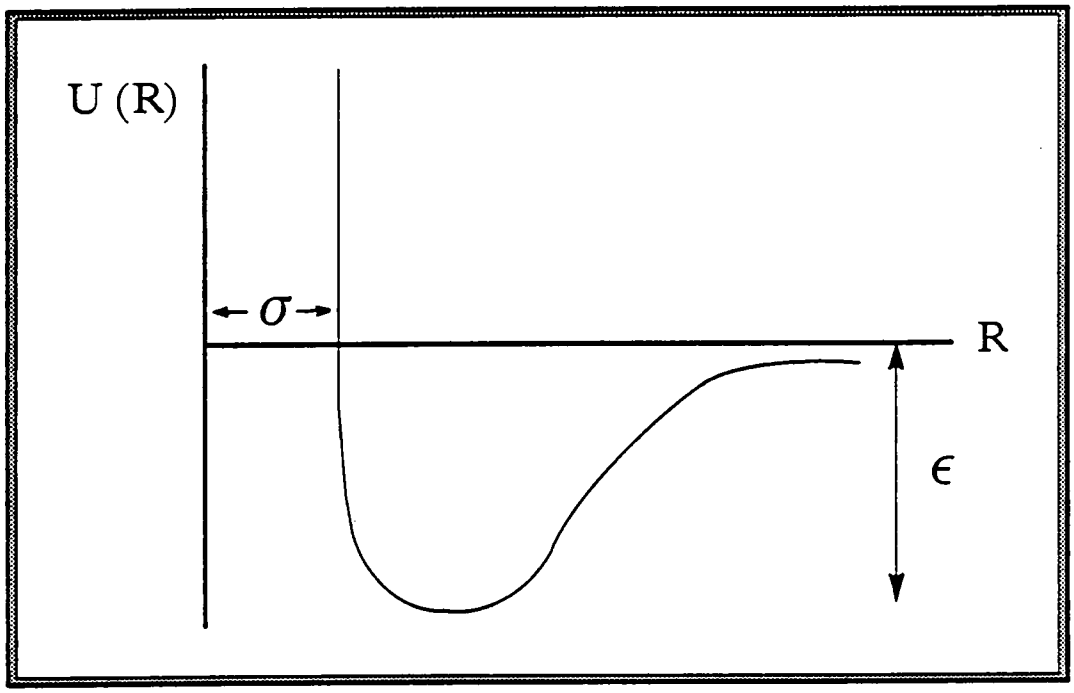

Figure 9. Schematic potential function defining σ as a distance and ε as the potential-well depth.

Table I. Lennard-Jones parameters and charge distributions used for monohydric alcohols, polyhydric alcohols and hydrocarbons in this work (Jorgensen)[27-40]

Atoms or Groups	q(e)	σ(Å)	ε(kcal/mol)
O(COH)	-0.700	3.070	0.170
H(COH)	0.435	0.0	0.0
CH_n(COH)	0.265	--	--
CH	--	3.850	0.080
CH_2	--	3.905	0.118
CH_3	--	3.775	0.207

Following Jorgensen,[38] charges are placed only on atoms of CH_n-O-H units. Lennard-Jones terms were used for CH_n groups from work on liquid hydrocarbons[29] and centered on the carbon atom, while the Lennard-Jones terms for OH are centered on the oxygen with the L-J term for the hydroxyl hydrogen set to zero (however the hydrogen is charged). For pure hydrocarbons such as propane only Lennard-Jones terms were used with the charges set to zero, which would be expected for hydrocarbons and as confirmed by other workers.[29,33,58,59,60] The bond lengths and bond angles were taken from experimental data if available; otherwise they were generated from the optimization. The optimized charges for simulation were taken from the Jorgensen optimized simulation potentials.[27-40] Table I shows the charges and Lennard-Jones terms employed in this work.

3. **Molecular Conformation**

In order to do all simulations in a self-consistent manner, an all-valance electrons semi-empirical molecular orbital (MNDO)[64,65] calculation was first carried out on each solute molecule and the lowest energy gas phase geometry was used as a starting molecular conformation. This was done because there is essentially no information in the literature on the geometry of the solutes in dilute aqueous solutions. Bond lengths and bond angles were started at values known from spectroscopy and optimized during the calculations. In addition, the geometry optimization was carried out to emphasize intramolecular hydrogen-bonding. As would be expected for molecules of this type, several conformational isomers existed, all very close

in energy. Since most of these isomers involved C-O rotations, the lowest energy geometry was selected and the solute-solvent interactions in the solution were allowed to fix the final conformation in the solute-water system. In the case of ethanol, several different locations of the OH group were used to start simulations, and in all cases the OH group was closest to the methyl group in the final conformation. For ethylene glycol both **gauche** and **trans** geometries were used and the final geometry was **gauche**, as experimental work had indicated.[16,21] The **gauche** conformation has a 60^0 angle between the C-O bonds when the molecule is viewed down the C-C axis. In the **trans** conformation, the angle is 180^0. In Tables II-VII, the optimized starting geometry for the solute molecules used in this calculation is given in terms of the standard Z-Matrix convention.[66] This defines the conformation in terms of the bond lengths, bond angles, and dihedral angles. For example, take propane in Table II. H_{11} is located at a distance 1.10 $\mathring{A}$ from C_3, forms a bond angle of 107.5^0 with H_6 about C_3, and is rotated 121.19^0 from C_2 when viewed along the C_3-H_6 axis in the direction indicated.

Table II. Starting molecular conformation in Z Matrix convention.[66]

Propane

Atom	Atom Number	Bond Length Å	Bond Angle (°)	Dihedral Angle(°)	Connectivity
C	1	0.000	0.00	0.00	000
C	2	1.530	0.00	0.00	100
C	3	1.530	115.39	0.00	210
H	4	1.109	111.76	60.98	123
H	5	1.115	108.77	237.47	231
H	6	1.109	111.77	299.58	321
H	7	1.110	107.52	238.83	142
H	8	1.109	107.80	123.22	142
H	9	1.115	108.78	237.46	213
H	10	1.109	107.80	236.81	362
H	11	1.110	107.51	121.19	362

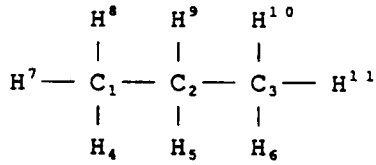

Propane

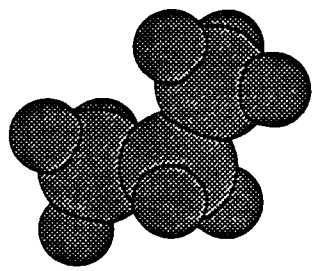

Table III. Starting molecular conformation in Z Matrix convention.[66]

Ethanol

Atom	Atom Number	Bond Length Å	Bond Angle (°)	Dihedral Angle (°)	Connectivity
C	1	0.000	0.00	0.00	000
C	2	1.539	0.00	0.00	100
O	3	1.396	110.40	0.00	210
H	4	0.947	111.01	93.63	321
H	5	1.108	111.89	60.53	123
H	6	1.108	111.88	238.53	125
H	7	1.109	109.21	119.26	125
H	8	1.124	109.39	237.65	213
H	9	1.124	109.38	122.34	213

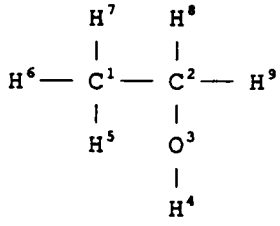

Ethanol

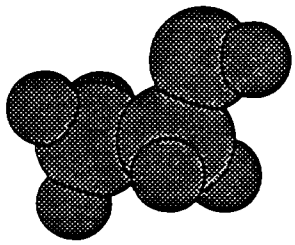

Table IV. Starting molecular conformation in Z Matrix convention.[66]

Ethylene Glycol

Atom	Atom Number	Bond Length A°	Bond Angle (°)	Dihedral Angle(°)	Connectivity
C	1	0.000	0.00	0.00	000
C	2	1.562	0.00	0.00	100
O	3	1.395	110.30	0.00	120
O	4	1.392	114.27	295.76	213
H	5	0.947	111.23	176.87	312
H	6	0.947	112.23	75.42	421
H	7	1.124	110.95	119.65	132
H	8	1.122	111.40	237.37	132
H	9	1.121	106.81	118.66	241
H	10	1.222	111.70	234.91	241

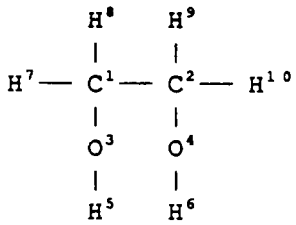

Ethylene Glycol

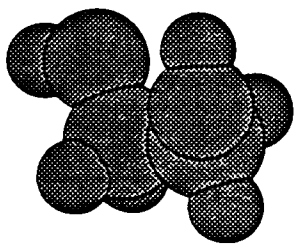

Table V. Starting molecular conformation in Z Matrix convention.[66]

1,2 Propylene Glycol

Atom	Atom Number	Bond Length A°	Bond Angle (°)	Dihedral Angle(°)	Connectivity
C	1	0.000	0.00	0.00	000
C	2	1.552	0.00	0.00	100
C	3	1.575	112.09	0.00	210
O	4	1.402	112.02	238.29	213
O	5	1.392	113.55	198.15	324
H	6	0.947	111.59	162.54	423
H	7	0.947	112.37	76.99	532
H	8	1.108	112.44	300.62	124
H	9	1.109	107.67	237.46	182
H	10	1.108	107.95	122.03	182
H	11	1.128	107.63	242.96	321
H	12	1.122	111.53	235.07	352
H	13	1.121	106.47	118.85	352

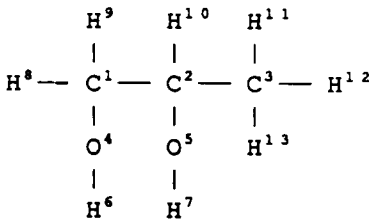

1,2 Propylene Glycol

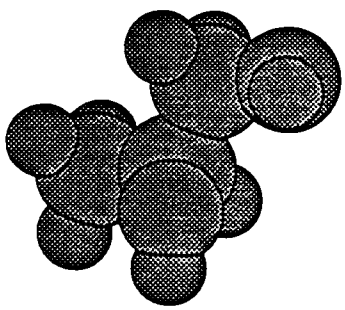

Table VI. Starting molecular conformation in Z Matrix convention.[66]

1,3 Propylene Glycol

Atom	Atom Number	Bond Length Å	Bond Angle (°)	Dihedral Angle (°)	Connectivity
C	1	0.000	0.00	0.00	000
C	2	1.548	0.00	0.00	100
C	3	1.554	117.34	0.00	210
O	4	1.396	111.32	76.33	123
O	5	1.396	115.01	-53.76	321
H	6	0.947	111.15	-156.29	421
H	7	0.946	112.54	92.31	532
H	8	1.124	110.69	122.60	142
H	9	1.124	110.93	239.40	142
H	10	1.115	107.04	240.85	231
H	11	1.113	110.11	126.19	231
H	12	1.122	106.10	119.25	352
H	13	1.123	111.29	234.22	352

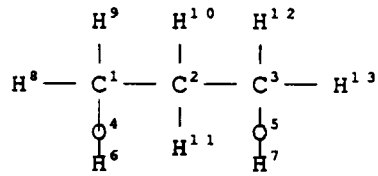

1,3-Propylene Glycol

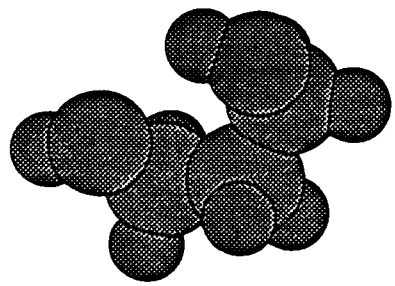

Table VII. Starting molecular conformation in Z Matrix convention.[66]

Glycerol

Atom	Atom Number	Bond Length Å	Bond Angle (°)	Dihedral Angle (°)	Connectivity
C	1	0.000	0.00	0.00	000
C	2	1.577	0.00	0.00	100
C	3	1.573	110.78	0.00	210
O	4	1.392	113.32	185.95	123
O	5	1.397	108.08	236.73	213
O	6	1.395	209.51	298.01	325
H	7	0.947	112.43	283.51	412
H	8	0.947	112.06	76.40	523
H	9	0.947	111.18	177.33	632
H	10	1.122	111.47	124.93	142
H	11	1.121	106.42	241.07	142
H	12	1.127	107.34	242.78	231
H	13	1.122	110.68	122.76	326
H	14	1.123	108.86	239.01	326

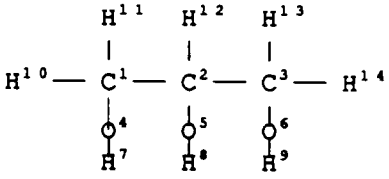

Glycerol

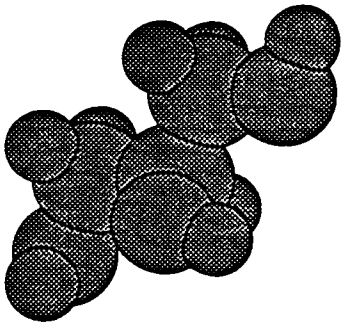

4. **Torsional Potential Energy**

Torsional rotational motion about C-O and C-C bonds was included in the simulation because of the complexity of the solute molecules. Unfortunately, there is very little experimental information available on the rotational barriers or the conformational populations for complex alcohols in dilute aqueous solution. Chao and Hall[61] and Melberg and Rasmussen[62] have reviewed the experimental gas phase microwave and infrared data for rotational barriers in ethanol, 1-propanol and 2-propanol. Jorgensen[38] has determined the torsional potentials by fitting to results obtained from MM2[28] molecular mechanics with full geometry optimization. Jorgensen's torsional potentials have been used in this work because the gas phase data from many investigators did not agree. Therefore, in this work torsional angle potential functions for terminal OH group C-O rotations are modeled after 1-propanol. Solutes such as ethanol, ethylene glycol, 1,3-propylene glycol, 1,2-propylene glycol and the terminal groups in glycerol fall into this group. Internal OH group C-O rotations in 1,2-propylene glycol and glycerol are modeled from 2-propanol. Rotations around C-C bonds are modeled from 1-propanol. Propane C-C rotations use potentials for n-butane taken from Jorgensen et al.[29] The C-O rotational barriers tend to be low (< 1.0 kcal/mol), and the interactions with the water molecules determined the average conformation in solution. In Table VIII the coefficients for the Fourier series form of the torsional potential energy

$$V(\Phi) = V_0 + V_1(1.0+\text{Cos}\Phi)/2.0 + V_2(1.0-\text{Cos}2\Phi)/2.0 + V_3(1.0+\text{Cos}3\Phi)/2.0 \quad (12)$$

are given. The graphs of the torsional potential functions are given in Figure 10.

Table VIII. Fourier coefficients for intramolecular rotational potential functions.[38]

Alcohol	Bond	V_0	V_1	V_2	V_3
Ethanol	C-O	0.0	0.834	-0.116	0.747
1-Propanol	C-O	0.0	0.834	-0.116	0.747
	C_1-C_2	0.0	0.702	-0.212	3.060
2-Propanol	C-O	0.429	0.784	0.125	-0.691
	C_1-C_2	0.0	1.522	-0.315	3.207

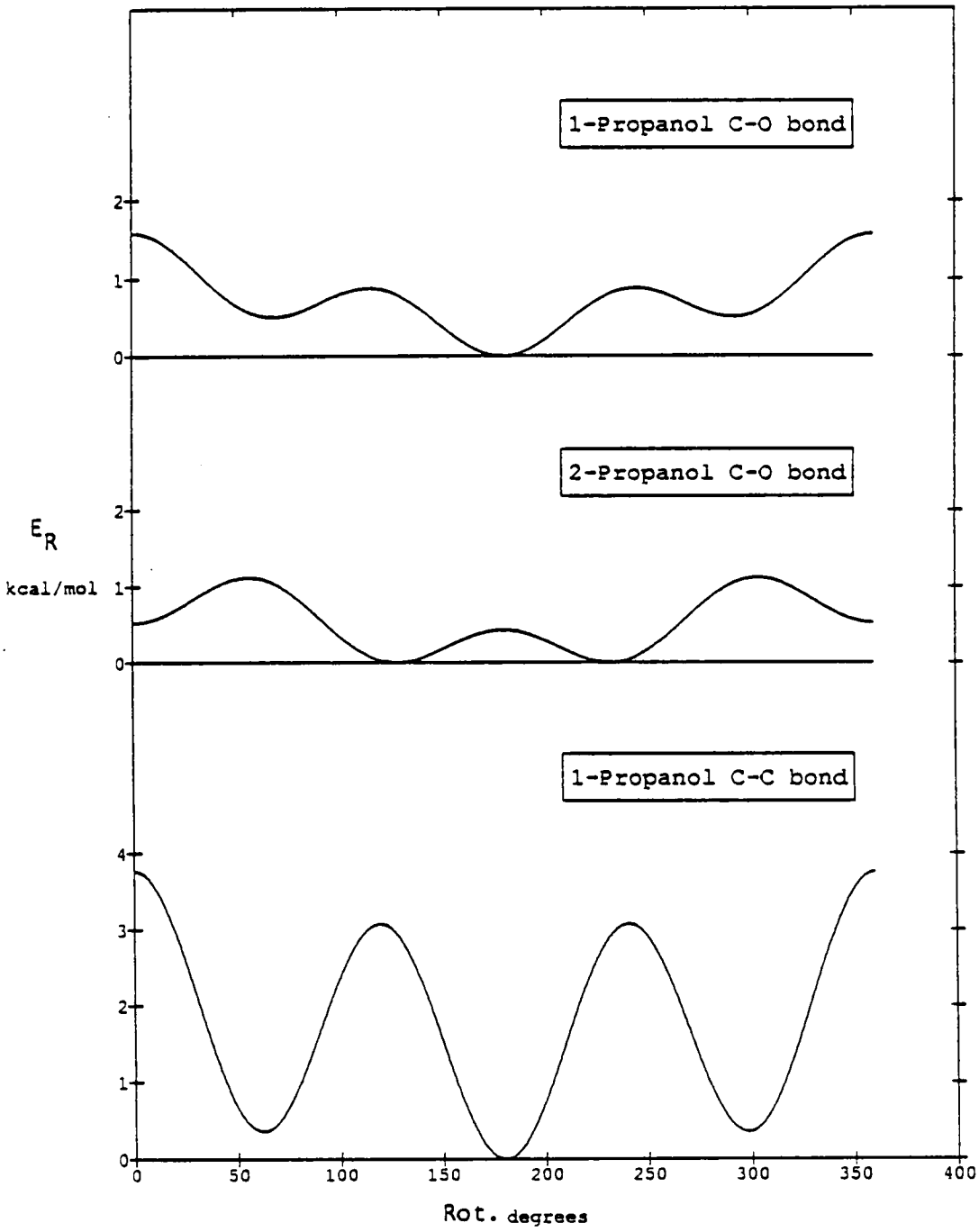

Figure 10. Plots of the C-O and C-C torsional rotation potential energy (E_R) functions for 1-propanol and 2-propanol.

5. Quantities Calculated From Simulation

As part of the NPT-ensemble averaging, the total average potential energy of the system is calculated including the torsional contribution. Also, the average density of the system is calculated. In this work several other quantities have been carried in the calculations and ensemble averaged. Since the position of each atom is known for each configuration, a distance scale can be established and the pair correlation function for any atom-pair can be calculated. The correlation functions can be averaged for output at the end of the simulation. Some of the most valuable pair correlation functions are those that Mehrotra and Beveridge[42] called quasi-component functions. In constructing these functions, first the total O-O, O-H, H-O and H-H pair correlation function is constructed for each atom in the solute (except the carbons) with each kind of atom in the solvent molecules. This allows the surrounding solvent system to be visualized in terms of how the water molecules would look as viewed from each of the solute atoms. Next, all of the solvent molecules (waters) are uniquely accounted for in either a primary (nearest neighbor) or secondary (next nearest neighbor) correlation function. This is done by selecting for each solvent atom the closest solute atom (primary) and the next-nearest solvent atom to the solute atom (secondary). Therefore, each solute atom has a primary function containing 108 atoms and a secondary function containing 108 atoms (or 216 if the solvent is water and the atom is hydrogen). Note that secondary solvent atoms to a solute atom can be in the primary functions for

another solute atom. The following notation is used for these correlation functions: $g^{i}(W,S)_{n}$ where i is blank for a total function, primed for a primary function and double-primed for a secondary function. W represents the particular solvent atom, either hydrogen (H) or oxygen (O), and S the solute atom, again either H or O in this case. n is the Z Matrix number of the solute atom; for example, oxygen 3 or hydrogen 4. With this construction the first peak of the primary distribution functions $g'(OO)_{n}$, $g'(OH)_{n}$, $g'(HH)_{n}$ and $g'(HO)_{n}$ will give an accurate interpretation of the number of hydrogen bonds (proton acceptor or proton donor) to each OH group on the solute. The number is obtained by integrating over the first peak in the appropriate primary radial distribution function to a distance called r(min), the first minimum in the primary pair distribution function. Also, for each of the solute-water systems the structure of the water is investigated by the calculation of water-water pair correlation functions, which allows a picture to be created of the effect of the solute on the water structure. The pair interaction energy distribution is calculated for both water-solute interactions and for water-water interactions. The water-water and water-solute pair interaction energy distributions are molecular-molecular interactions calculated from the Coulomb and Lennard-Jones site-site interactions which are summed over each molecule to give molecular interactions. For example, the energy of interaction of two water molecules would consist of a Lennard-Jones term for the two oxygen atoms and Coulomb terms involving the interaction of each of the three

charges on water molecule 1, with the three charges on water molecule 2 as described by equation (11). This allows the number of water molecules whose interaction energy with a water molecule is between E and E + ΔE to be plotted as a function of interaction energy, producing the pair interaction energy distribution function which can be averaged over all of the configurations of the system. The integral from approximately -2.5 to -10.0 kcal/mol in the solute-water pair distribution gives the number of solvent molecules interacting with the entire solute molecule in the energy range associated with hydrogen-bonding. Finally, the binding energy distribution is calculated for water-solute and for water-water interactions. For each configuration of the system, the solute molecule is surrounded by solvent molecules so that all solute-solvent interaction energies can be calculated. The sum of all solute-solvent interaction energies gives a solute-solvent binding energy which will vary configuration to configuration. The average over all ensembles gives a solute-solvent binding energy distribution. This distribution gives the overall strength of the water binding to the solute and also the effect of the solute on the water-water binding energy. During the calculation a configuration is saved every 50k configurations. These saved configurations were used to assess the effect of the molecules beyond cutoff and to give a visual picture of solute-water systems by using the saved configurations near final equilibrium. The additional computations incurred by carrying so many ensemble averages was to increase the computer time by about a factor of two. However, this

must be done if the details of solvent interactions near selected atoms in the solute are to be analyzed.

III. RESULTS AND DISCUSSION

1. General

Regarding the use of computer simulation to model liquids, and in particular dilute aqueous solutions, several comments are in order. First, Monte Carlo and Molecular Dynamics are becoming increasingly important as techniques to study liquids and solutions. Computers are now fast enough to handle the heavy computational load, and intermolecular potentials are being developed which are transferable system to system and give realistic results for a large array of liquids. These advancements have been led by Jorgensen, Scheraga, Stillinger, Karplus and Clementi among others. However, as Mehrotra et al.[73] and Jorgensen and Madura[27] have pointed out, care must be exercised, particularly in simulating dilute solutions. The addition of a single solute molecule to a collection of H_2O molecules (usually 108 to 216) increases the complexity of the system enormously in that solute-solvent interactions (and for higher concentrations solute-solute effects) must be accounted for, and radial distribution functions must be calculated on an atom-by-atom basis for the solute. The addition of solute motion and solute conformational changes introduces further complexity. The other problem is that many more configurations of the system must be averaged to obtain reliable information on details such as heats of solution, solute conformation and hydrogen bonding. In general, solute displacements and intramolecular rotations are attempted at frequencies much lower (by a factor of 100 or more) than attempts to

move solvent molecules. Thus, techniques to sample preferentially solvent molecules near the solute molecule (Owicki)[56,57] or convergence acceleration techniques such as "force-bias" sampling are employed.[73] In this work the use of an inverse square weighting factor is used as suggested by Owicki. Jorgensen[27] also employed a $1/(r^2 + c)$ weighting factor. In addition, moving the solute molecule helps to speed up the convergence. In this work, the solute molecule is translated every 210 configurations and torsional bond rotations are attempted every 110 configurations.

When solute molecules are added to water, solute-solvent interactions have to be included in the energy calculations. Also, the number of possible radial distribution functions expands greatly. In this work the standard pair correlation functions g(OO) and g(OH) are calculated for the solvent molecule along with the binding energy distribution and the pair interaction energy distribution. To analyze the solute-solvent interactions the total pair correlation function for each solute atom (excluding carbons because of shielding) has been calculated for both oxygen and hydrogen in the solvent. In addition, the quasi-component correlation functions called primary (nearest-neighbor) and secondary (next nearest-neighbor) have been calculated to assess better the details of atom-to-atom interactions of the solvent.

2. **Water**

As was mentioned earlier, the TIP4P model[30] was taken for water because it is being used extensively by other workers and

because it gives good values for the structural properties and the density and potential energy of water at atmospheric pressure. In Table IX a comparison is made of the values obtained here, using the TIP4P potential to simulate water, with those that Jorgensen and co-workers[30] obtained in NPT-ensemble simulations of TIP4P water. The agreement is very good except for the 2 percent higher density in this work and the higher number of nearest neighbors per monomer obtained from the integral of the g(OO) first peak out to 3.5 $\mathring{A}$, 5.43 compared to 5.1. However, if comparisons are made with the recent neutron diffraction results by Soper and Phillips[67] which are compared in Table X, it is seen that 5.43 is 3 percent higher than the experimental value while Jorgensen et al.[27] results are 3 percent lower. In Figure 11 and Figure 12, the complete experimental results for g(OO) and g(OH) of Soper and Phillips[67] are compared with results from this simulation using TIP4P water. Overall, the results here are in line with both Jorgensen[30] and Soper and Phillips.[67]

Table IX. Values obtained in Monte Carlo Simulation of TIP4P water at 1 atmosphere and 25°C.

	This Calculation	Jorgensen et al.[27]
Density, (g/cm^3)	1.024	0.999
Internal Energy ($-E_i$ (kcal/mol)	10.07	10.07
Integral of 1st g(OO) Peak	5.43	5.1
Integral of 1st g(OH) Peak	1.92	1.95
Peak Binding Energy per mole	-20.3 kcal/mol	-20.5 kcal/mol (est. from curve)

Table X. Comparison of TIP4P water from NPT Monte Carlo with neutron scattering experiment.

Pair Correlation Function	r (min) (Å)	Integral to r(min)
This Work		
g(OO)	3.5	5.428
g(OH)	2.5	1.916
Jorgensen, Chandrasekhar, Madura, Impey, & Klein[30]		
g(OO)	3.5	5.1
g(OH)	2.5	1.950
Neutron Scattering		
Soper and Phillips[67]		
g(OO)	3.5	5.271
g(OH)	2.5	1.974

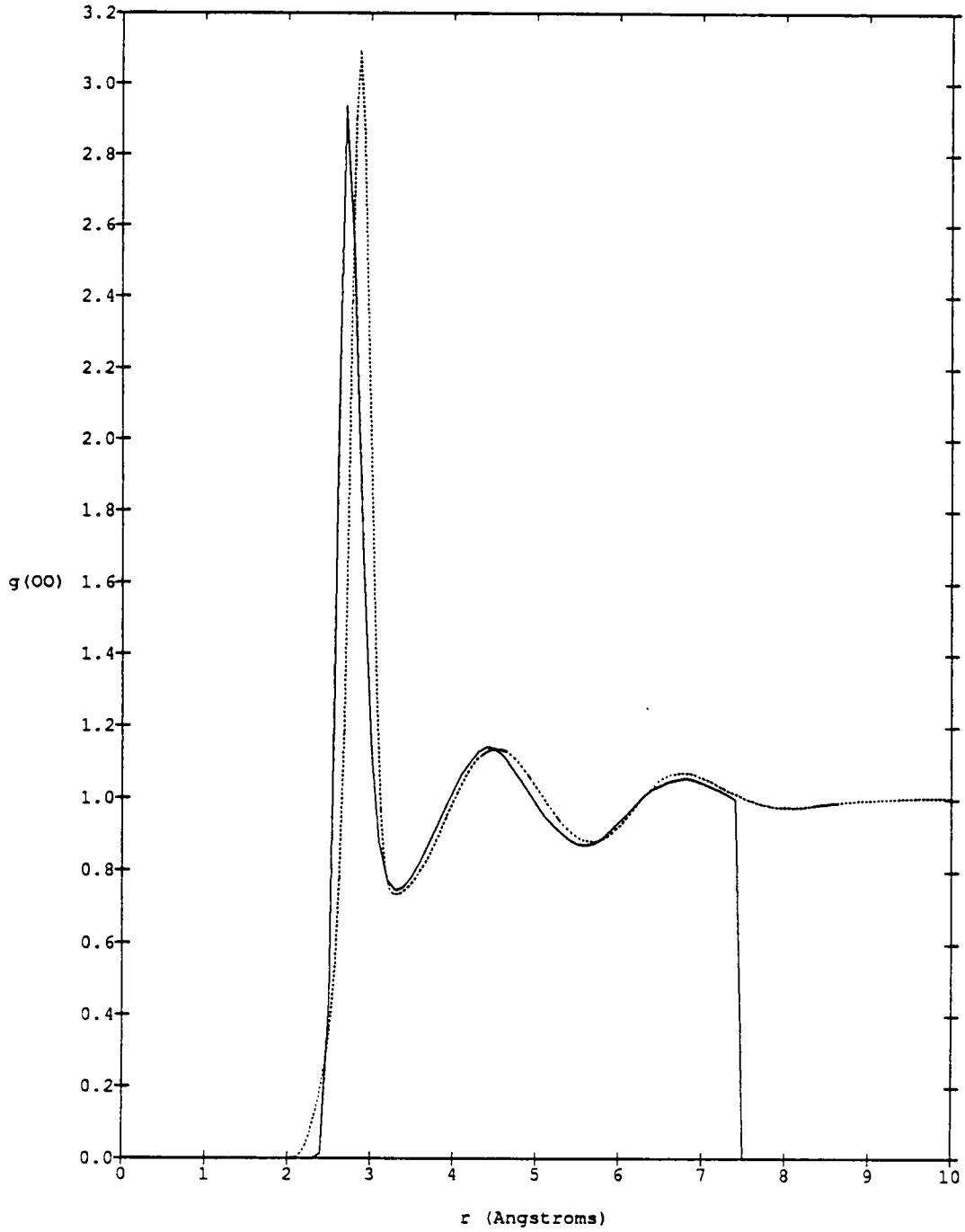

Figure 11. Neutron diffraction results of Soper and Phillips[67] for g(OO) compared with the results from this work using TIP4P water.[30] The dotted line is experimental and the solid line is calculated.

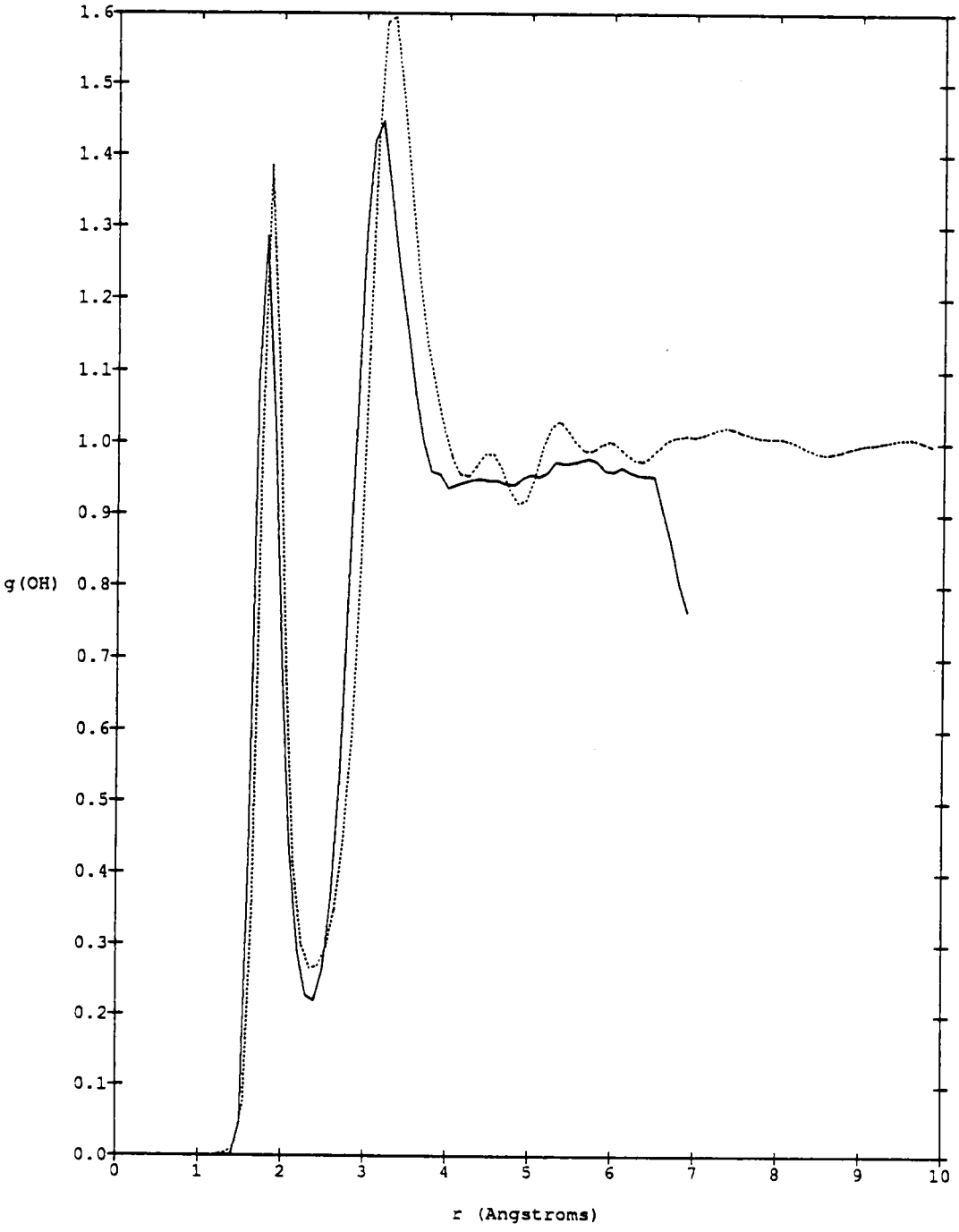

Figure 12. Neutron diffraction results of Soper and Phillips[67] for g(OH) compared with the results from this work using TIP4P water.[30] The dotted line is experimental and the solid line is calculated.

3. **Propane**

Propane (C_3H_8) was used in this series of solutes for aqueous simulation because it represents both a C_3 hydrocarbon of approximately the same size as the polyhydric alcohols and a hydrophobic system that is a well known Type II (large cavity) hydrate former.[68-72] Gas hydrates are crystalline compounds which form from pure gases, or mixtures of gases, such as methane, ethane and propane, and water. With this in mind, simulations of the water-propane system were run at atmospheric pressure and 25°C and also at a pressure of 27 bar and 4°C, conditions that exist in the propane hydrate-forming region.

Generally, the simulation results show propane has the properties of a hydrophobic molecule. The total pair correlation function g(HH) or g(OH) relates a hydrogen on the propane to interactions with either a water hydrogen or water oxygen and is very broad. The functions have amplitudes which increase with distance and are almost without structure for both the low pressure and high pressure examples (see Figure 13). Also, the primary (nearest neighbor) g'(HH) and g'(OH) functions (Figures 14a and 14b and 15a and 15b) show uniform peaks around the entire molecule essentially at equal distance from the propane hydrogens except broadened in the case of the high pressure (27 bar) simulation. In other words, the radial distribution functions indicate that the propane molecule is surrounded by a uniform, almost spherical shell of water molecules

which broadens with increased pressure in a clathrate or hydrate structure.

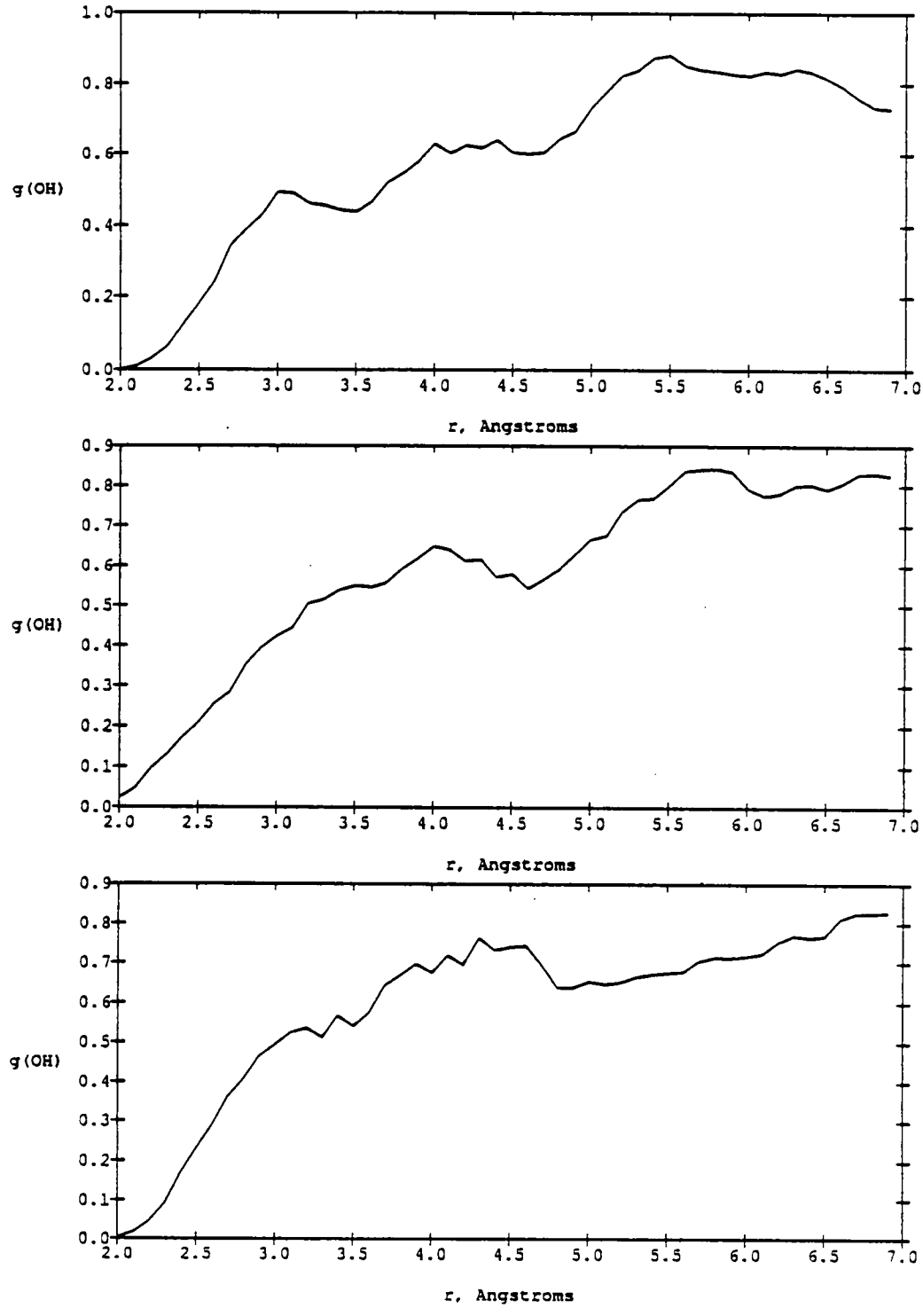

Figure 13. Examples of g(OH) correlation functions around propane hydrogen atoms four, five and six in propane-water atmospheric pressure.

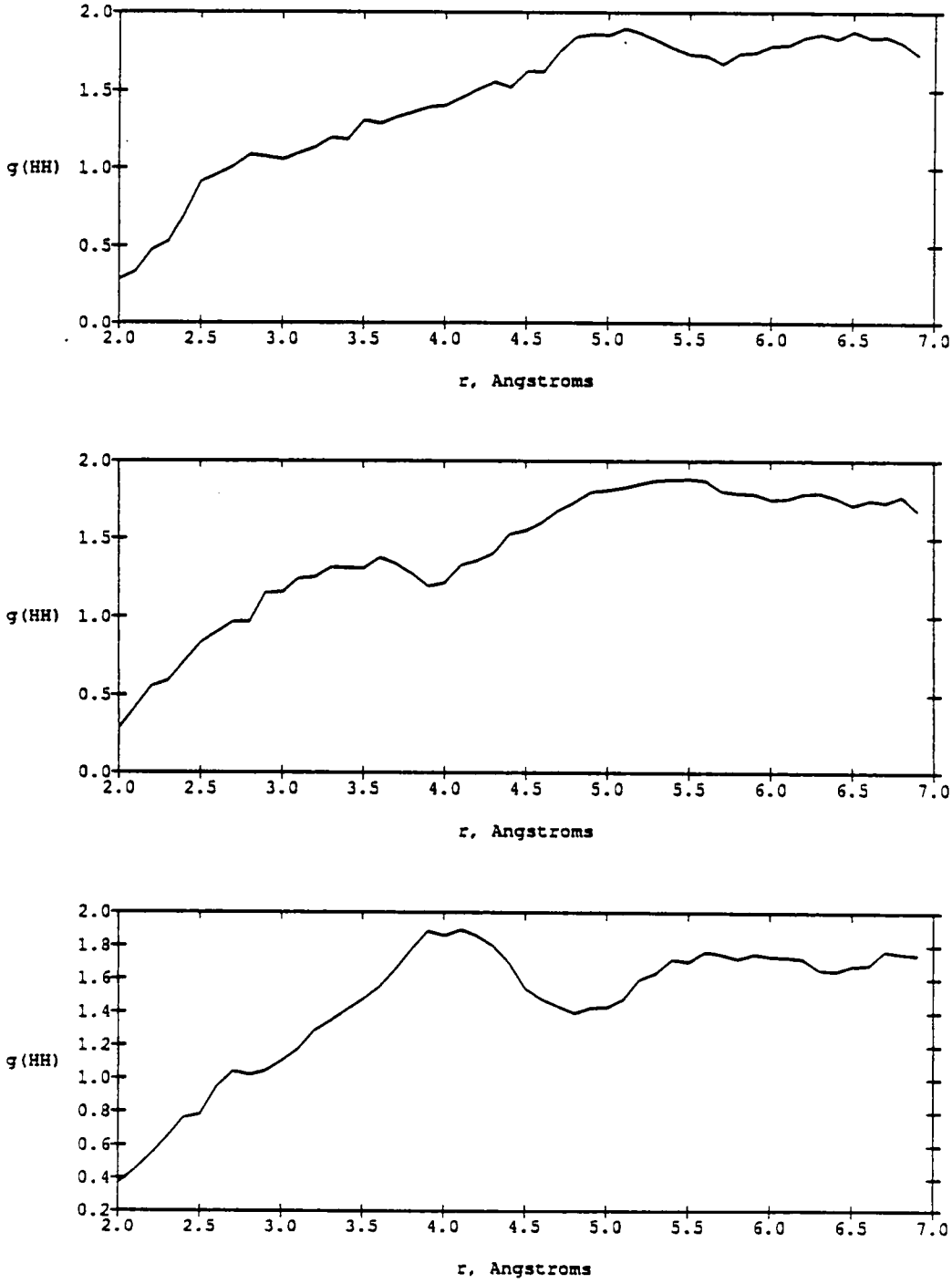

Figure 13. (cont.) Examples of g(HH) pair correlation functions around propane hydrogen atoms four, five and six in propane-water at atmospheric pressure.

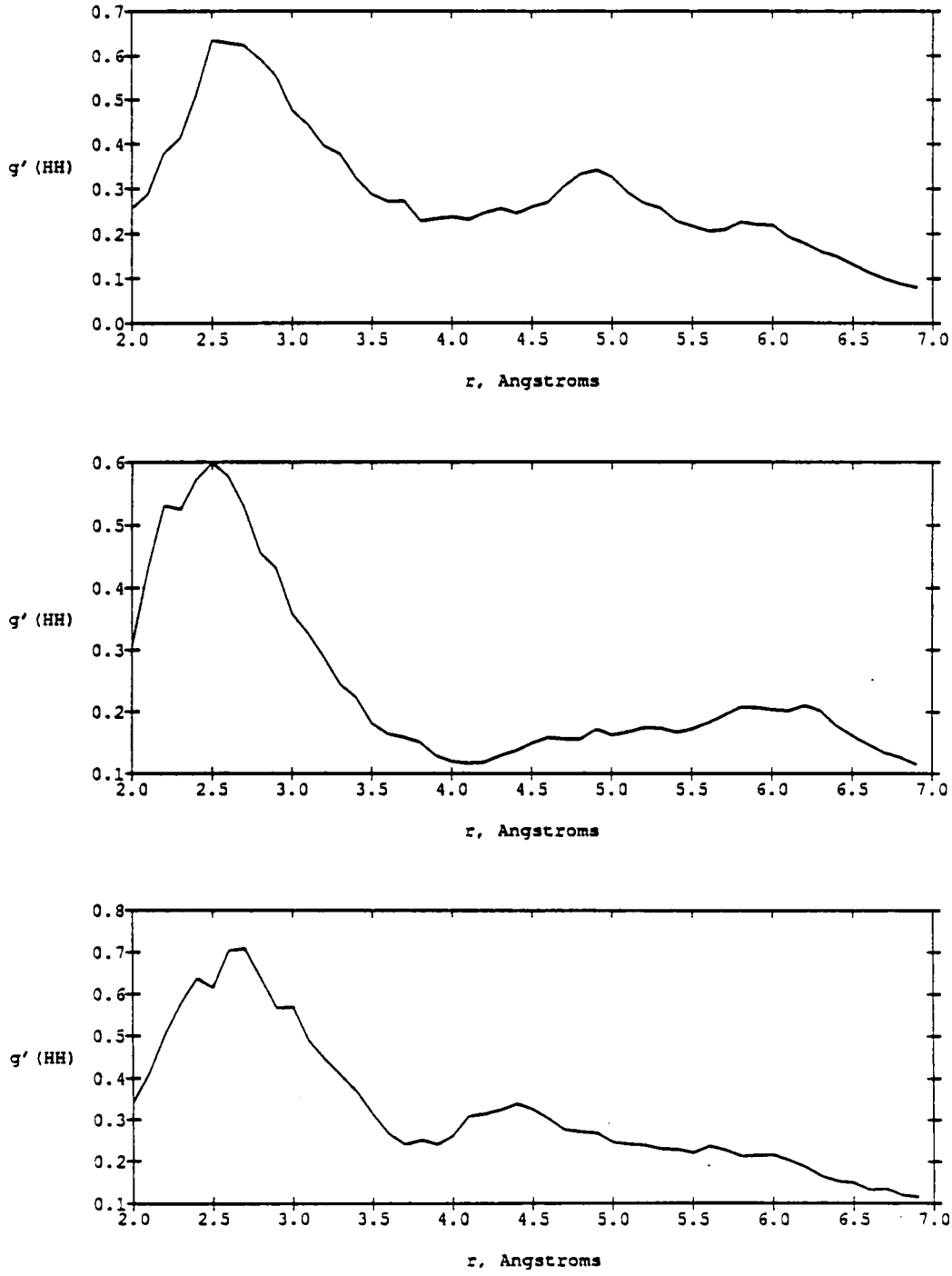

Figure 14a. Examples of primary pair correlation functions $g'_n(HH)$ around solute hydrogen atoms four, five and six in propane-water at atmospheric pressure.

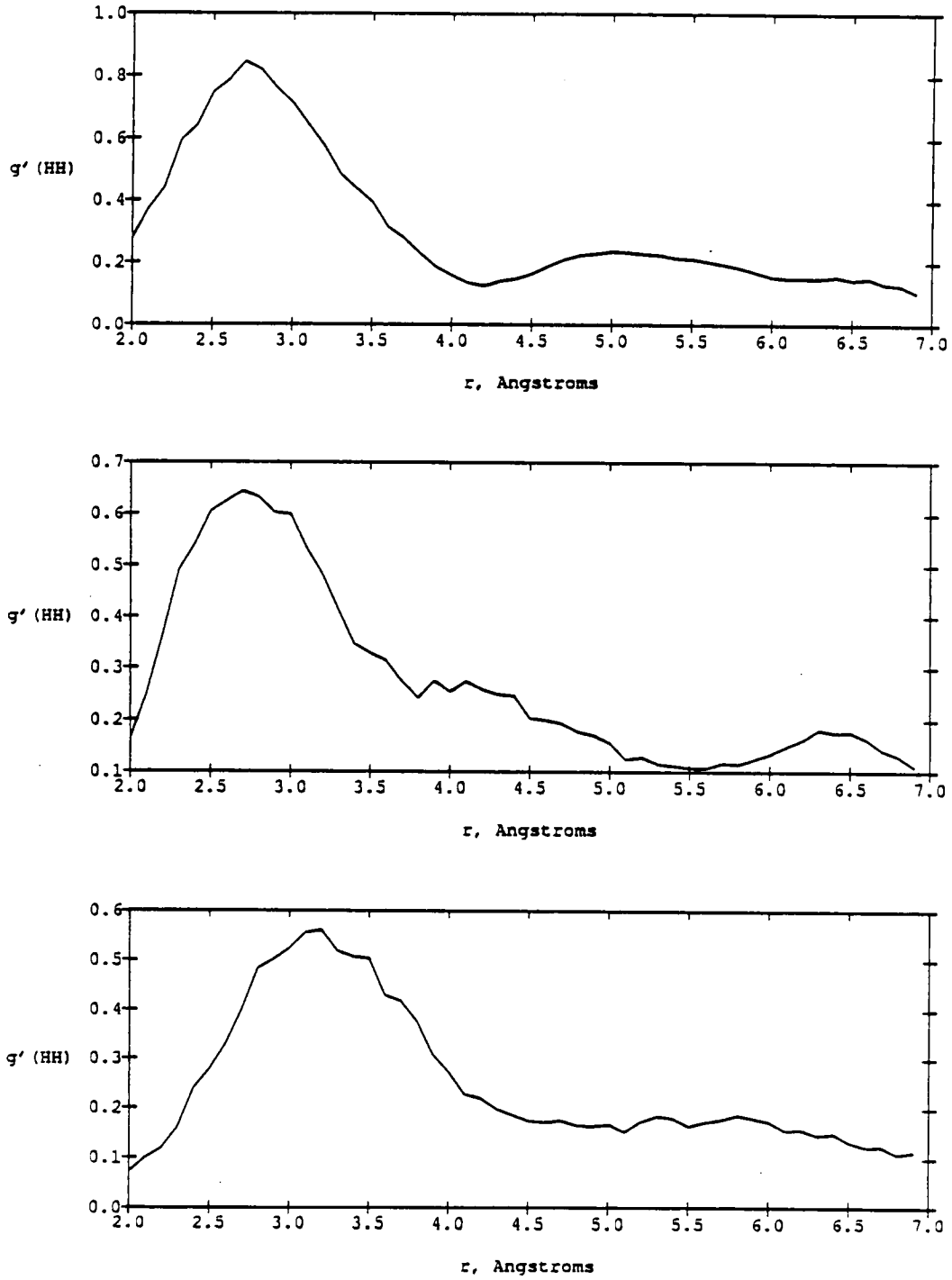

Figure 14b. Examples of primary pair correlation functions g'(HH) around solute hydrogen atoms four, five and six in propane-water at 27 bar and 277°K.

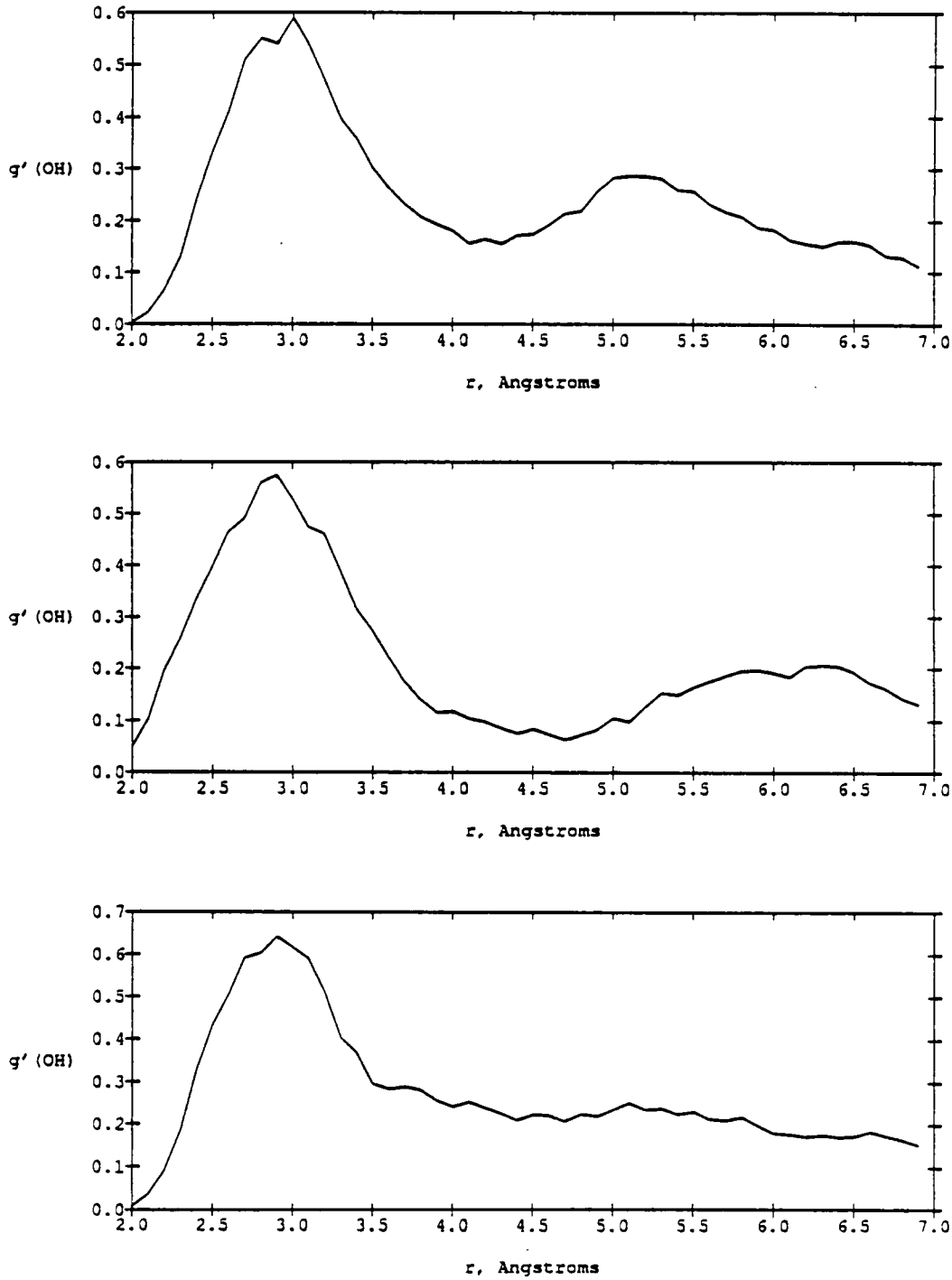

Figure 15a. Examples of primary $g'(OH)_n$ pair correlation functions around solute hydrogen atoms four, five and six in propane-water at atmospheric pressure.

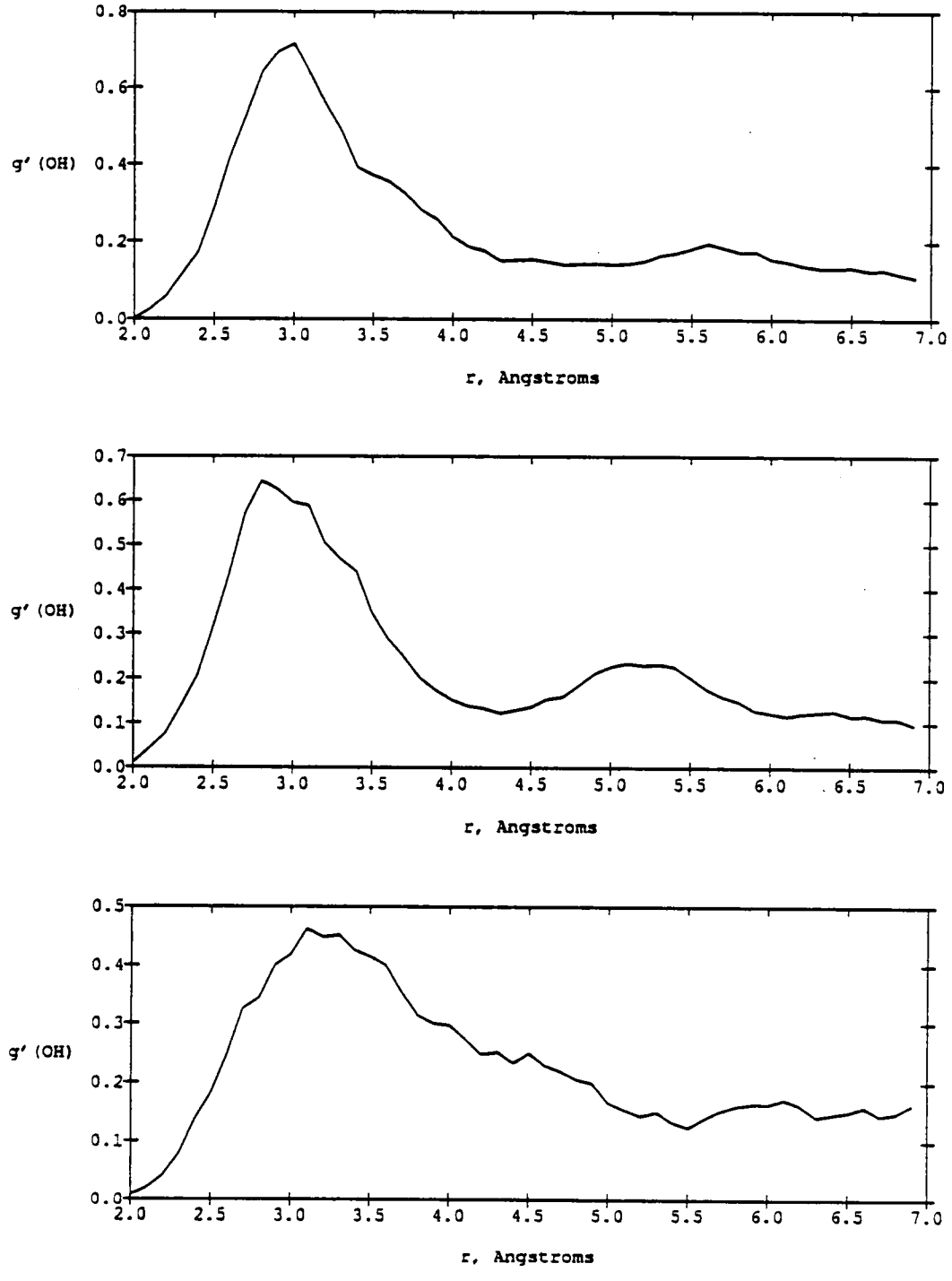

Figure 15b. Examples of primary $g'(OH)_n$ pair correlation functions around solute hydrogen atoms four, five and six in propane-water at 27 bar and 277°K.

An examination of the energy distribution functions such as the water-propane pair interaction energy distribution shows a very narrow peak extending from -0.75 kcal/mol to greater than +1.50 kcal/mol centered at -0.25 kcal/mol (Figure 16). This behavior indicates extremely weak (slightly attractive) interactions between propane and water and, of course, no hydrogen bonding. The water-water pair interaction energy distribution shows a distribution very similar to pure water while the water-water binding energy peaks at -20.5 kcal/mol for atmospheric pressure and -21.5 kcal/mol for the 27 bar simulation. The propane-water binding energy distribution is very narrow (Figure 17), extending from -2.0 kcal/mol to -9.0 kcal/mol and peaking at -7.5 kcal/mol. Plots of the Wood control functions for energy and density (Figure 18) show that a very stable equilibrium is obtained. In Figure 19, a saved configuration is shown near the end of the simulation. Although a small sampling of the system, the configuration gives a visual picture of the water shell around the propane molecule. The conformation of the propane is essentially the starting conformation. Note the surface outlined around the propane molecule by placing 2.5 $\mathring{A}$ radius circles centered on each carbon atom of the solute. On future configuration displays, the circles are centered on each oxygen and carbon atom of the solute. This allows one to view an interaction surface outside of which the interactions are hydrophobic, and inside of which hydrogen bonding may occur.

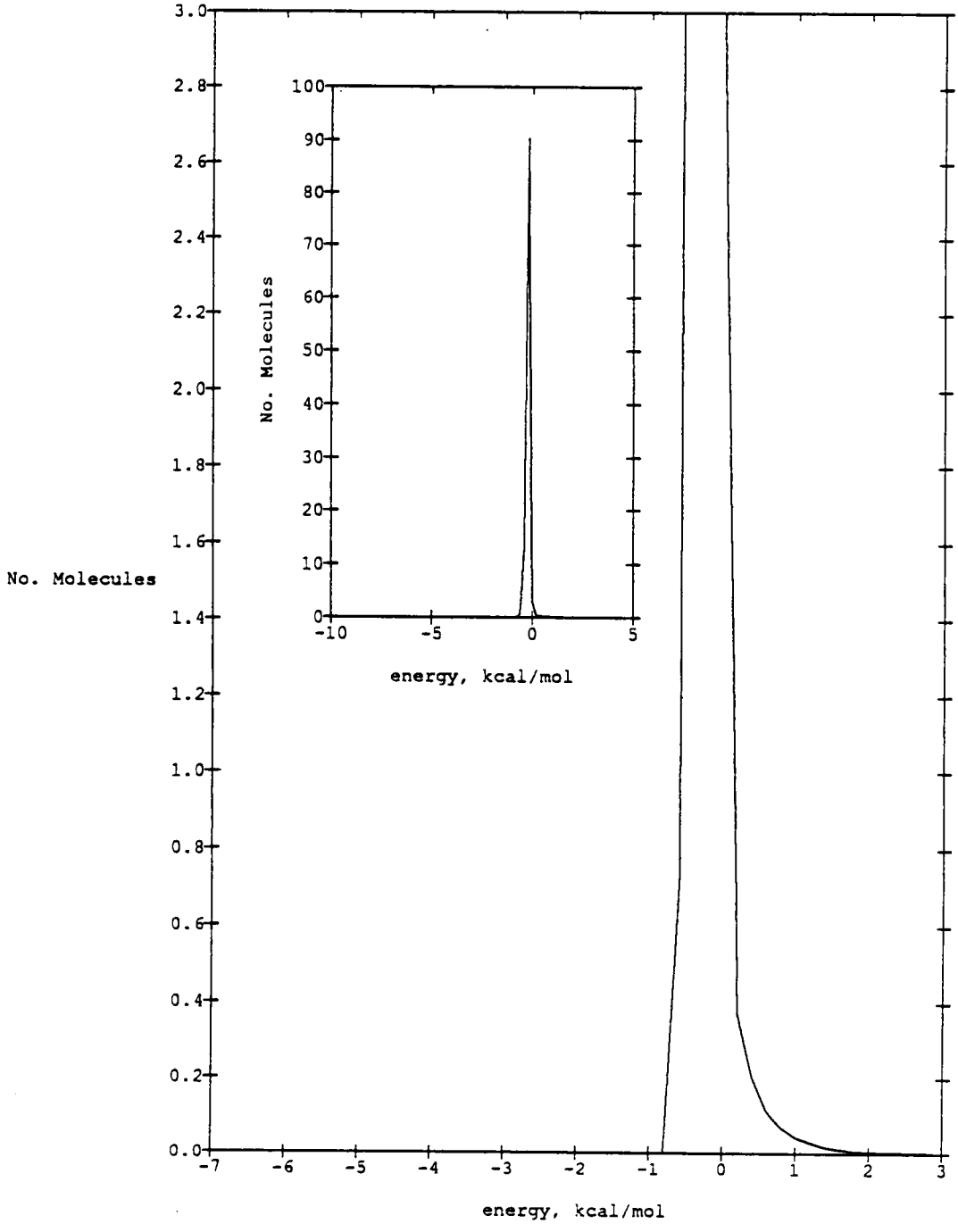

Figure 16. The water-propane pair interaction energy (kcal/mol) distribution.

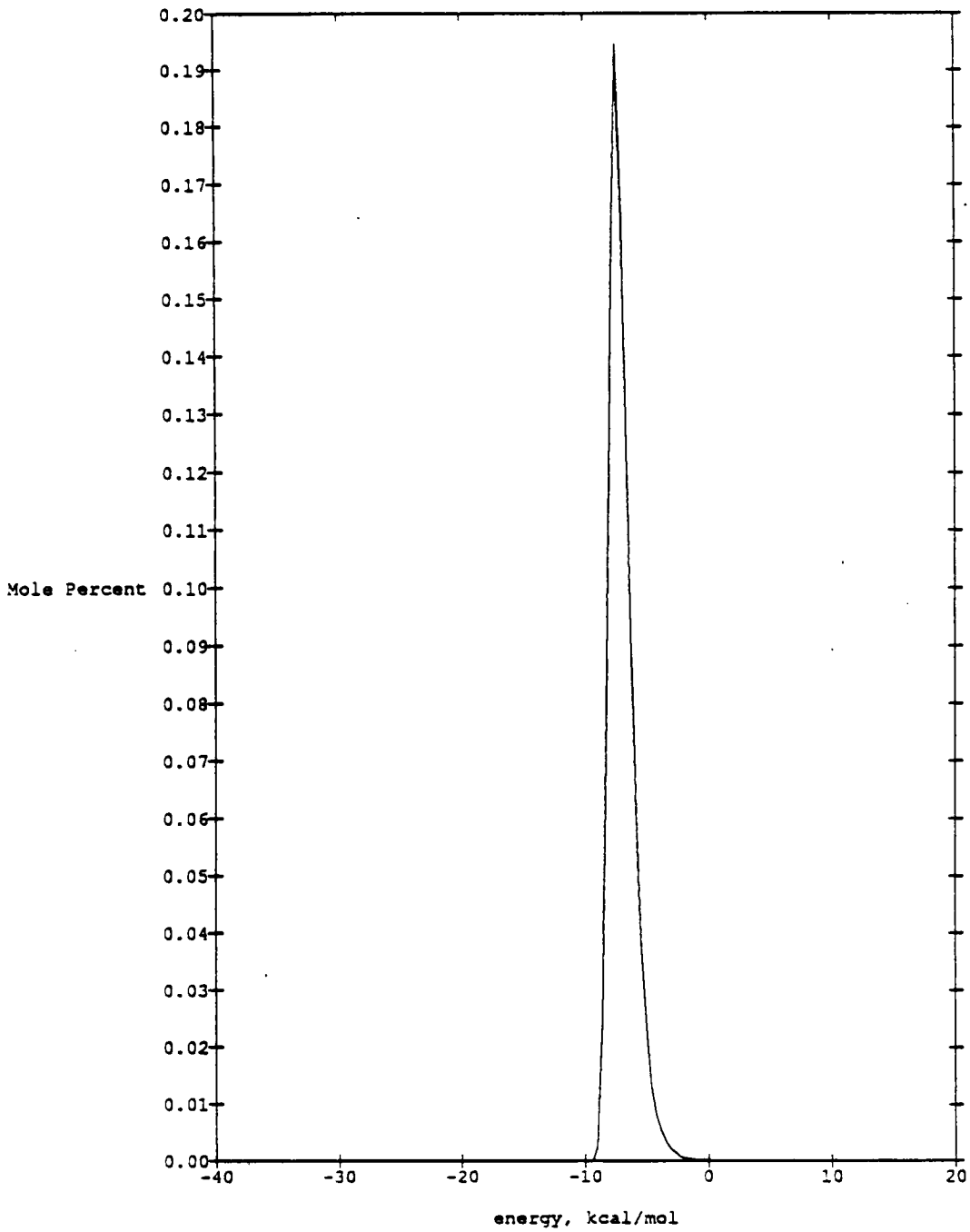

Figure 17. The distribution of propane binding energy (kcal/mol) for propane in water.

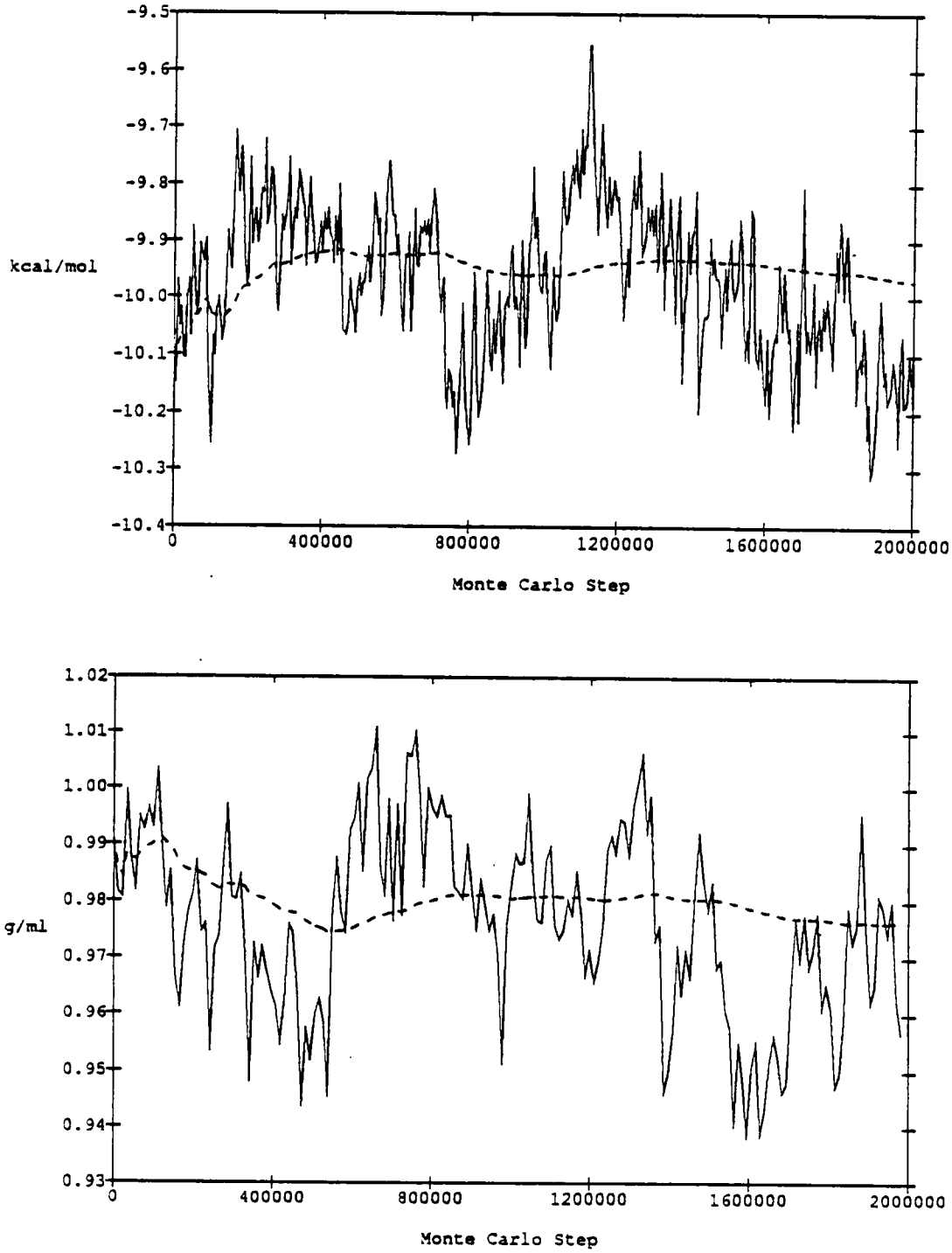

Figure 18. The Wood control function for density and internal energy in propane-water. The cumulative averages are displayed by the dotted lines. 5000 configurations are averaged for each Wood control point for energy and 100 configurations for density.

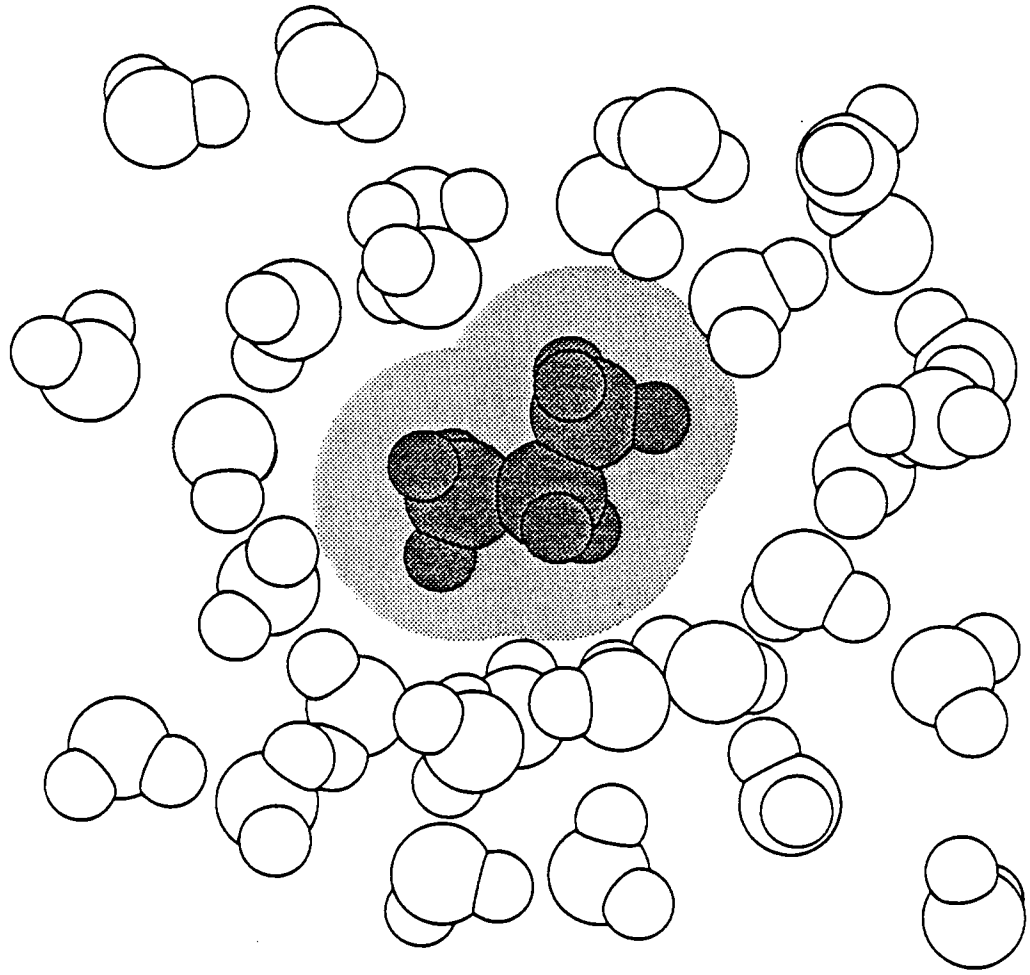

Figure 19. Saved configuration of propane in water near the end of an NPT-Ensemble Monte Carlo Simulation with the system at 27 bar and 277°K. A 4.0 Å thick slab-section is displayed. The shaded surface is created by 2.5 Å radius circles centered on carbon atoms.

As discussed previously, propane forms at high temperatures and pressures a gas hydrate of the large cavity or Type II structure. In these systems the propane molecule is surrounded by a fairly uniform shell of water molecules. The propane interacts very weakly with the water, and the strongest interactions in the system are the water-water hydrogen bond interactions. To analyze the hydrate systems, two simulations were carried out. First, one propane molecule in 108 waters was simulated at 25°C and one atmosphere pressure. Then the same system was simulated at 27 atmospheres and 4°C. The $g'(OH)_n$ and $g'(HH)_n$ were calculated (Figures 14 and 15) to show the uniformity of the clathrate (cage) structure of the solvent molecules. The first peak in the $g'(OH)_n$ function is uniformly 2.8-3.0 Å away from each of the propane hydrogens and broadens significantly with the increase in pressure. The first peak in the g'(HH) function is approximately 2.6 Å away from the propane hydrogens and broadens with the increased pressure. In fact, by visual observation of the saved configurations one can see the water shell becoming thicker and more organized in going from atmospheric pressure to 27 bar. Therefore, the system ends up with a propane molecule in a large cavity with a broad, almost spherical shell (~4.0 Å wide) of water hydrogen bonded to itself around it. The conformation of the propane remains the starting lowest energy gas phase conformation. The water-water radial distribution functions show some changes in the water-water pair correlation functions. The 1.85 Å g(HO) peaks increase in amplitude as does the 2.8 Å g(OO) peak as the pressure

increases. The water-water binding energy distribution peak goes from -20.5 kcal/mol to -21.5 kcal/mol with increasing pressure, but no changes are seen in the water-water pair interaction energy distribution curves. The energy functions related to the propane-water interaction do not change in going to higher pressure. This indicates that the propane hydrate is a water organization phenomenon rather than a solute specific (other than solute size) phenomenon. This is further evidenced by Table XI in which the total potential energy of all the solutes studied in water is presented. Notice that the hydrate-forming conditions reduce the system potential energy from -9.97 kcal/mol/H_2O to -10.31 kcal/mol/H_2O or by 0.34 kcal/mol/H_2O.

Table XII gives the value of the integrals of g'(OH) around each propane hydrogen over the first peak in a distance called r_{min}. This integral gives the number of water molecules coordinated with each propane hydrogen and the sum of this integral over all propane hydrogens gives the coordination number. In the hydrate-forming pressure and temperature region, the total propane water coordination number is increased from 24 to 30. John and Holder[70] have given a coordination number of 28 for Type II hydrate structures.

Table XI. Internal energy and system density.

T = 298 K
Warm-up - 1000K Configurations
Statistics - 2000K Configurations
(One Solute and 108 Waters)

	Total Potential Energy per H_2O (kcal/mol)	Density (g/cm^3)
Propane (1 Atmosphere)	- 9.97	0.976
Propane (27 Atomspheres, 277°K)	-10.31	0.987
Water	-10.07	1.024
Ethanol	-10.14	0.999
Ethylene Glycol	-10.20	0.966
1,2-Propylene Glycol	-10.12	1.004
1,3-Propylene Glycol	-10.25	0.995
1,3-Propylene Glycol (linear)	-10.23	0.993
Glycerol	-10.33	1.002

Table XII. Propane coordination number with water in aqueous solution.

1.0 Bar, 25°C

Energy -9.97 (kcal/mol) - Density 0.976 (g/cm^3)

r(min) (Å)	Integral of g'(OH) to r(min) (n)
4.1	2.61
4.7	2.82
4.7	4.10
4.7	4.11
3.7	1.83
3.7	1.96
4.1	2.60
4.1	3.82
Coordination Number	23.85

27.0 Bar, 5°C

Energy -10.31 (kcal/mol) - Density 0.987 (g/cm^3)

r(min) (Å)	Integral of g'(OH) to r(min) (n)
4.7	3.95
4.3	3.07
5.5	5.39
4.9	4.43
4.5	2.99
4.6	2.69
4.5	3.53
4.5	3.98
Coordination Number	30.03

r(min) is defined as the distance to the first minimum of the g'(OH) function after the first peak. The error in the integral values is estimated to be ±2.0 percent.

4. **Ethanol**

Ethanol (C_2H_5OH) is an example of a monohydric alcohol. Recently Alagona and Tani[44,45] have carried out NVT ensemble Monte Carlo simulations of dilute aqueous solutions of **trans**-ethanol (See Table III). In the present work, the ethanol was started in two conformations, one with the hydroxyl hydrogen pointing away from the methyl group and the second with the hydroxyl hydrogen pointing toward the methyl group. The pair correlation functions important to the analysis of hydrogen bonding are shown in the next few figures. Figure 20 shows the primary pair correlation function between the OH oxygen and water hydrogen $g'(HO)_3$ and the primary pair correlation function between the OH hydrogen and water hydrogen $g'(HH)_4$. Note that the subscript numbers refer to Table III rotation.

Figure 21 shows the primary pair correlation function between the hydroxyl (OH) oxygen and nearest neighbor water oxygen $g'(OO)_3$ and between hydroxyl (OH) hydrogen and nearest neighbor water oxygen $g'(OH)_4$. The close approach of a solvent (H_2O) proton to an OH osygen is an OH group proton acceptor hydrogen bond, and the close approach of an OH hydrogen to a solvent (H_2O) is an OH group proton donor hydrogen bond. Integrals over the first peak in $g'(HO)_3$ and the first peak in $g'(OH)_4$ give the number of OH group proton acceptor hydrogen bonds and OH group proton donor hydrogen bonds, respectively. Figure 22 shows the total pair correlation functions $g(HO)_3$ and $g(HH)_4$, and Figure 23 shows the total pair correlation functions $g(OO)_3$ and $g(OH)_4$.

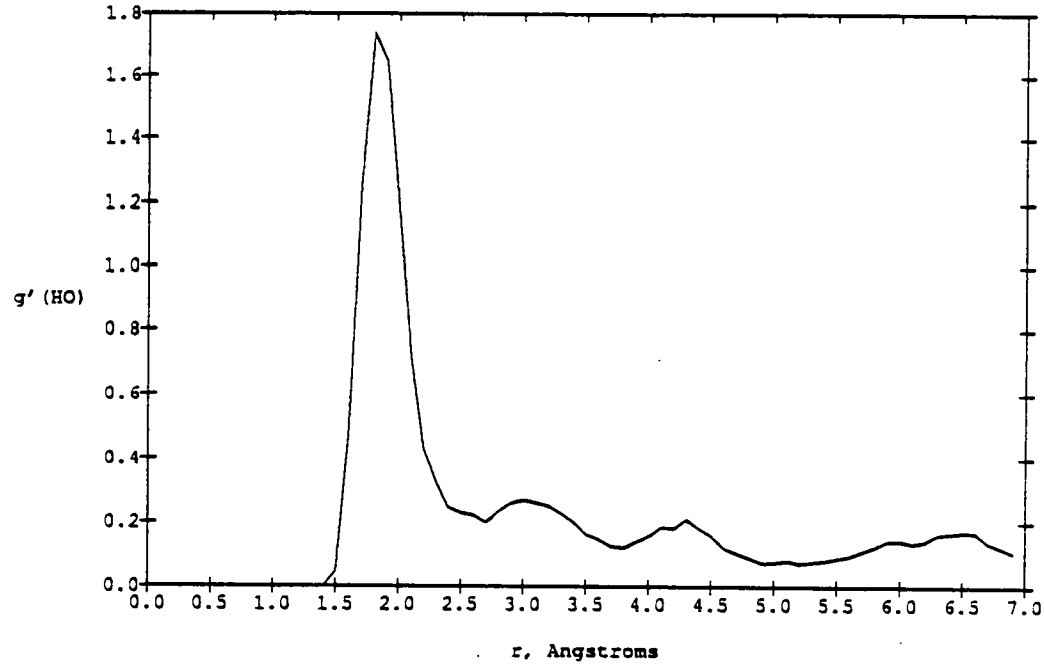

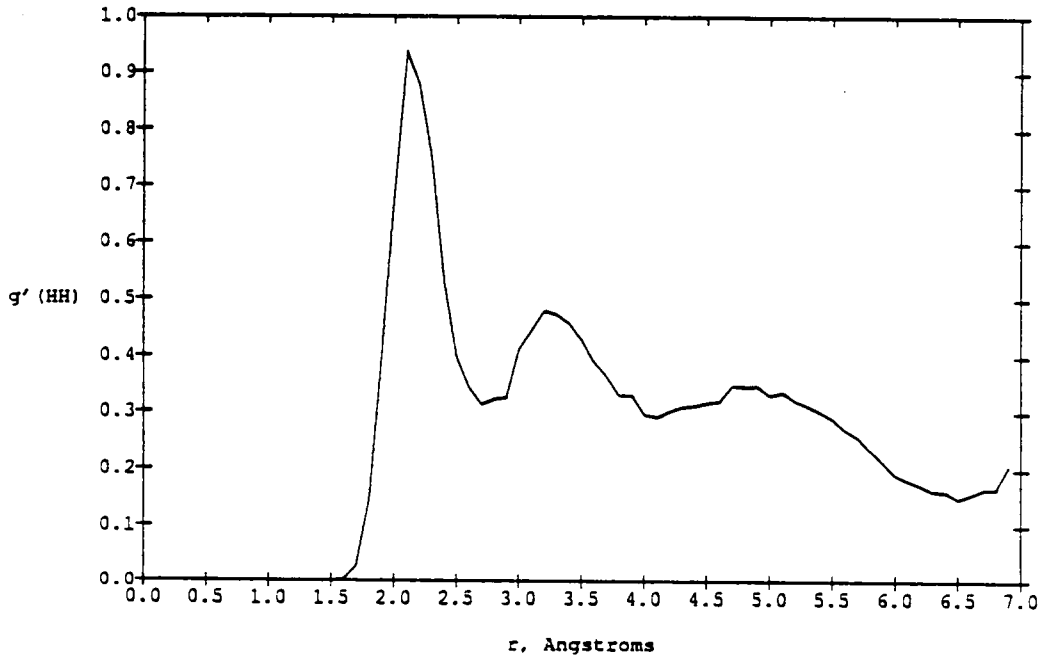

Figure 20. Primary pair correlation functions $g'(HO)_3$ and $g'(HH)_4$ for ethanol-water.

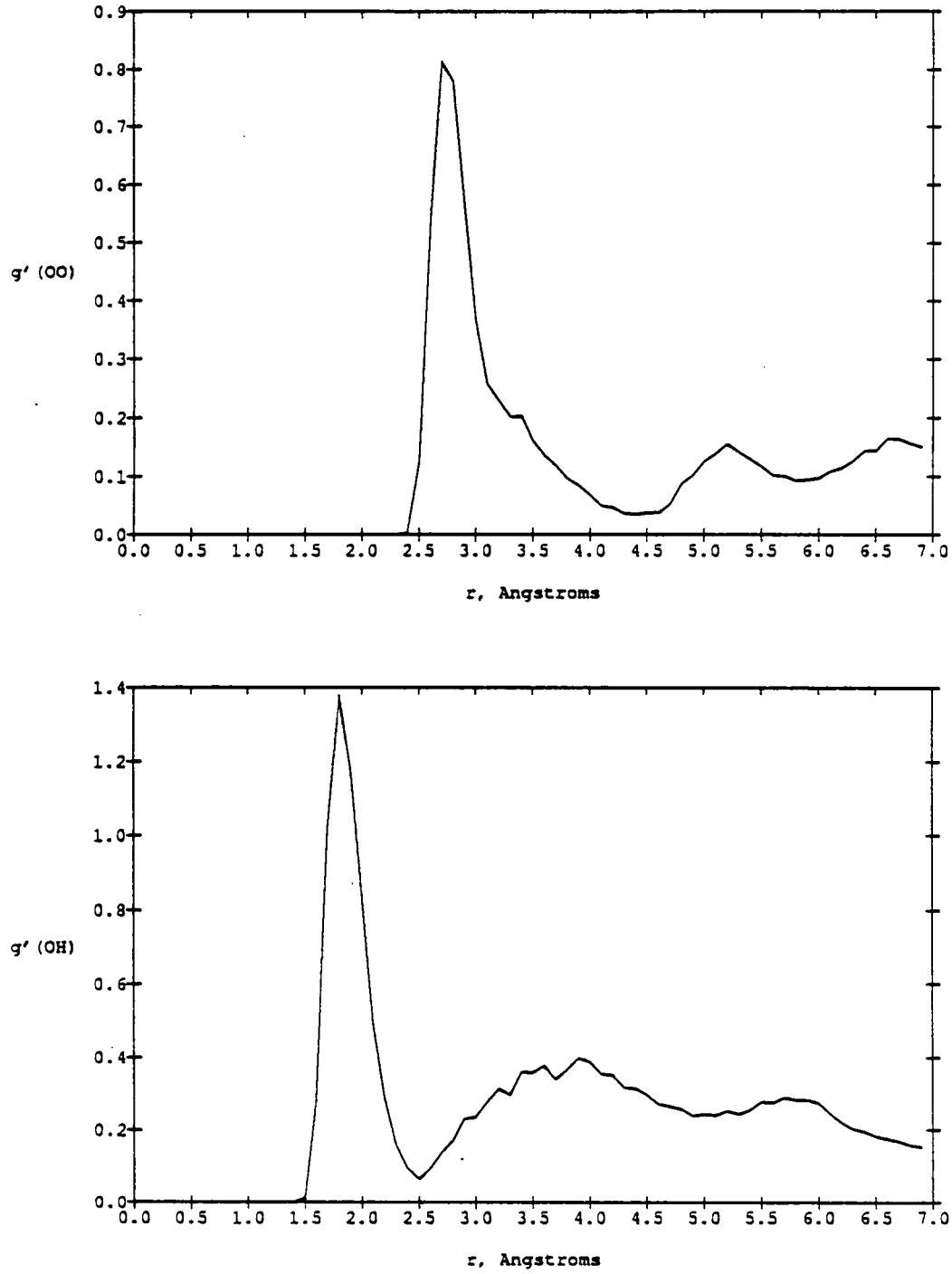

Figure 21. Primary pair correlation functions $g'(OO)_3$ and $g'(OH)_4$ for ethanol-water.

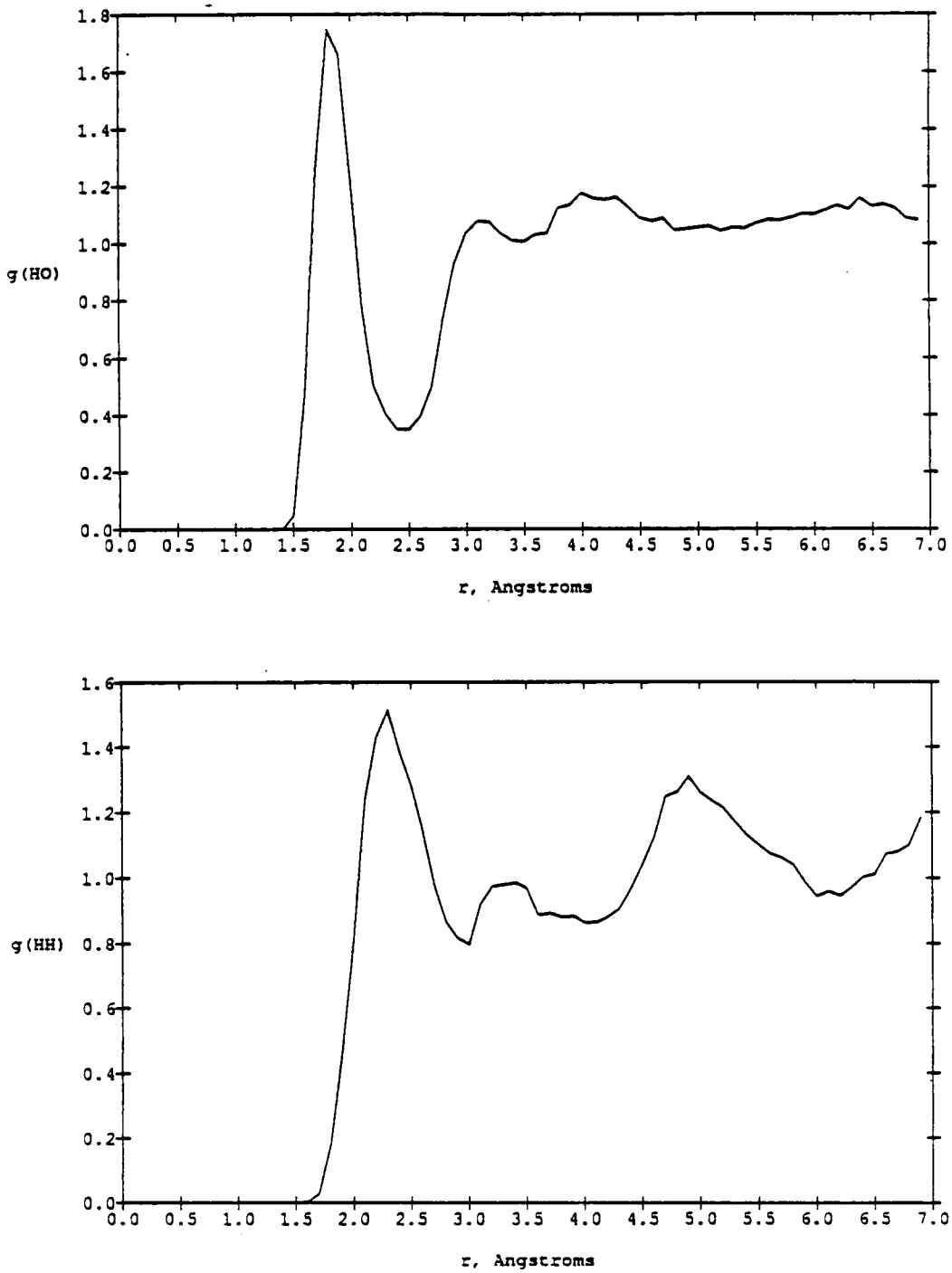

Figure 22. Total pair correlation functions $g(HO)_3$ and $g(HH)_4$ for ethanol-water.

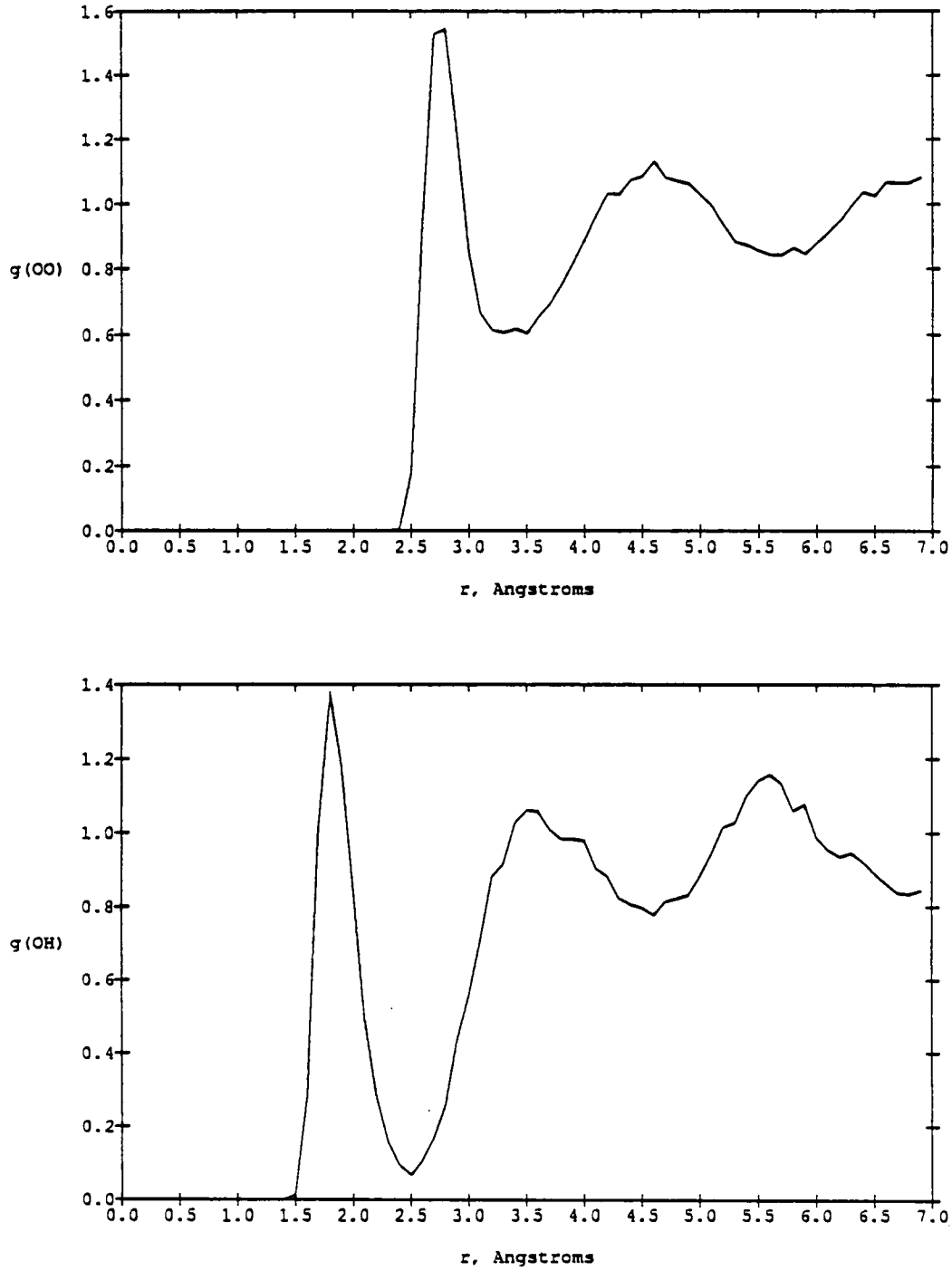

Figure 23. Total pair correlation functions $g(OO)_3$ and $g(OH)_4$ for ethanol-water.

Notice that the general shape of $g(HO)_3$ is similar to that in pure water, Figure 12. $g(HH)_4$ is very similar to the curve reported for g(HH) in Reference 44, including the small peak at 3.4 Å. This is interesting because it was expected that some distortions in the total ethanol-water pair correlation functions would take place due to the rotational degrees of freedom employed in this calculation. $g(OO)_3$ looks very similar to free water in shape, Figure 11; however, the amplitude of the peaks are reduced by a factor of two. $g(OH)_4$ is very similar to the Alagona and Tani[44,45] results. They interpreted their calculations to represent the ethanol OH group as both a proton acceptor and a proton donor in water.

In addition, Figure 24 shows the ethanol-water pair interaction energy distribution function plotted against interaction energy. Remember that most interactions contributed by remote molecules are close to zero. The distribution at positive energy represents interaction with the nonpolar part of the ethanol molecule. The distinct attractive interactions occurring from -3.0 kcal/mol to -6.5 kcal/mol represent hydrogen bonding of water with ethanol.

The integral of methanol-water pair interaction energy distribution function from -7.0 kcal/mol to -2.6 kcal/mol gives a value of 2.29 water molecules attractively interacting with and assumed to be hydrogen bonds between the solvent water molecules and the ethanol molecule. In Figure 25 the ethanol-water binding energy distribution is given. The binding energy ranges from -10.0 kcal/mol to -29.0 kcal/mol, with the peak at -20.0 kcal/mol. The results are

very similar to those for TIP4P water and are in keeping with the oxygen-centered $g(OO)_3$ on ethanol having a similar shape for pure water. Finally, Figure 26 presents a 4 Å-thick slab of a sample configuration near the completion of the calculation. Notice the conformation of ethanol with the OH proton toward the methyl group, and the two waters close to the OH group which act as proton donors and acceptors. Also observe the five-membered ring-forming tendencies in the water molecules around the nonpolar part of the ethanol molecule.

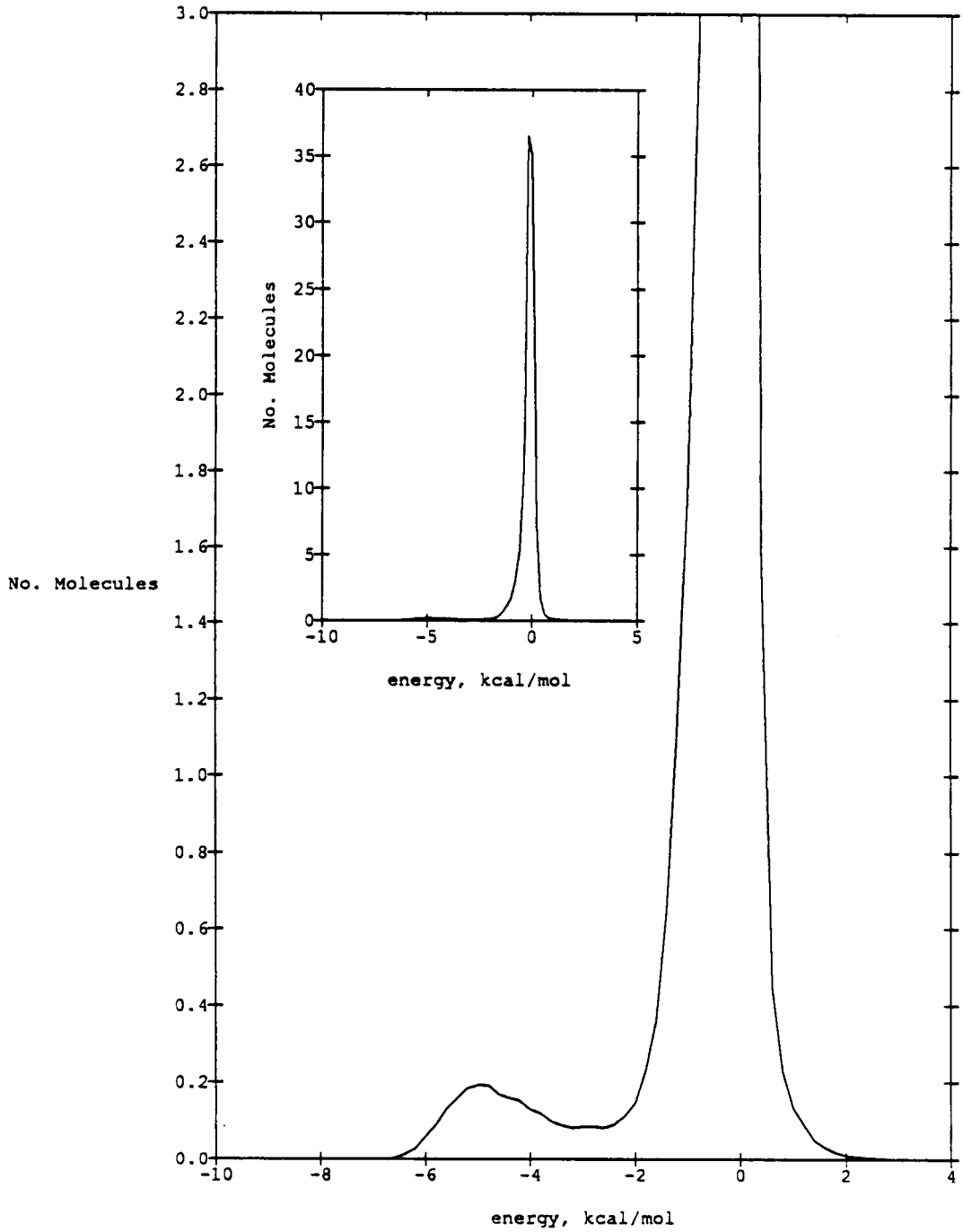

Figure 24. Pair interaction energy distribution function for ethanol-water.

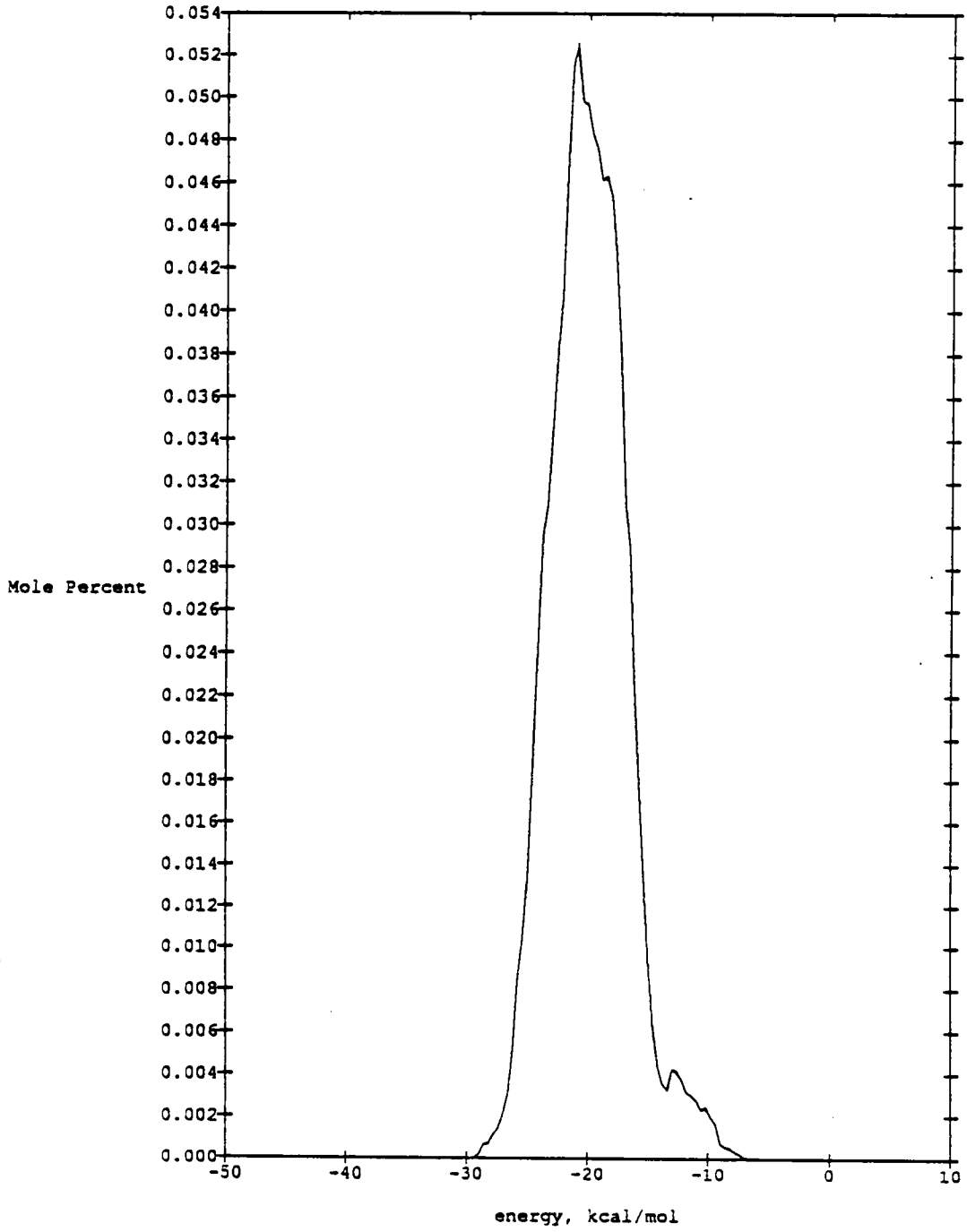

Figure 25. Binding energy distribution of ethanol in water.

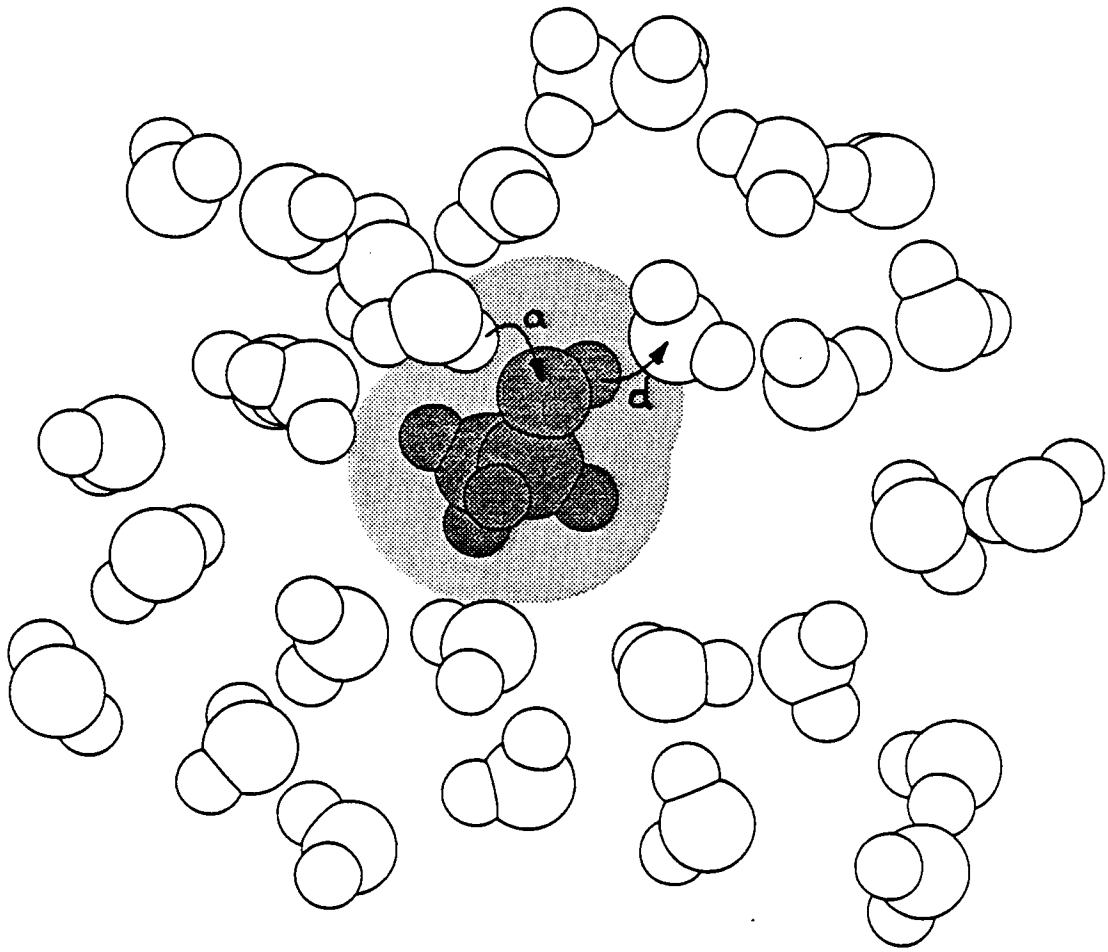

Figure 26. Saved configuration of ethanol in water showing the ethanol conformation and the OH group proton acceptor and donor properties designated by arrows with a and d labels. A 4.0 Å slab is shown. The shaded surface is created by 2.5 Å circles centered on oxygen and carbon atoms.

Alagona and Tani[45] used a **trans** conformation for ethanol in water, and their NVT-ensemble Monte Carlo simulation showed two hydrogen bonds to ethanol with the OH group being a proton acceptor in one and a donor to nearby water molecules in the other. This work agrees with their conclusion. In Figure 20 $g'(HO)_3$ indicates the OH oxygen acting as a proton acceptor while $g'(OH)_4$ in Figure 21 indicates the OH hydrogen being shared with a solvent oxygen. In addition, the integral over $g'(HO)_3$ integrates to 1.42 hydrogen bonds while the integral over $g'(OH)_4$ integrates to 0.89 hydrogen bonds. The integral from -10.0 kcal/mol to -2.6 kcal/mol over the ethanol-water pair interaction energy distribution (Figure 24) gives a value of 2.29 hydrogen bonds. The ethanol-water correlation function $g(OO)_3$ (Figure 23), is almost identical to that of pure water, which indicates that even though significant hydrogen bonding occurs between ethanol and water, the water structure is not greatly changed.

In examining the conformation of ethanol in water, alcohol molecules were started with the OH groups in several conformations. However, the final conformation of the OH group always indicated that the hydroxyl hydrogen was close to the methyl group. Table XI reveals that the effect on the total potential energy of water by adding ethanol is slight, -10.14 kcal/mol compared to -10.07 kcal/mol in pure water. Also, the water-water binding energy and the ethanol-water binding energy are both approximately -20.0 kcal/mol.

5. **Ethylene Glycol**

Ethylene glycol $C_2H_4(OH)_2$ is the simplest polyhydric alcohol and was earlier characterized in the Introduction of this work as a good analogue of water and slightly hydrophobic in dilute solution. The molecule is also known from NMR experiments[16] to have its OH groups in the **gauche** conformation in aqueous solution, with a tendency to for intramolecular hydrogen bonds. The results of the NPT-ensemble simulation of ethylene glycol (EG) in water are best illustrated by showing the pair correlation functions which detail the interactions around the two OH groups in EG.

Figure 27 shows $g'(HO)_3$ and $g'(HO)_4$, Figure 28 shows $g'(HH)_5$ and $g'(HH)_6$, Figure 29 shows $g'(OO)_3$ and $g'(OO)_4$, and Figure 30 shows $g'(OH)_5$ and $g'(OH)_6$. The pair correlation functions $g'(HO)_{3 \text{ and } 4}$ clearly represent the close approach of a proton to each of the two OH oxygens. In a similar fashion, $g'(HH)_{5 \text{ and } 6}$ demonstrate approach of a solvent hydrogen to each of the hydroxyl hydrogens, indicating the presence of a water molecule near each OH group. The $g'(OO)_{3 \text{ and } 4}$ and $g'(OH)_{5 \text{ and } 6}$ pair correlation functions indicate water molecules from the solvent in close proximity with the OH groups of ethylene glycol, although there is some asymmetry in peak amplitude. $g'(OH)_{5 \text{ and } 6}$ indicates that the OH proton is hydrogen bonded to a solvent oxygen.

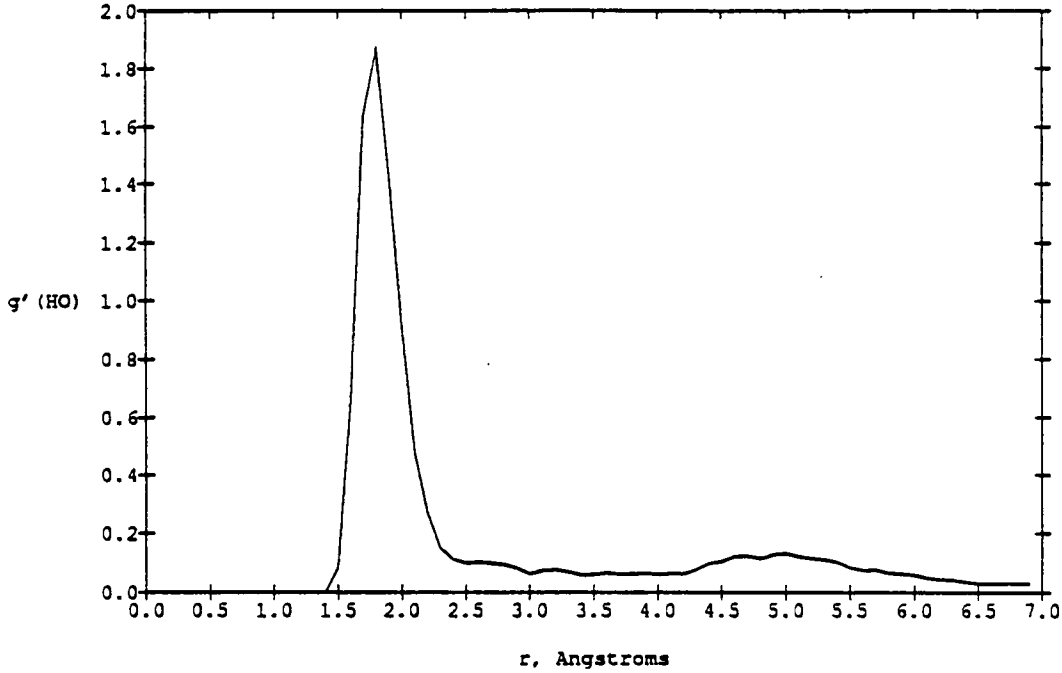

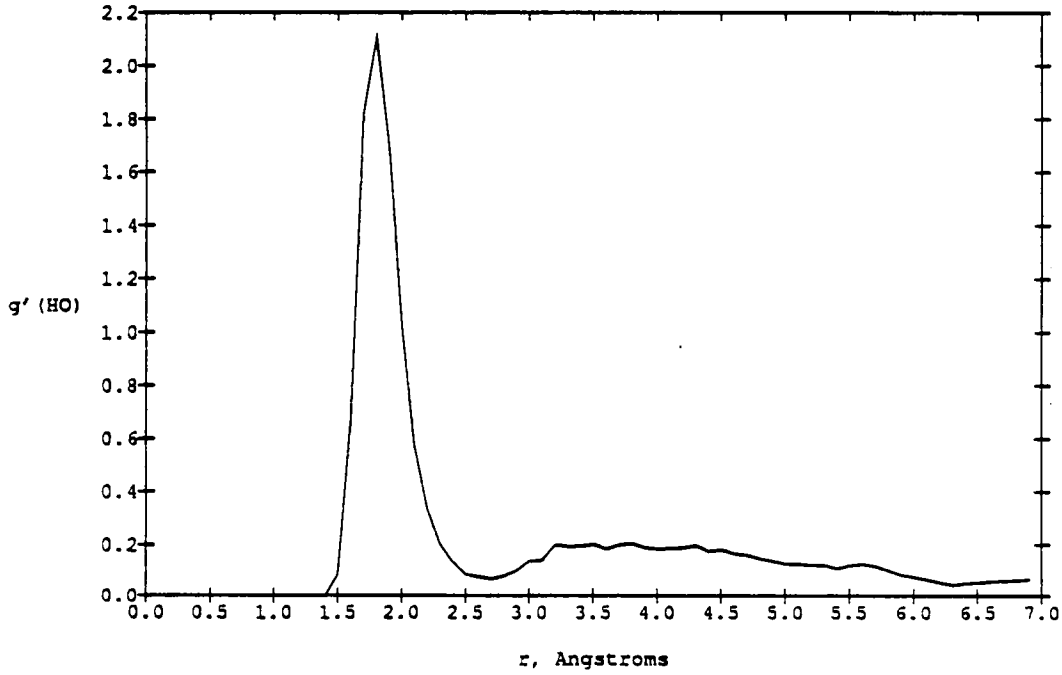

Figure 27. Pair correlation functions $g'(HO)_3$ and $g'(HO)_4$ of ethylene glycol in water.

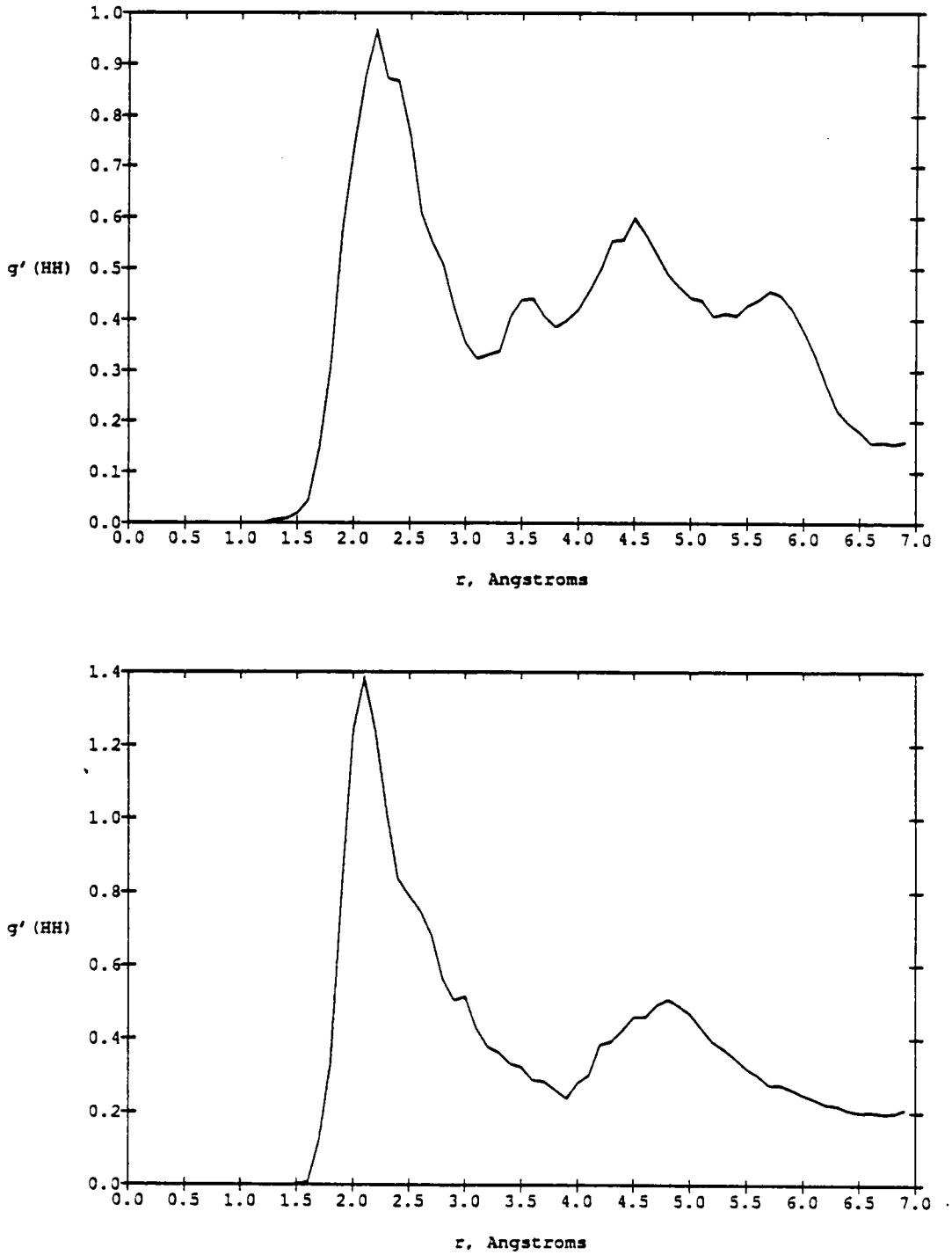

Figure 28. Pair correlation functions $g'(HH)_5$ and $g'(HH)_6$ of ethylene glycol in water.

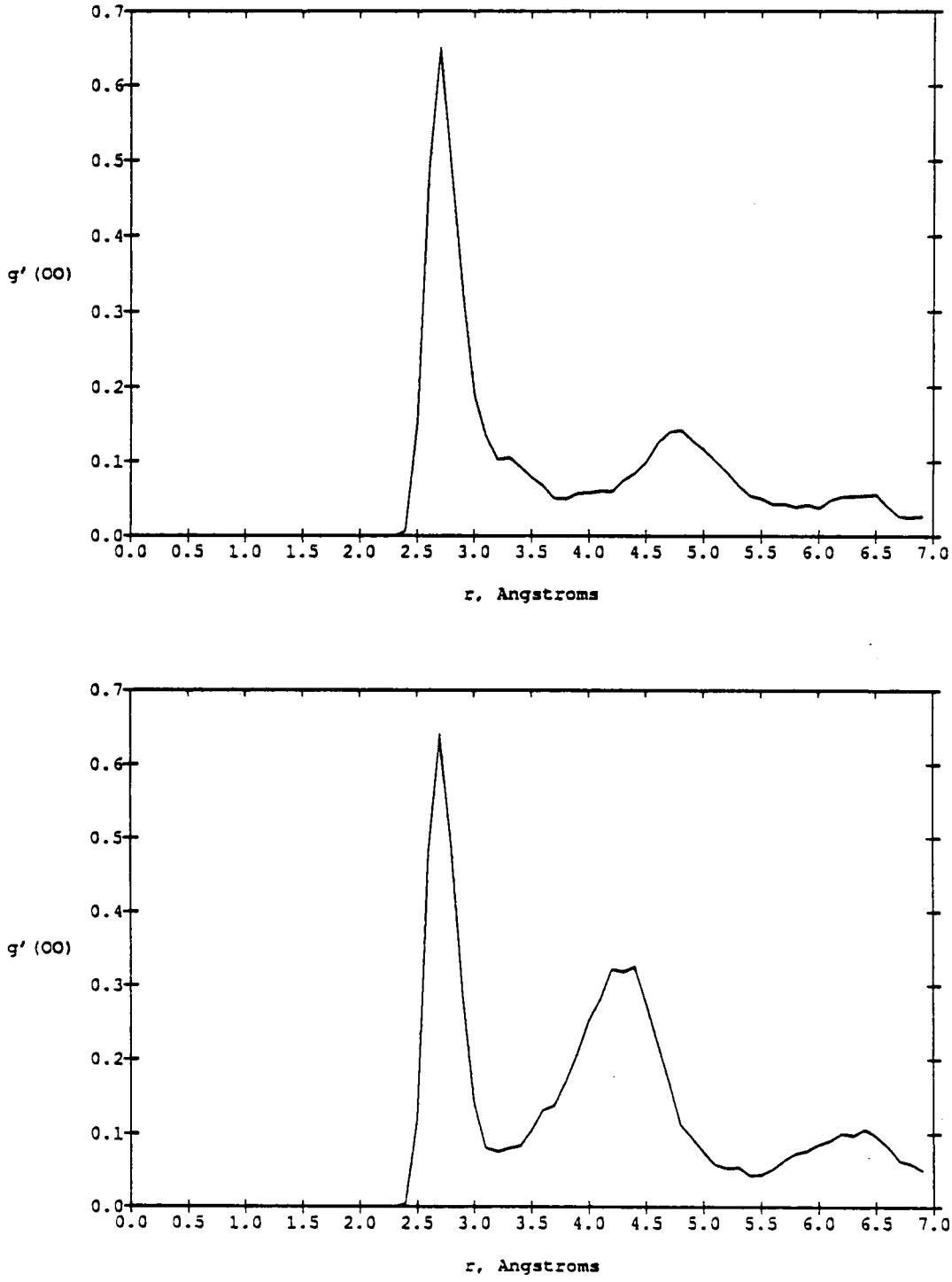

Figure 29. Pair correlation functions $g'(OO)_3$ and $g'(OO)_4$ of ethylene glycol in water.

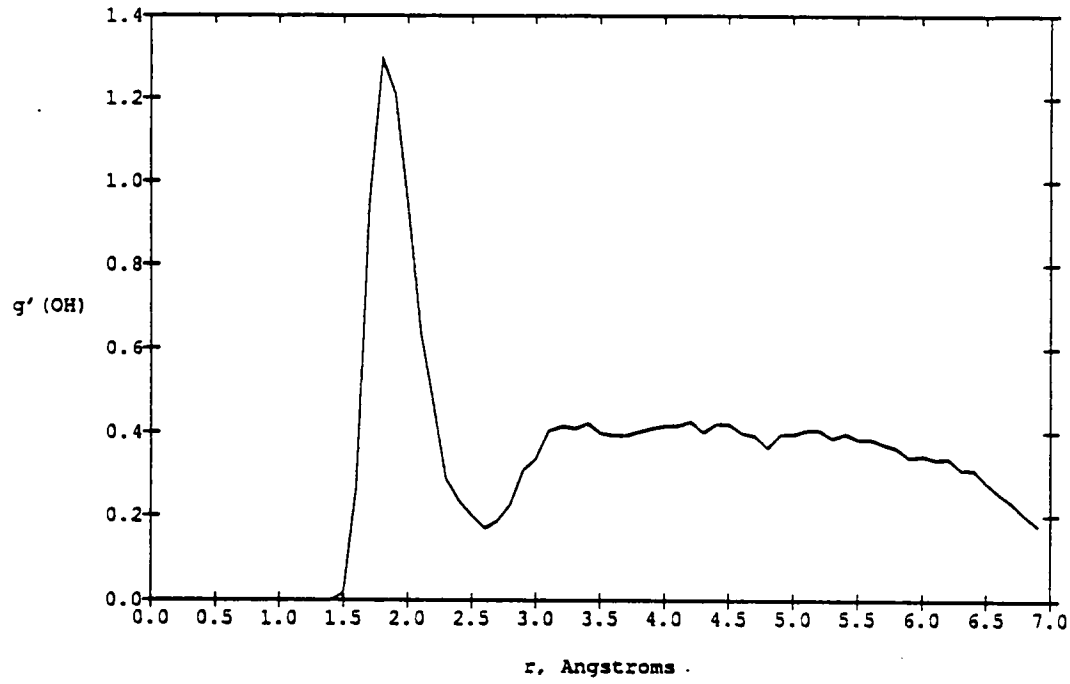

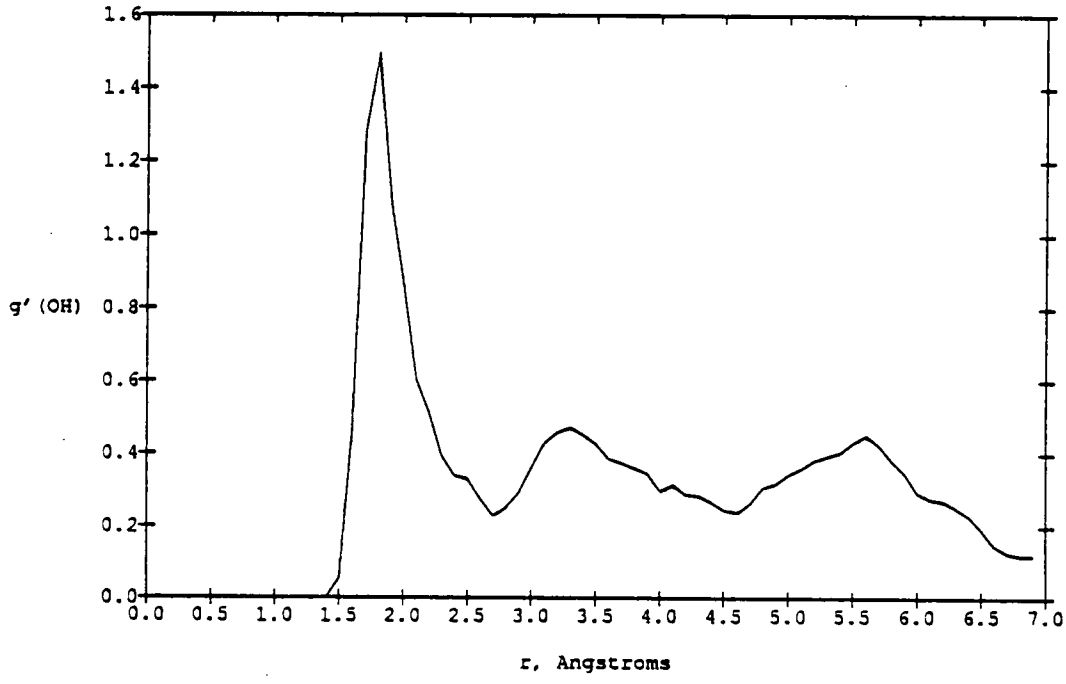

Figure 30. Pair correlation functions $g'(OH)_5$ and $g'(OH)_6$ of ethylene glycol in water.

Integrals of the first peak in the $g'(HO)_{3 \text{ and } 4}$ functions to 2.6 Å give 1.07 and 1.24, respectively, for the OH proton acceptor hydrogen bonds. Integrals of the first peak in the $g'(OH)_{5 \text{ and } 6}$ function to 2.4 Å give 0.94 and 1.05, respectively, for the OH proton donor hydrogen bonds.

Figure 31 is a plot of the water-EG pair interaction energy distribution functions, and Figure 32 is a plot of the EG-water binding energy distribution. The pair interaction function shows, as usual, most pair interactions near zero energy. However, there is also a strong positive interaction energy extending beyond 2.0 kcal/mol. The attractive interactions range from -2.5 kcal/mol to -9.0 kcal/mol and seem to be made up of two peaks, one at -6.5 kcal/mol and one at -5.0 kcal/mol. The integral of the pair interaction distribution from -10.0 kcal/mol to -2.5 kcal/mol gives 4.29 water molecules hydrogen-bonded to EG. The binding energy curve ranges from -20.0 kcal/mol to -38.0 kcal/mol and peaks at -26.0 kcal/mol.

In Figure 33, a configuration is shown near the completion of the simulation. It shows the **gauche** conformation of the EG molecule in dilute solution and the ring-forming tendencies of some of the solvent waters. The waters hydrogen bonded to the OH groups are clearly seen, with water molecules donating protons to the OH groups and accepting protons from the OH groups.

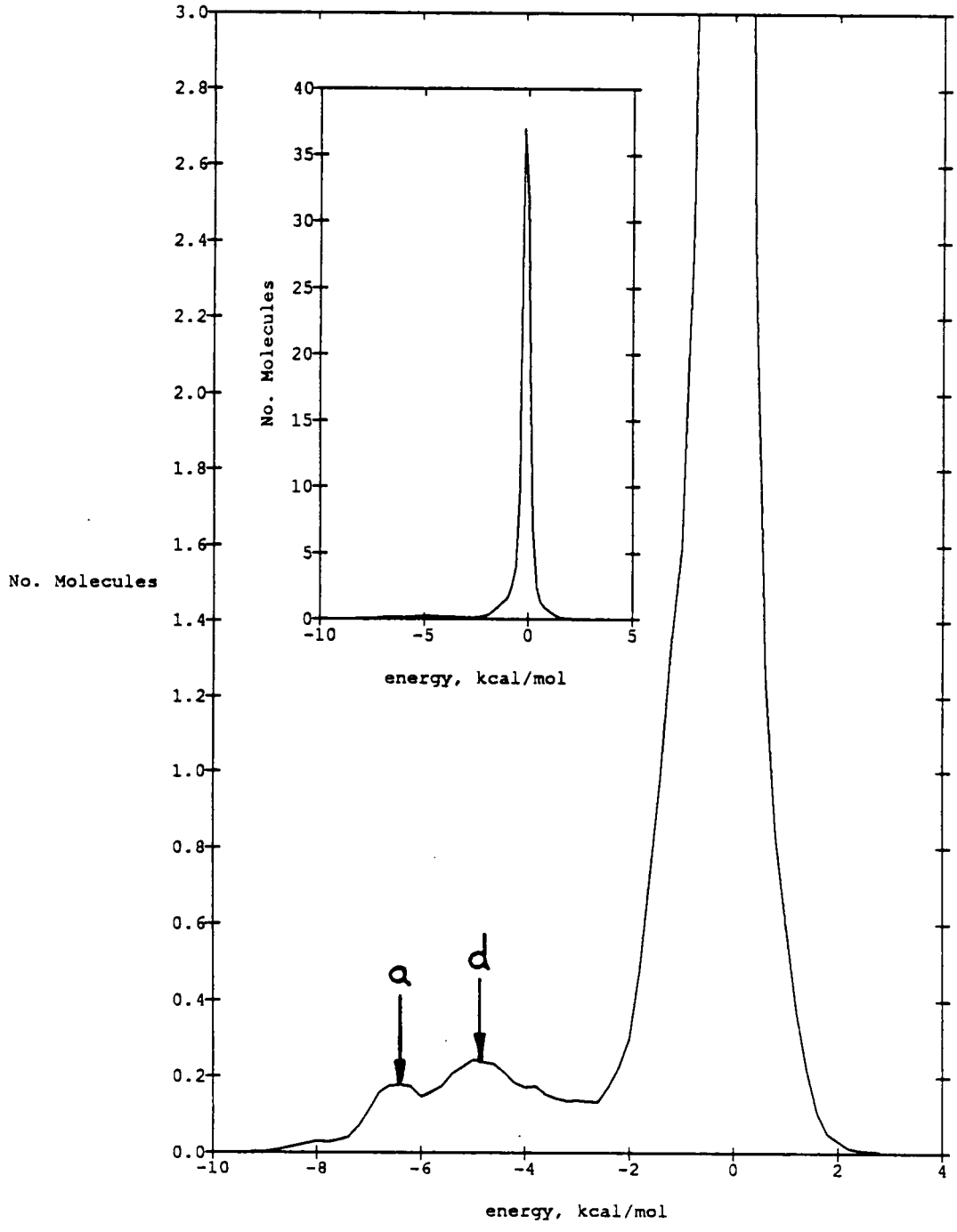

Figure 31. Water-ethylene glycol pair interaction energy distribution functions. The arrows denote structure, and could indicate the region of OH proton acceptor bonds (a) and the region of OH proton donor bonds (d).

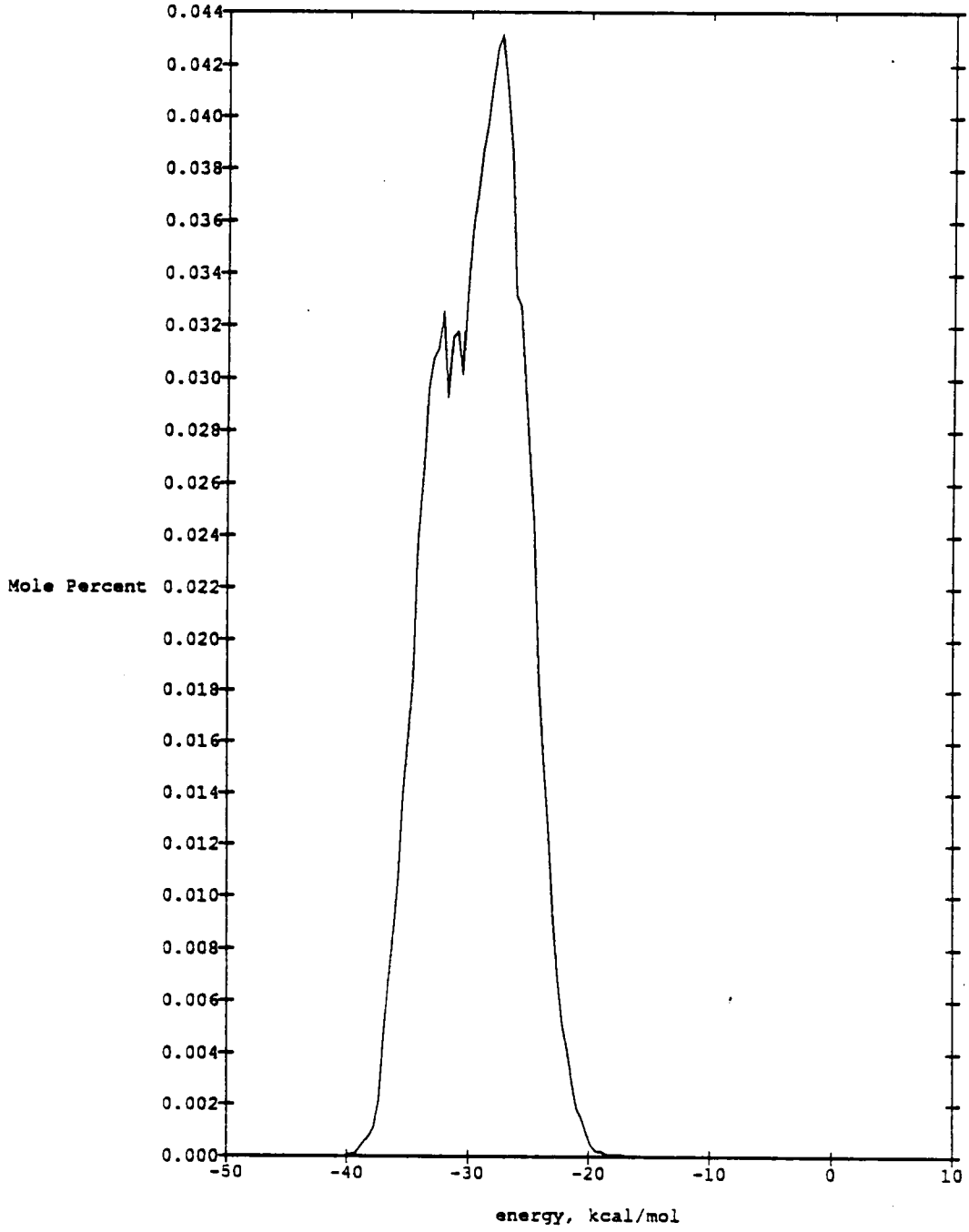

Figure 32. Ethylene glycol binding energy distribution function in water.

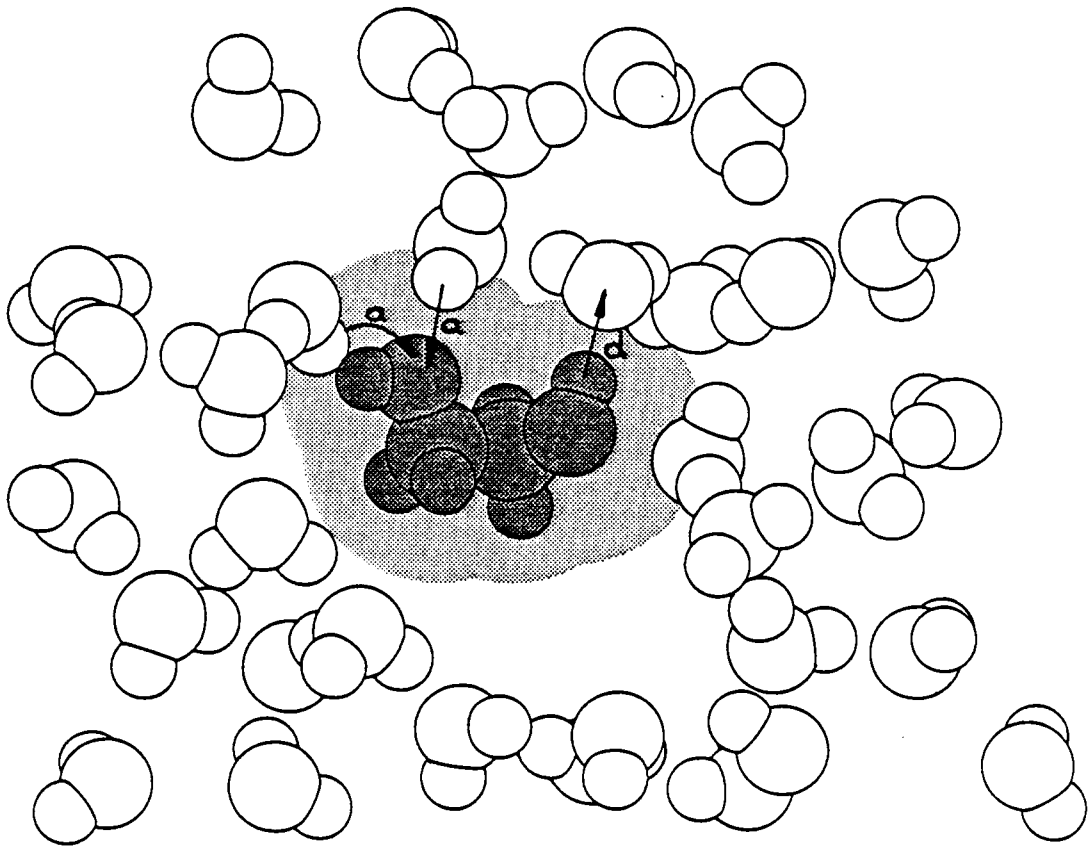

Figure 33. Saved configuration of the system showing the **gauche** conformation of ethylene glycol and the hydrogen bonding of the water to the OH groups. Arrows denoted by (a) show proton acceptor bonds and arrows denoted by (d) show proton donor bonds. A 4.0 Å slab of the simulation box is shown. The shaded surface is created by 2.5 Å circles centered on oxygen and carbon atoms.

Ethylene glycol in aqueous solution has been reported to be in the **gauche** or contracted conformation from experimental results.[16,21] In this work the molecule was started with the OH groups in both a trans and in a **gauche** conformation, and the final conformation always ended up **gauche**. The integral of the pair interaction energy distribution from -10.0 kcal/mol to -2.5 kcal/mol (4.29 hydrogen bonds) implies each of the two OH groups may act as a proton donor and a proton acceptor. The peak of the water-EG binding energy being at -28.0 kcal/mol is in keeping with the increased amount of hydrogen bonding.

6. <u>1,2 Propylene Glycol and 1,3 Propylene Glycol</u>

Propylene glycol (PG) $C_3H_6(OH)_2$ was the basis in this work for the study of several systems. First the 1,2-PG geometry places the two OH groups very close together so that OH intramolecular interactions and screening can be investigated. 1,3-PG has the OH groups at the terminal ends of the molecule so that they might be expected to be isolated enough from each other to hydrogen bond like ethanol. Since both 1,2-PG and 1,3-PG evolved to the **gauche** form in solution, a linear isomer of 1,3-PG was run. In the higher energy linear conformation of 1,3-propylene glycol, the C-C rotational potential barrier kept the molecule linear throughout the simulation. Figures 34 and 35 show the $g'(HO)_{4 \text{ and } 5}$ and $g'(OH)_{6 \text{ and } 7}$ for 1,2-Propylene glycol. The $g'(HO)_{4 \text{ and } 5}$ curves are similar in structure and demonstrate the close approach of a proton to each oxygen of the two OH groups. The $g'(OH)_{6 \text{ and } 7}$ functions indicate proton donor

activity to a solvent oxygen from each hydroxyl group because of the close approach (1.85 Å) of the solvent oxygen to the OH proton. Figure 36 shows the pair interaction energy distribution function and Figure 37 shows the 1,2-propylene glycol water binding energy distribution. The integral from -10.0 kcal/mol to -3.0 kcal/mol over the pair interaction energy function gives 3.75 solvent waters hydrogen bonded with 1,2-propylene glycol. The binding energy distribution function ranges from -20.0 kcal/mol to -40.0 kcal/mol, peaking at -33.0 kcal/mol.

Figure 38 is a stored configuration which shows the final **gauche** conformation of the 1,2-PG and indicates proton acceptance by the OH oxygens and proton donation by the hydrogen on the OH groups.

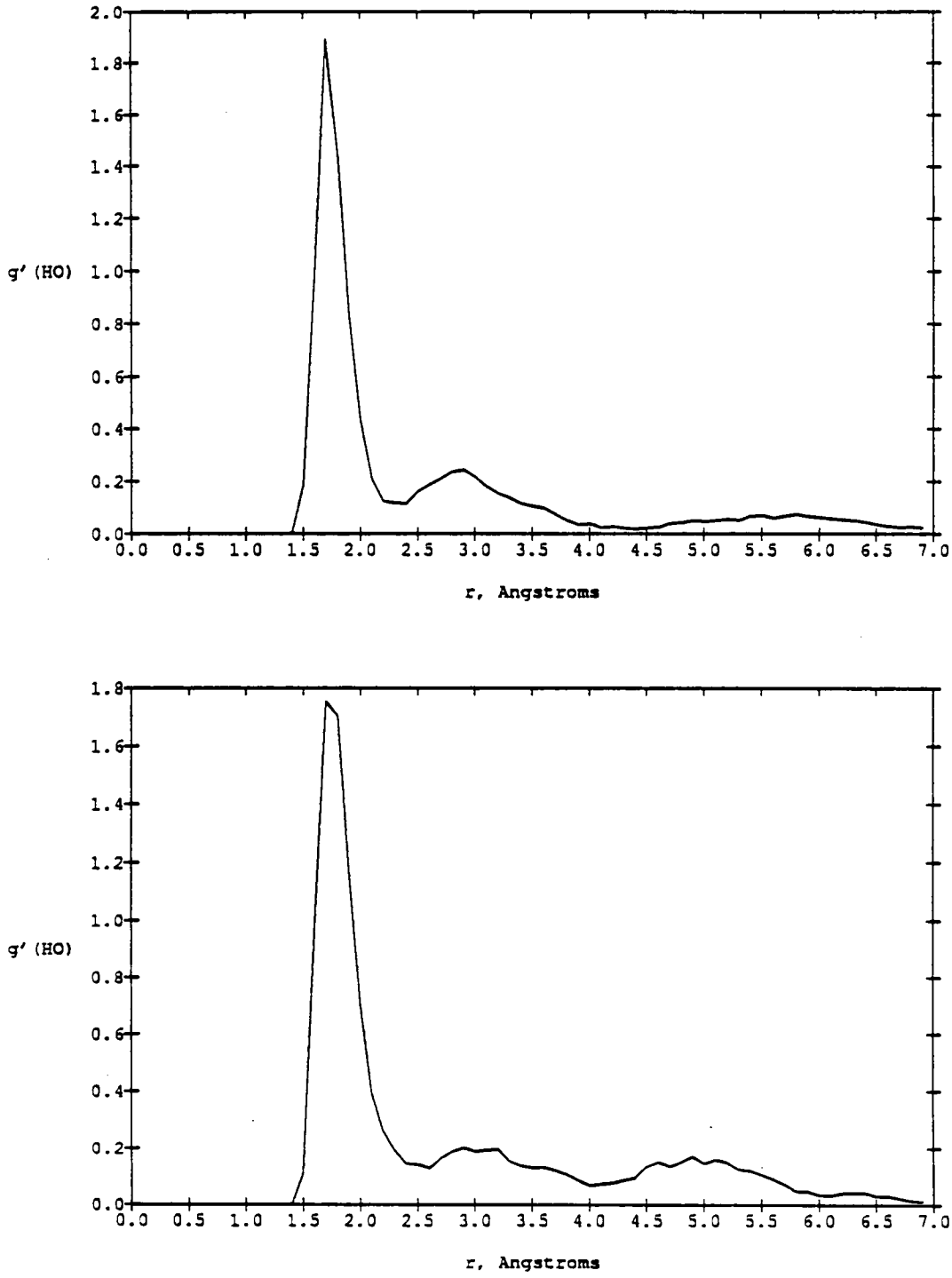

Figure 34. Pair correlation functions $g'(HO)_{4 \text{ and } 5}$ for 1,2-propylene glycol.

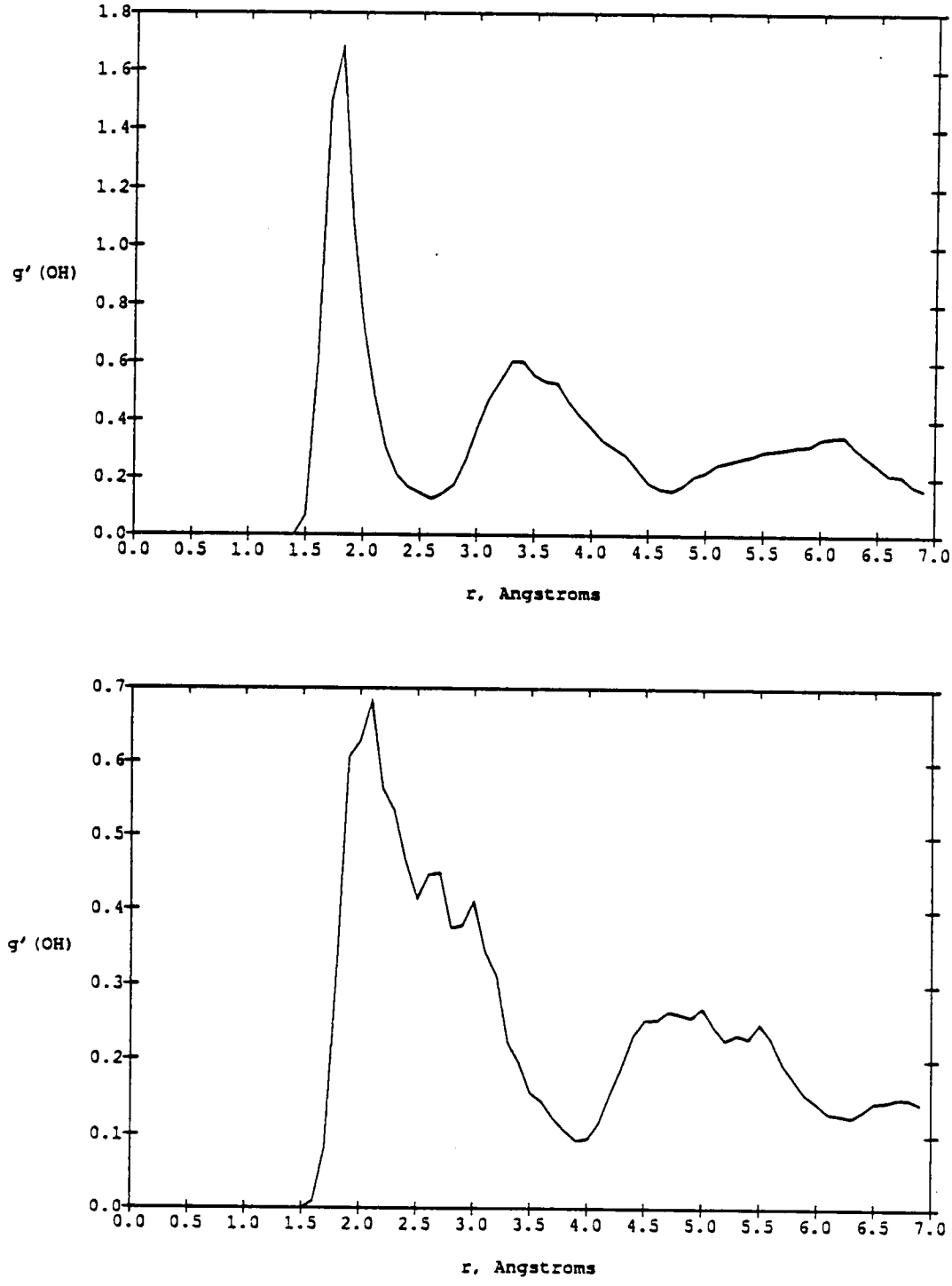

Figure 35. Pair correlation functions $g'(OH)_{6 \text{ and } 7}$ for 1,2-propylene glycol.

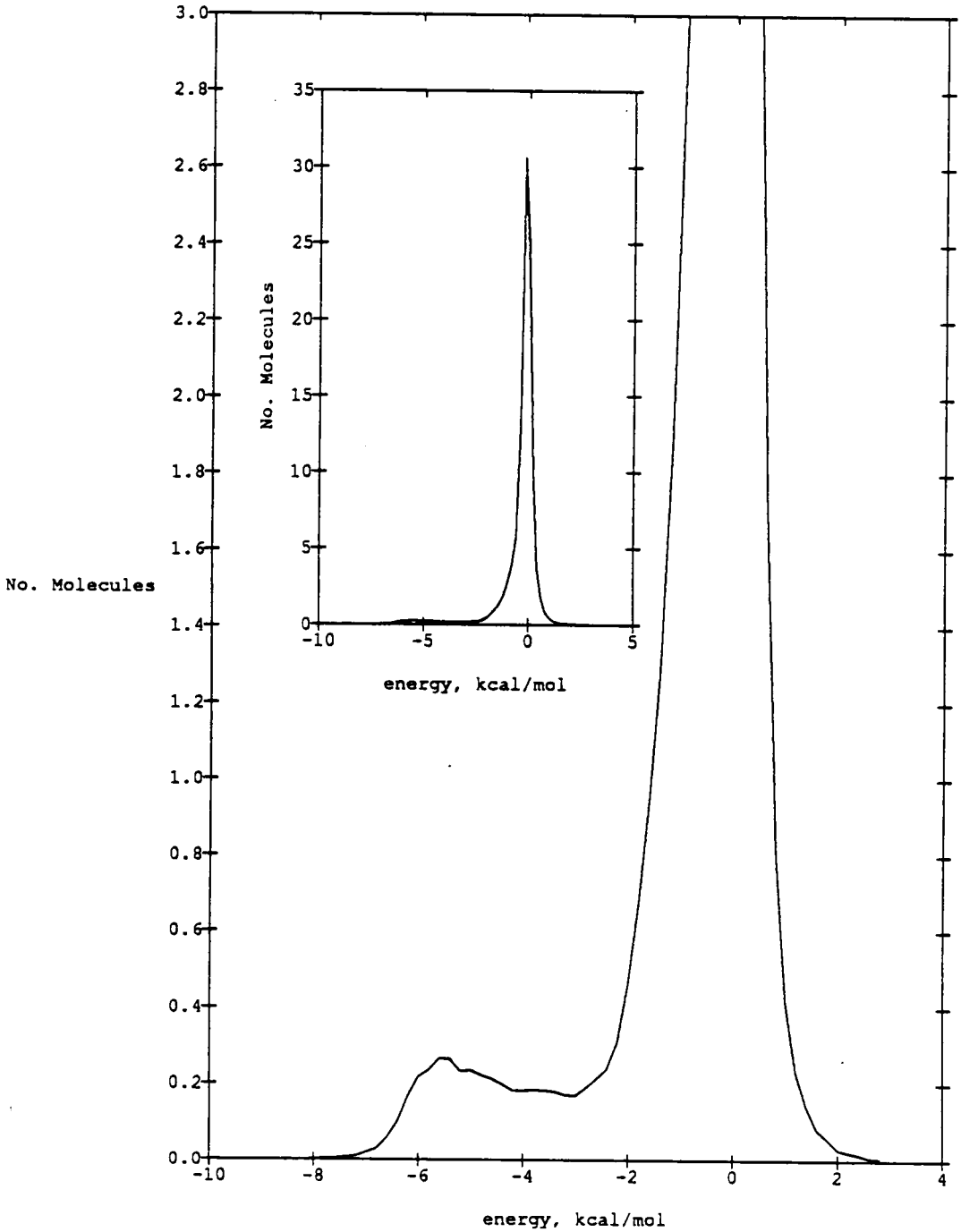

Figure 36. 1,2-Propylene glycol-water pair interaction energy distribution function.

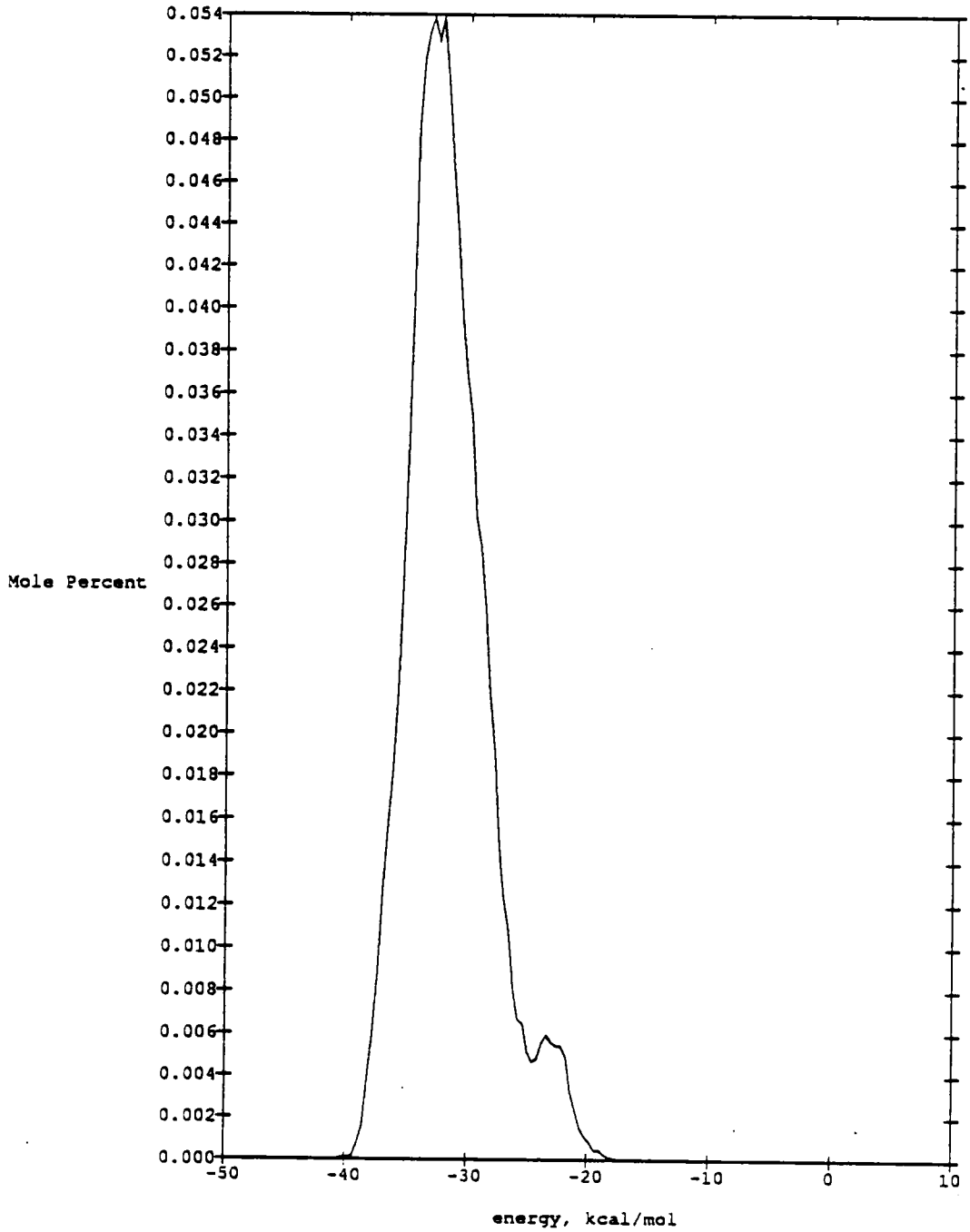

Figure 37. 1,2-Propylene glycol-water binding energy distribution.

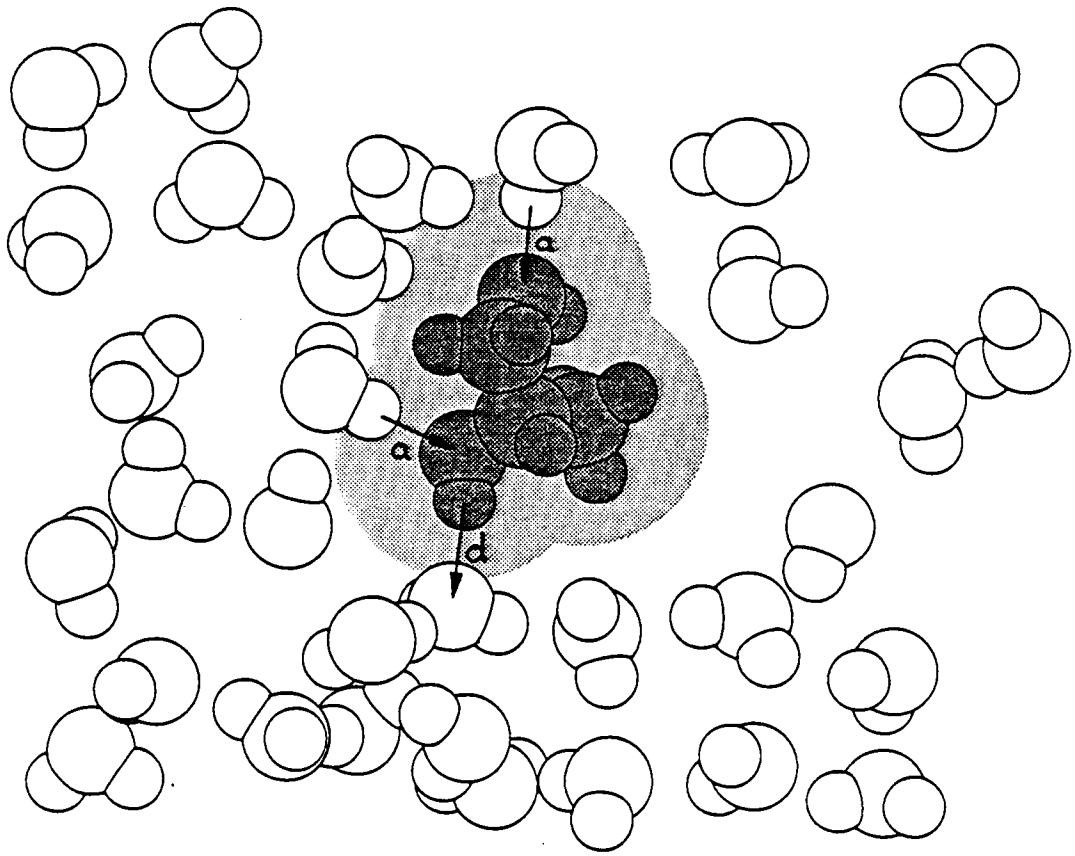

Figure 38. Saved configuration of 1,2-propylene glycol in water near the end of an NPT-Ensemble simulation. The arrows with a and d labels indicate OH acceptor (a) and donor (d) hydrogen bonds. A 4.0 Å slab of the simulation box is shown. The shaded surface is created by 2.5 Å circles centered on oxygen and carbon atoms.

In 1,3-PG with the OH groups on the terminal ends of the molecule, the lowest energy gas phase conformation is **gauche** with respect to the C-O bonds and with respect to the backbone C-C bonds, and both OH groups are on the same side of the molecule. The molecule maintained this conformation during the simulation. A higher energy linear geometry was also used in a simulation test.

Figure 39 gives the plots of $g'(HO)_{4 \text{ and } 5}$ for 1,3 PG. Figure 40 shows $g'(OH)_{6 \text{ and } 7}$ for the 1,3-PG. Figure 41 gives the 1,3-PG-water pair interaction energy distribution and Figure 42 the 1,3-PG-water binding energy distribution. The attractive part of the pair interaction integrals from -10.0 kcal/mol to -3.4 kcal/mol gives 3.86 water molecules hydrogen bonded or interacting with 1,3 PG in this energy range.

The binding energy distribution ranges from -32.0 kcal/mol to -53.0 kcal/mol, peaking at -44.0 kcal/mol. The higher binding energy and extended attractive pair distribution function indicates that the water-hydrogen bonding to 1,3-PG is stronger than to 1,2-PG. This is probably due to less screening of the OH groups in 1,3-PG as compared to the spatial crowding of the OH groups in the 1,2-PG conformation. Also, 1,3-PG has a higher boiling point (214°C) than 1,2-PG (189°C) in the pure liquid form, indicating strong hydrogen bonding in the pure 1,3-PG liquid. Figure 43 shows a configuration near the end of the simulation. Note the conformation of the 1,3-PG and what appears to be an OH oxygen acting as a proton acceptor to hydrogen bond water, and an OH hydrogen being donated to water oxygen.

The linear conformational isomer of 1,3-PG is very similar to the **gauche** 1,3-PG in terms of the pair correlation functions. However, although the curves are not shown, the pair interaction energy distribution function is more attractive, and the integral from -10.0 kcal/mol to -3.4 kcal/mol gives 4.76 water molecules bonded in this energy range. Also, the linear 1,3-PG-water binding energy distribution curve indicates stronger binding, giving a range of -35.0 kcal/mol to -57.0 kcal/mol and peaking at -49.0 kcal/mol. Figure 44 shows a saved configuration of linear 1,3-PG, which shows the elongated nature of the molecule and water bonded to each OH group.

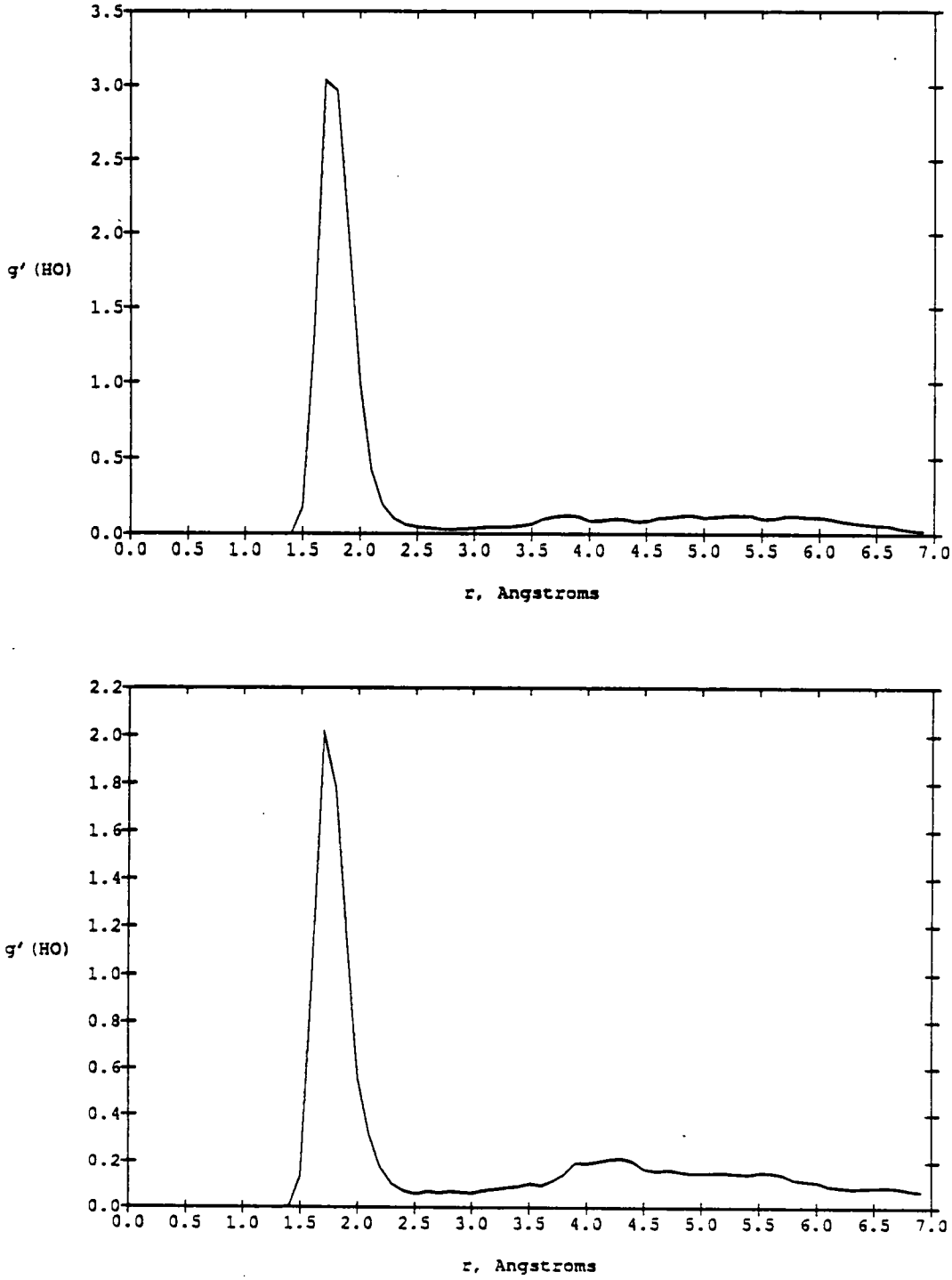

Figure 39. Pair correlation functions $g'(HO)_4$ and $g'(HO)_5$ for 1,3-propylene glycol.

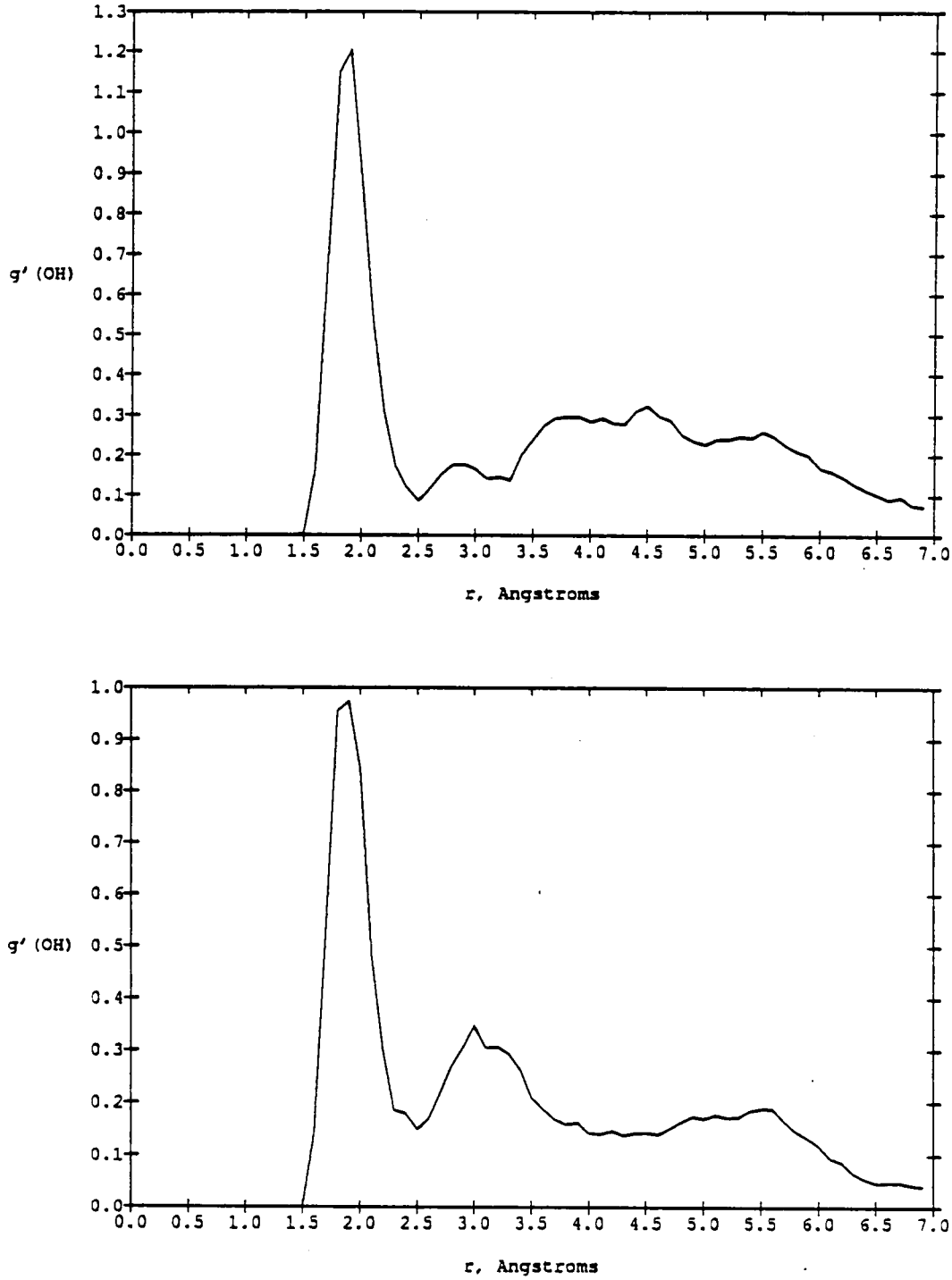

Figure 40. Pair correlation functions $g'(OH)_6$ and $g'(OH)_7$ for 1,3-propylene glycol.

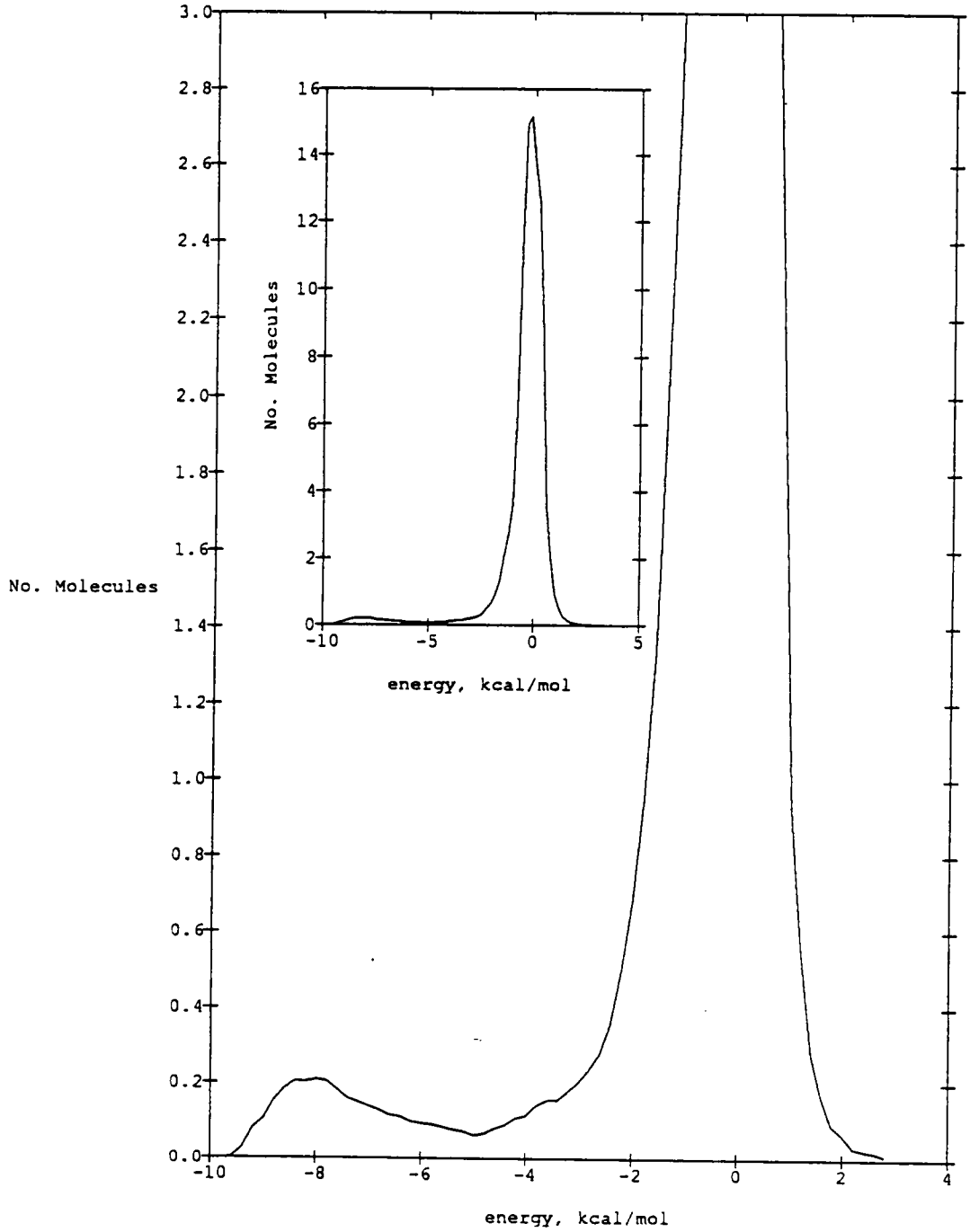

Figure 41. 1,3-Propylene glycol-water pair interaction energy distribution function.

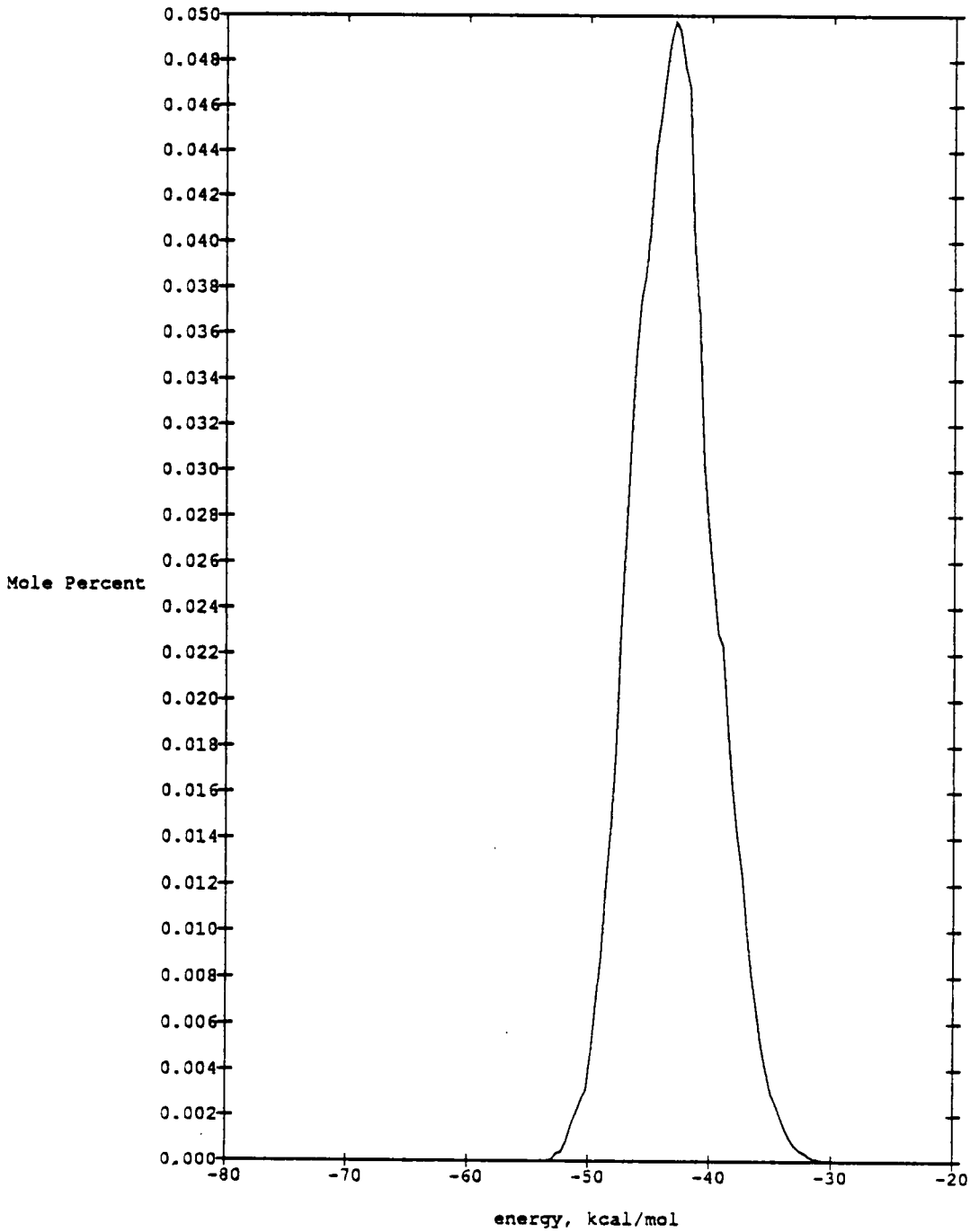

Figure 42. 1,3-Propylene glycol-water binding energy distribution curve.

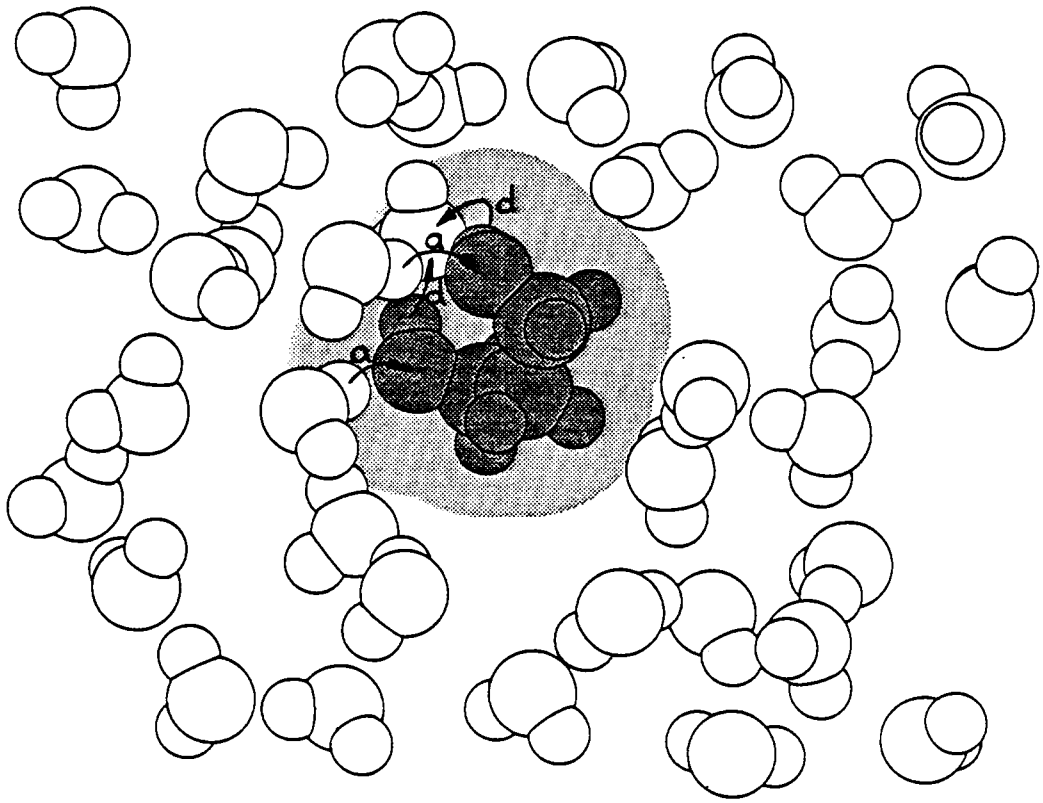

Figure 43. Saved configuration of 1,3-propylene glycol in water near the completion of an NPT-Ensemble Monte Carlo simulation. The arrows labeled (a) and (d) indicate OH proton acceptor bonds (a) and OH proton donor bonds (d), respectively. a 4.0 Å slab of the simulation box is shown. The shaded surface is created by 2.5 Å circles centered on oxygen and carbon atoms.

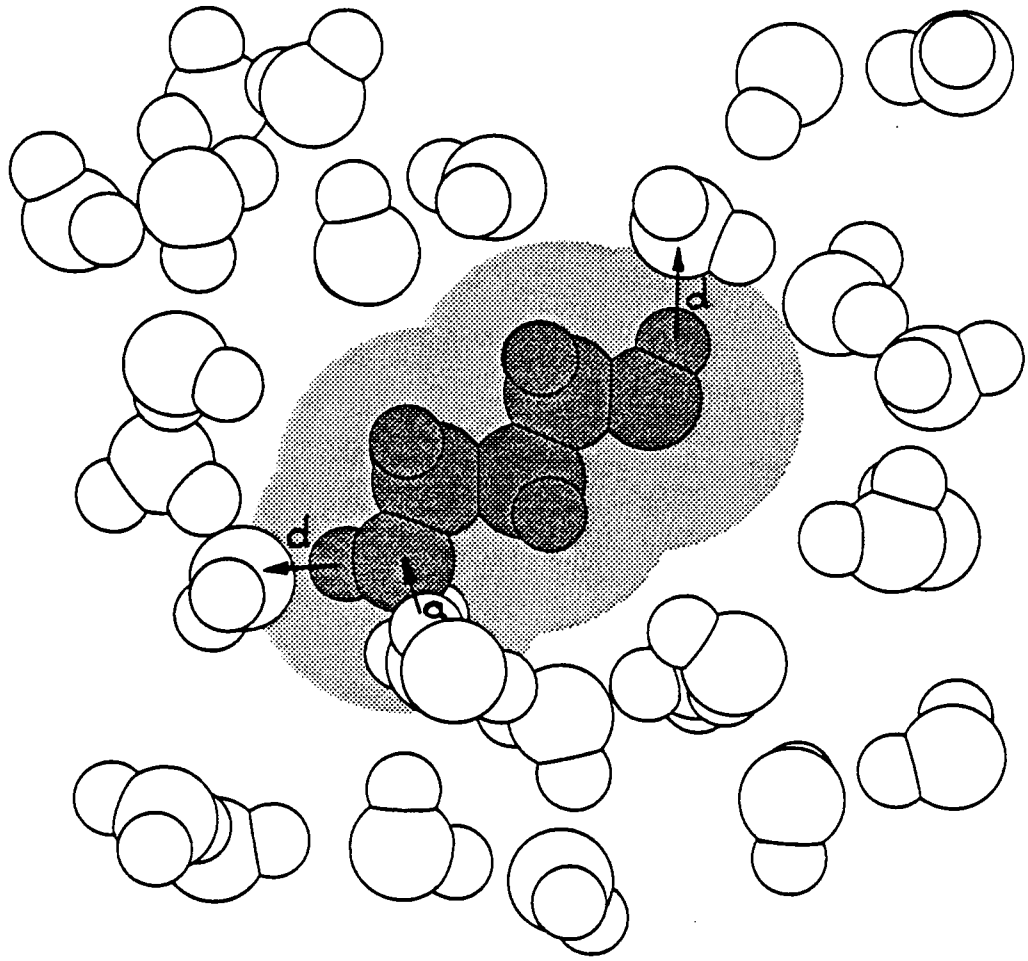

Figure 44. Saved configuration of linear 1,3-propylene glycol in water at the end of a simulation run. The arrows labeled (a) and (d) indicate OH proton acceptor bonds (a) and OH proton donor bonds (d), respectively. A 4.0 Å slab is shown. The shaded surface is created by 2.5 Å circles centered on oxygen and carbon atoms.

In analyzing propylene glycol (PG), both the 1,2 form with adjacent OH groups and the 1,3 form with terminal OH groups were investigated. This was done to assess the effect of separating the OH groups on the hydrogen bonding. In addition, in the 1,3-PG case the system was simulated with the final conformation of the 1,3-PG in the contracted or **gauche** form and in the elongated or linear conformation. This was done to assess whether the terminal OH's begin to approach ethanol behavior as they become more isolated. Generally, as before, the conformation in solution was contracted or **gauche** at the end of all simulations except for the linear isomer 1,3-PG case, in which case the system stayed in the starting geometry. The pair interaction energy distribution integrals from -10.0 kcal/mol to -3.0 kcal/mol show more hydrogen bonding as the OH group separation increases from 1,2-PG to 1,3-PG (**gauche**) to 1,3-PG (linear), viz. 3.75, 3.86 and 4.76, respectively.

The pair correlation functions give more details about the hydrogen bonding. The $g'(HO)_{4 \text{ and } 5}$ (Figure 34) show OH oxygens in 1,2-PG acting as proton acceptors with the pair correlation function for the two OH groups also equal in amplitude.

The integrals of the first peaks in $g'(HO)_{4 \text{ and } 5}$ give the extent of the hydrogen bonding in 1,2-PG where the OH oxygen is the proton acceptor, which integrals are 0.79 and 1.04 respectively. In addition, $g'(OH)_{6 \text{ and } 7}$ (Figure 35) show the OH donor bonding of 1,2-PG with the solvent oxygen . The extent of this hydrogen bonding is given by the integrals over the first peaks of $g'(OH)_{6 \text{ and } 7}$ with the

values 1.02 and 0.79, respectively. The water-1,2-PG binding energy is -34.0 kcal/mol and the pair interaction energy distribution shows a peak hydrogen bonding region at -5.5 kcal/mol.

In the 1,3-PG with the final **gauche** conformation, $g'(HO)_{4 \text{ and } 5}$ (Figure 39) shows oxygen proton acceptor bonding in the OH groups with an asymmetry in amplitude. The integrals over the first peaks in $g'(HO)_{4 \text{ and } 5}$ give the extent of this bonding and have values of 1.54 and 1.00. In addition, $g'(OH)_{6 \text{ and } 7}$ (Figure 40) show oxygens at less than 2 $\mathring{A}$ from the OH hydrogens. This proton donor bonding from the 1,3-PG OH groups can be assessed by integrals over the first peaks of $g'(OH)_{6 \text{ and } 7}$. The values for these integrals are 0.82 and 0.75, respectively. The **gauche** 1,3-PG water binding energy peaks at -43.0 kcal/mol while the pair interaction energy distribution is again a bimodal distribution with peaks near -4.0 kcal/mol and -8.0 kcal/mol.

In the simulation carried out on the linear isomer of 1,3-PG, the molecular geometry stayed in the starting conformation. $g'(HO)_{4 \text{ and } 5}$ shows OH group proton acceptor bonding. The integrals of $g'(HO)_{4 \text{ and } 5}$ give the extent of this bonding as 1.64 and 1.11, respectively. In addition, $g'(OH)_{6 \text{ and } 7}$ indicate symmetric OH group donor bonding in which the integrals of the first peaks of $g'(OH)_{6 \text{ and } 7}$ give the values of 0.93 and 0.97, respectively. The peak binding energy in this geometry is -48.0 kcal/mol.

7. **Glycerol**

Glycerol ($C_3H_5(OH)_3$) has three hydroxyl groups and a large number of conformational isomers. Because of the many rotational degrees of freedom, glycerol is the most complex of the solutes studied in aqueous solution. As was mentioned earlier, the solution chemistry of aqueous glycerol solutions is complex and very nonideal. Glycerol-water solutions contract at low concentrations and the molecule in the pure liquid is thought to be in an elongated conformation.[7,8] In the calculations presented here, the lowest energy intramolecular bonded conformation (which is an elongated [linear] conformation) is used as a starting geometry. The ending geometry is shown in Table XIII in which the glycerol molecule is in a contracted geometry created by the terminal OH groups moving to a **gauche** conformation by C-C bond rotations with respect to the central carbon and with all those O-H groups on the same side of the molecule. Figures 45 and 46 give the calculated values of the primary (nearest neighbor) pair correlation functions $g'(HO)_{4,5,6}$ and $g'(OH)_{7,8,9}$ describing the solute OH groups' interaction with the solvent. $g'(HO)_{4,5,6}$ in Figure 45 indicate a solvent proton in close association with each of the OH oxygens. In Figure 46, $g'(OH)_{7,8,9}$ show the very symmetric three peaks of the solvent oxygens near the OH hydrogens.

Figure 47 shows the water-glycerol pair interaction energy distribution and Figure 48 the binding energy distribution function. The attractive region of the pair interaction function, Figure 47,

shows hydrogen bonding from the shoulder at -2.0 kcal/mol of the zero energy peak to the long tail of a peak at -6.0 kcal/mol extending to beyond -10.0 kcal/mol. The integral from -10.0 kcal/mol to -2.5 kcal/mol gives a value of 6.45 hydrogen bonds per glycerol molecule. However, the integral from -10.0 kcal/mol to the local minimum at -4.4 kcal/mol gives 3.47 hydrogen bonds. In Figure 48 the water-glycerol binding energy distribution is also very broad, ranging from -35.0 kcal/mol to -67.0 kcal/mol with a peak at -52.0 kcal/mol. Both of these curves indicate the strong hydrogen bonding ability of glycerol in water solution. Figure 49 shows a saved configuration of the glycerol-water simulation. Note the contracted conformation of the molecule and the close association of water molecules with the OH groups of glycerol. If one visually scrolls through the saved configurations, the C-C rotations that bring the OH groups to the **gauche** conformation can be observed along with the water reorganization because of the hydrophobic and hydrophylic division of the molecule, with the three OH groups on the hydrophylic side.

Table XIII. Z-Matrix of the ending conformation of glycerol in dilute aqueous solution.

Glycerol

Atom	Atom Number	Bond Length Å	Bond Angle (°)	Dihedral Angle(°)	Connectivity
C	1	0.00	0.00	0.00	000
C	2	1.58	0.00	0.00	100
C	3	1.57	110.78	0.00	210
O	4	1.39	113.32	100.05	123
O	5	1.40	108.08	-123.27	213
O	6	1.40	109.51	-3.08	325
H	7	0.95	112.43	-115.36	412
H	8	0.95	112.06	76.79	523
H	9	0.95	111.18	-141.72	632
H	10	1.12	111.47	124.93	142
H	11	1.12	106.42	-118.93	142
H	12	1.13	107.34	-117.22	231
H	13	1.12	110.68	122.76	326
H	14	1.12	108.86	-120.99	326

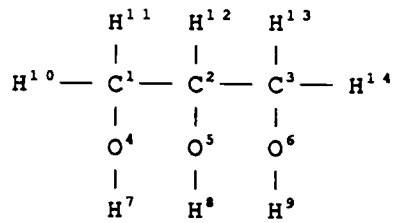

Glycerol

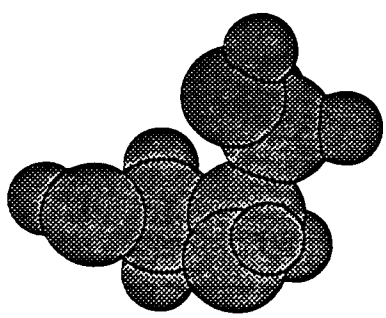

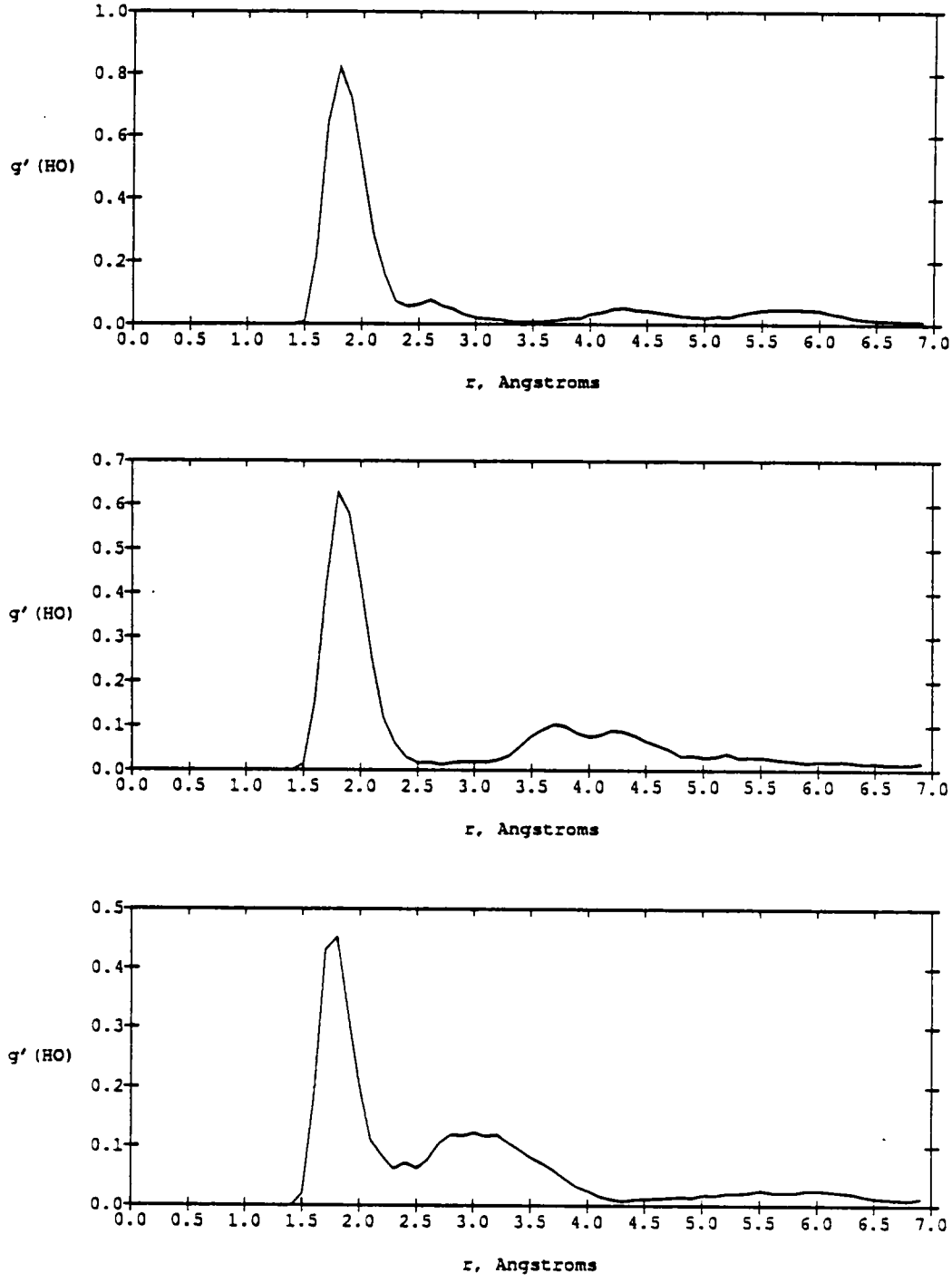

Figure 45. Pair correlation functions $g'(HO)_4$, $g'(HO)_5$ and $g'(HO)_6$ for glycerol-water.

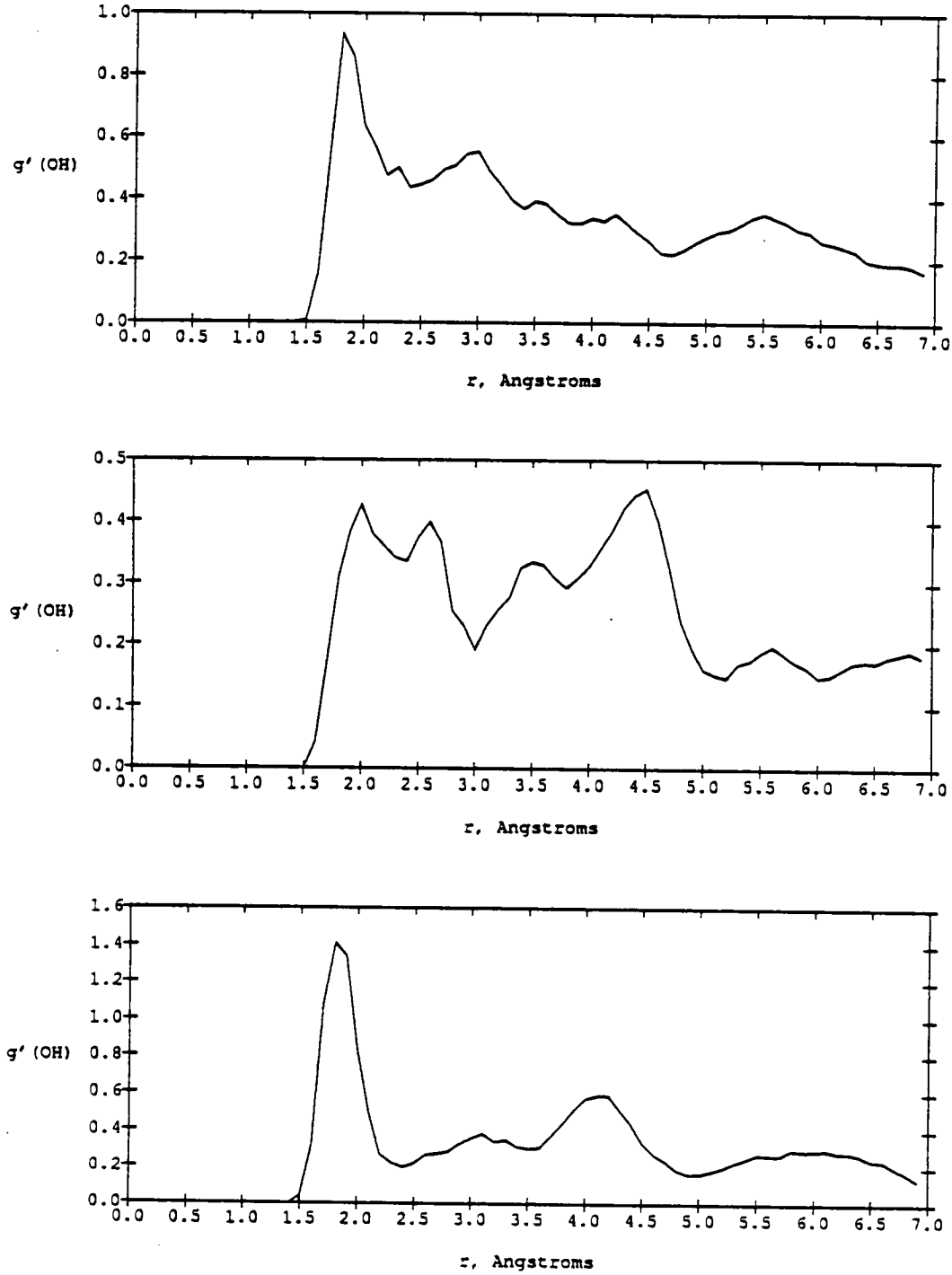

Figure 46. Pair correlation functions $g'(OH)_7$, $g'(OH)_8$ and $g'(OH)_9$ for glycerol-water.

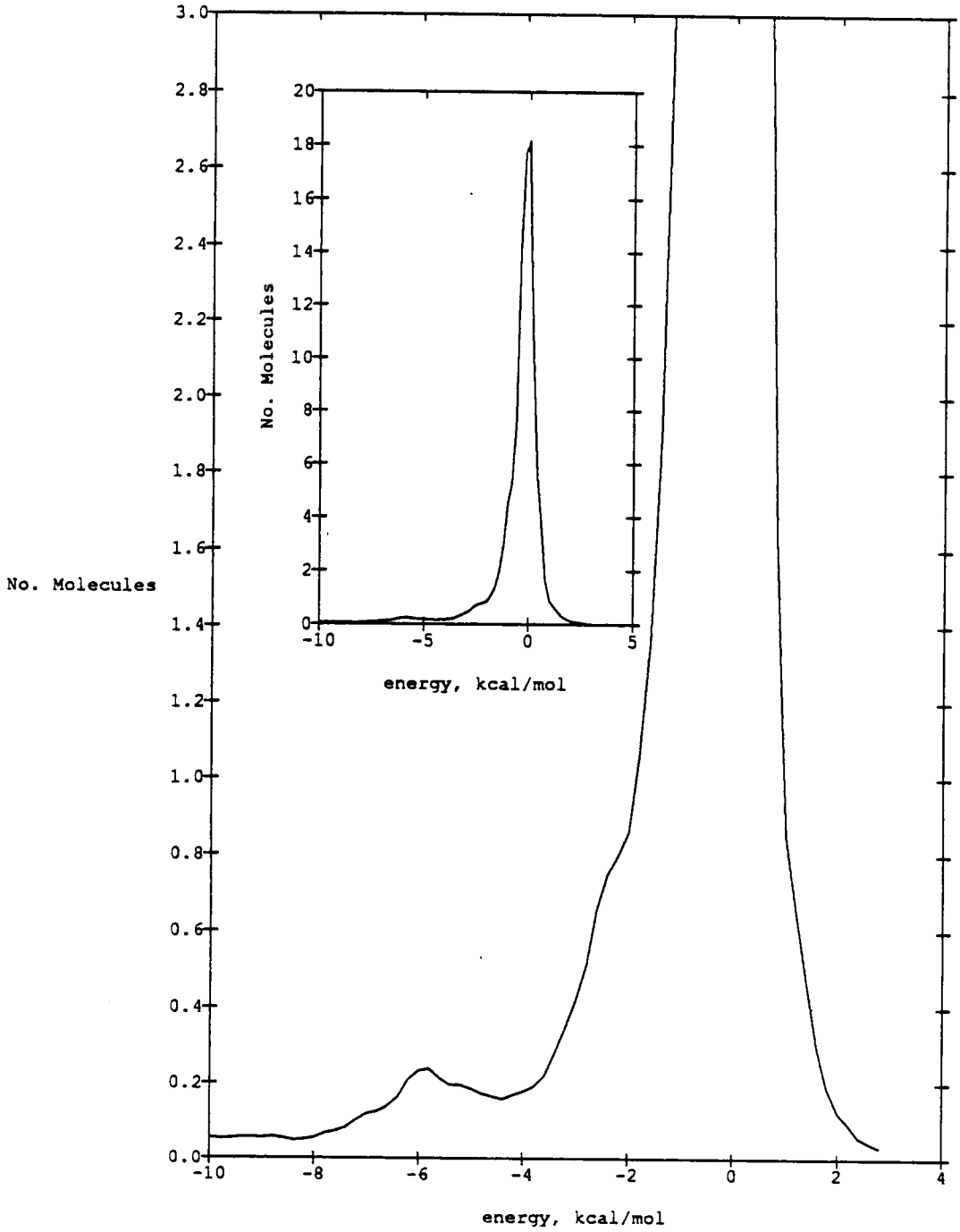

Figure 47. Glycerol-water pair interaction energy distribution function.

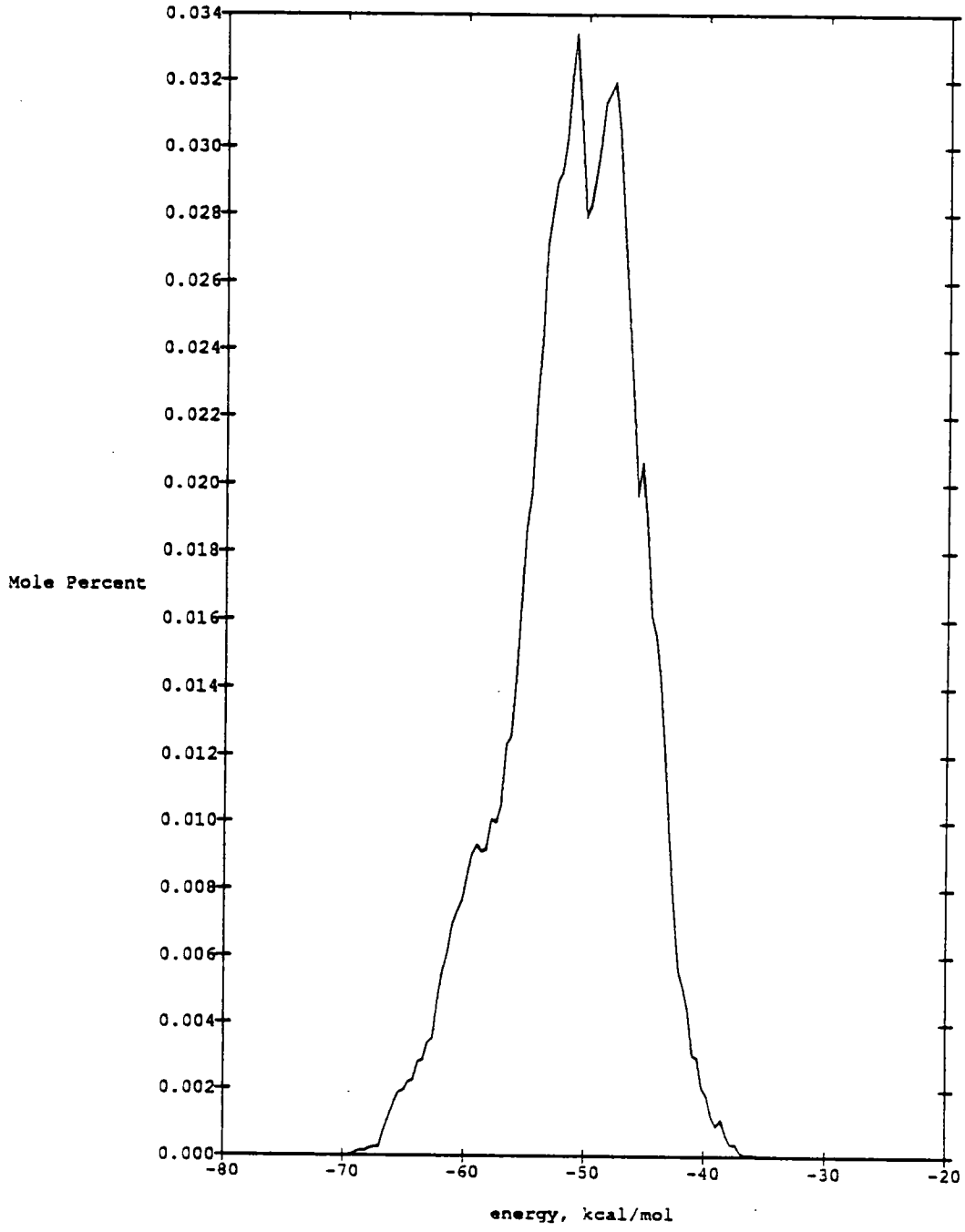

Figure 48. Glycerol-water binding energy distribution.

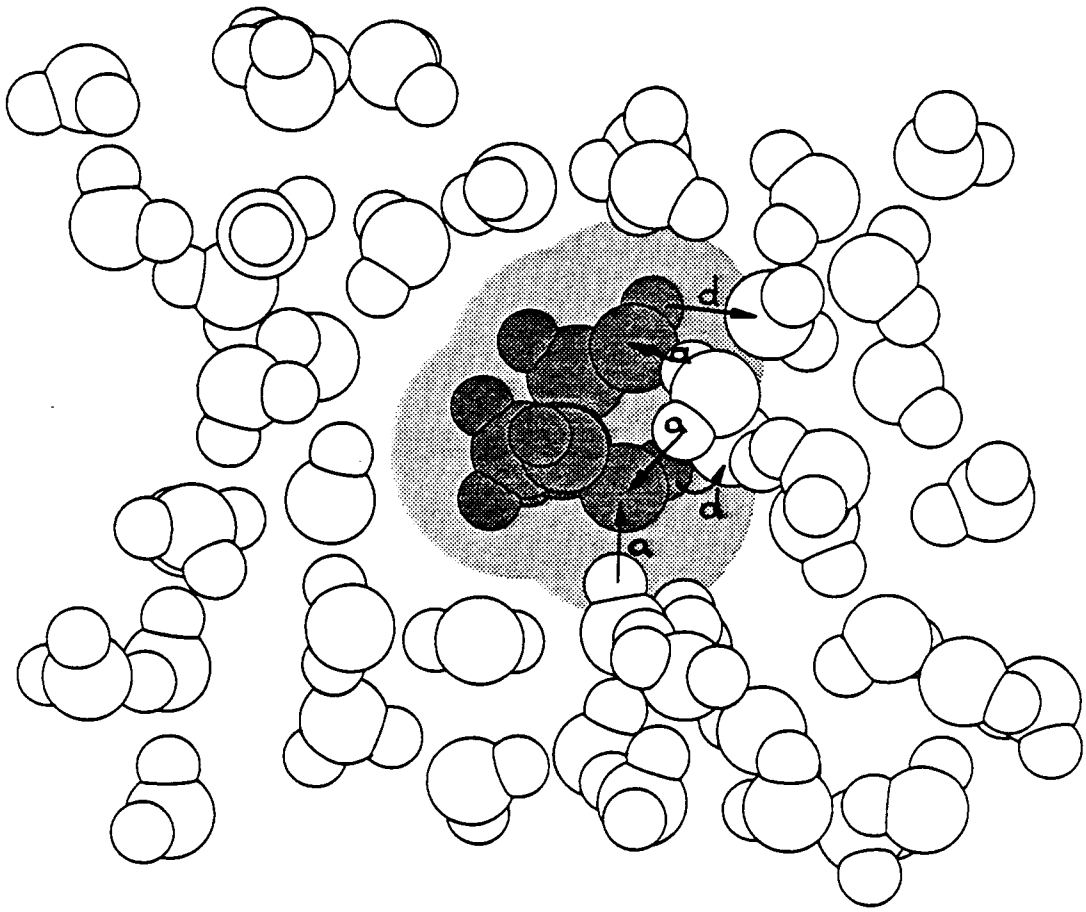

Figure 49. Saved configuration of the glycerol-water system. The arrows labeled (a) and (d) point out OH proton acceptor bonds (a) and OH proton donor bonds (d), respectively. A 4.0 Å slab is shown of the simulation box. The shaded area is created by 2.5 Å circles centered on oxygen atoms and carbon atoms.

The simulation results show that the complex glycerol molecule ended up with the gas phase elongated geometry rotating in the liquid to a contracted **gauche** geometry. In this case, the conformation change not only requires rotations around low potential barrier C-O bonds but also the 60^0 torsional rotation of the terminal C-C bonds. MNDO[65] calculations of the energy difference between the starting conformation and the final one gave 9.7 kcal/mol, with the ending geometry in the higher energy state. All of the solutes investigated here tended to seek a contracted geometry with the OH groups on one side of the molecule, probably driven by the fact that the polyhydric alcohols have both hydrophobic and hydrophilic regions close together. The hydrophobic interaction would tend to force the hydrocarbon (CH_2) part of the molecule spherical. Coupled with the attractive water-OH interaction in a "floppy" molecule, the tendency is to drive the OH groups to one side of the molecule in a **gauche** conformation, or in a more contracted geometry.

An analysis of $g'(HO)_{4,5, \text{ and } 6}$ (Figure 45) indicates OH proton acceptor bonding with an asymmetry among OH groups. The integrals over the first $g'(HO)_{4,5 \text{ and } 6}$ peaks give the values of 0.50, 0.40 and 0.27, respectively, for the number of OH-proton acceptor bonds. $g'(OH)_{7,8 \text{ and } 9}$ (Figure 46) exhibit the OH-proton donor bonding to solvent oxygen which appears to be most prominent at the glycerol terminal OH groups. The integrals over the first peaks of $g'(OH)_{7,8 \text{ and } 9}$ give values of 0.61, 0.47, and 0.90 hydrogen OH donor bonds, respectively. The total OH group hydrogen bonding

numbers are 1.11, 0.87 and 1.17 for the three hydroxyl groups, or a total of 3.14. The integral from -10.0 kcal/mol to the minimum at -4.0 kcal/mol on the pair interaction distribution curve (Figure 47) gives 3.47. However, if the integral is carried to -2.5 kcal/mol to include the low energy shoulder, the value is 6.45. This is due to closely associated water molecules which show up in Figure 49. These molecules are more weakly bonded to glycerol, with binding energies in the range -2.5 kcal/mol to -4.0 kcal/mol.

8. **General Discussion**

Table XIV lists the average solute-water binding energy for all of the solutes for which simulations were carried out in this work. Shown in the same table is the moisture content of several of the solutes obtained from experimental sorption isotherm data of Sloan and Labuza[74] at 23°C and 20.0 percent relative humidity RH. The water content closely parallels the calculated binding energy, as would be expected. In Table XV the partial molar heats of solution are derived from the calculations by assuming liquid-liquid mixing and the results for total potential energy and solution volume (Table VII). The experimental partial molar heats of solution are derived from the tangent of the heat of solution curve[76] at the molar concentrations used for each solute. For all solutes except glycerol the Redlich and Kister[77] fit to the heat of solution data was used. The function representing the data was differentiated, evaluated at 0.0093 mol fraction and extrapolated to the pure solute in order to calculate the partial molar heat of solution. For glycerol, the value was obtained

from the derivative of a parabolic fit to the glycerol data.[3] Graphical results, by drawing the tangent to the experimental heat of solution versus concentration, give equivalent values in all cases. For ethanol, Alagona and Tani[45] obtained values of -57.0 kcal/mol to -80.0 kcal/mol, much more negative than the experimental value (-2.4 kcal/mol). They argue that the water organization near the hydrophobic part of the ethanol molecule causes the discrepancy. The -7.7 kcal/mol obtained here is more reasonable but still too negative. Also, the partial molar heats of solution obtained for ethylene glycol, 1,2-propylene glycol and 1,3-propylene glycol are more negative than the experimental values. The value calculated for glycerol (-19.4 kcal/mol) is also more negative than the value derived from the experimental heat of solution (-5.1 kcal/mol).

Table XVI gives the total potential energy calculated in each simulation along with the standard deviation associated with the average value. Table XVII shows the average calculated solution density and standard deviation along with experimental densities for the molar concentration that was simulated. Table XVIII gives the pair interaction energy distribution integrals over the hydrogen bonding energy range for both water-water interactions and for water-solute interactions. Figure 50 is an example of the water-water pair interaction energy distribution for pure water. Note that the alcohols all reduce the water-hydrogen bonding, so they are water-hydrogen bond breakers at this concentration. The water-solute numbers are the total hydrogen bonds to the solute in the energy range

for hydrogen bonding. Table XIX derives the hydrogen bonding in a different way. In this table the pair correlation functions g'(HO) and g'(OH) are used to separate the hydrogen bonding to the alcohol's hydroxyl groups into the proton acceptor and proton donor bonds. This is done by integrating the first peak of the primary pair correlation function (g'(HO) for acceptor and g'(OH) for donor) to the function minimum at r(min). Note that in general the hydrogen bonding to the alcohol's OH groups tends to be more acceptor than donor-like, as would be expected from the stronger interaction[45] for oxygen acceptor bonds. Glycerol is an exception because the oxygens are inaccessible to the waters in the contracted geometry that the molecule has in dilute solution. Glycerol has few linear hydrogen bonds in that geometry, but has a number of water molecules weakly interacting with it as shown in Table XIII.

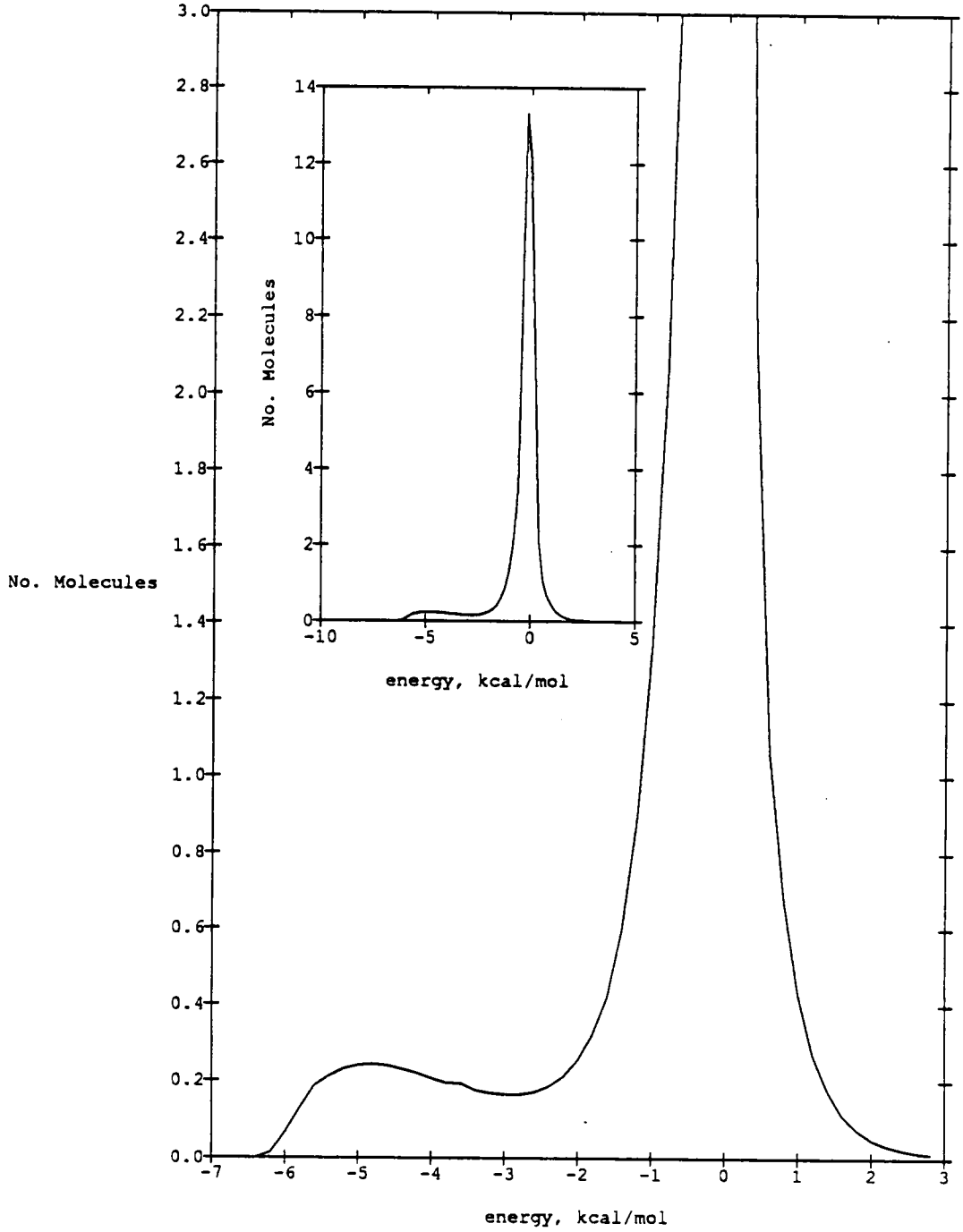

Figure 50. Water-water pair interaction energy distribution for pure water.

Table XIV. Peak of water-solute binding energy distribution from NPT-Ensemble Monte Carlo simulation. The second column gives the water content in weight percent of the solutes at 23°C and at relative humidity of 20.0 percent.

Solute	1.0 Atmos., 25°C Binding Energy (kcal/mol)	1.0 Atmos., 23°C Moisture Content[74] (gH_2O/100g Solids)
Propane	- 7.0	--
Water	-20.0	--
Ethanol	-20.0	--
Ethylene Glycol	-28.0	4.0
1,2-Propylene Glycol	-33.0	6.0
1,3-Propylene Glycol (**gauche**)	-43.0	8.0
1,3-Propylene Glycol (linear)	-48.0	--
Glycerol	-52.0	10.0

Table XV. Calculated Partial Molar Heat of Solution.

Table XV. Calculated Partial eats of Solution.

	V_{Sol} ($\AA^3$)	ΔV_{Sol} (kcal/mol)	ΔE_{Sol} (kcal/mol)	ΔH_{Sol} (kcal/mol)	ΔH_{Sol} (Exp) (kcal/mol)
Propane	226.8	0.003	10.8	10.8	--
Propane (27 bar, 4°C)	189.0	0.075	-25.9	-25.8	--
Ethanol	152.0	0.002	- 7.6	- 7.6	-2.4[76,78]
Ethylene Glycol	293.0	0.004	-14.0	-14.0	-1.5[76,79]
1,2-Propylene Glycol	185.4	0.003	- 5.4	- 5.4	-2.3[76,79]
1,3-Propylene Glycol	215.7	0.003	-16.2	-16.2	-1.9[76,79]
1,3-Propylene Glycol (linear)	225.9	0.003	-17.3	-17.3	--
Glycerol	219.0	0.003	-19.4	-19.4	-5.1[3]

For solution mixing $\Delta H_{Sol} = \Delta E_{Sol} + P\ \Delta V_{Sol}$ [27,75]

AE_{Sol} (Table VII) Energy of solution minus energy of pure water times 108.0

ΔV_{Sol} (Table VII) Volume of solution minus volume of pure water.

The experimental ΔH_{Sol} are partial molar heats of solution.[75]

Table XVI. Simulation results for solution total energy (kcal/mol).

Compound	Total Energy (kcal/mol)	
Water	-10.07	(.003)
Propane	- 9.97	(.007)
Propane (27 bar)	-10.31	(.007)
Ethanol	-10.14	(.006)
Ethylene Glycol	-10.20	(.007)
1,2-Propylene Glycol	-10.12	(.007)
1,3-Propylene Glycol	-10.25	(.005)
1,3-Propylene Glycol	-10.23	(.007)
Glycerol	-10.33	(.006)

Standard deviation for the energy is shown in parenthesis. 4000K configurations were averaged.

Table XVII. Simulation Results for Solution Total Density.

Compound	Density (g/cm^3)		Experimental Density (g/cm)
Water	1.023		0.997[30]
Propane	0.976	(0.001)	—
Propane (27 bar)	0.987	(0.001)	—
Ethanol	0.999	(0.001)	0.993[81]
Ethylene Glycol	0.966	(0.001)	0.993[13]
1,2-Propylene Glycol	1.004	(0.001)	1.001[80]
1,3-Propylene Glycol	0.995	(0.001)	0.999[80]
1,3-Propylene Glycol (linear)	0.992	(0.001)	--
Glycerol	1.002	(0.001)	1.0004[13]

The number in parenthesis is the standard deviation for the calculated density. 4000K configurations were averaged.

Table XVIII. Pair interaction energy distribution integrals.

Integrals (-10.0 kcal/mol to -2.5 kcal/mol) for TIP4P water and to the minimum of the bimodal curve for the water/solute)

	Hydrogen Bonds Water/Water	Hydrogen Bonds Water/Solute
Water	3.45	
Propane	3.44	0.00
Ethanol	3.41	2.29
Ethylene Glycol	3.43	4.29
1,2-Propylene Glycol	3.42	3.75
1,3-Propylene Glycol	3.39	3.86
1,3-Propylene Glycol (linear)	3.39	4.76
Glycerol	3.38	*3.47

*For glycerol there is additional low energy binding of water between -4.0 kcal/mol and -2.5 kcal/mol (Figure 47). The integral from -10.0 kcal/mol to -2.5 kcal/mol gives 6.45 water-solute hydrogen bonds. The estimated error in the integral values is $\pm$2.0 percent.

Table XIX. Pair correlation function hydrogen bond integrals.

	r(min) Å	g'(HO) Integrals (Proton Acceptor)	r(min) Å	g'(OH) Integrals (Proton Donor)
Ethanol	2.7	1.42	2.5	0.89
Ethylene Glycol				
	2.5	1.07	2.4	0.94
	2.6	1.24	2.4	1.05
1,2-Propylene Glycol				
	2.3	0.79	2.6	1.02
	2.5	1.04	2.5	0.79
1,3-Propylene Glycol				
	2.6	1.54	2.5	0.82
	2.5	1.00	2.5	0.75
1,3-Propylene Glycol (anti)	2.6	1.64	2.5	0.93
	2.5	1.11	2.6	0.97
Glycerol				
	2.4	0.50	2.2	0.61
	2.7	0.40	2.4	0.47
	2.4	0.27	2.4	0.90

The estimated error in the integral values is ± 2.0 percent.

IV. CONCLUSIONS

The general conclusion of this work is that a careful use of the NPT-ensemble Monte Carlo technique can give important details of the hydrogen-bonding in complicated alcohols. However, internal motion must be accounted for and preferential sampling of the solvent near the solute must be added along with solute motion to improve the sampling of phase space for these complex systems. Even so, long runs must be made to give smooth radial distribution functions and smooth energy distribution functions before bonding details can be seen. Primary and secondary pair correlation functions must be computed to give the details of the solvent structure near solute OH groups. The results obtained for thermodynamic quantities such as heat of solution are still not completely satisfactory, still being too negative for the simplest alcohol (ethanol), and for the polyhydric alcohols. Other important conclusions are:

1. In dilute solutions the contracted molecular conformation for the solute (all OH groups on one side of the molecule) is energetically preferred. This is consistent for all of the solutes simulated in dilute solution.
2. The use of quasi component radial distribution functions representing nearest neighbor and next nearest neighbor approach of the solvent molecule to each solute atom allows for straight-forward interpretation of hydrogen bonding. There is a tendency for the alcohols to act as proton acceptors rather than donors.

3. A reasonable picture of propane-hydrate formation can be obtained by running the simulation at pressures higher than atmospheric.
4. Stored configurations, particularly near the end of a simulation run, give instructive visual pictures of the solute conformation and show whether the alcohol bonding is acting as a proton acceptor or a proton donor. In addition, observations can also be made of solvent configurations (such as five-membered H_2O rings) in hydrophobic regions.
5. The T1P4P water model of Jorgensen is a good model for this type of simulation. Also, optimized potential functions for molecular groups developed by Jorgensen and coworkers can be transported to other molecules and give reasonable results.
6. The water-solute binding energies correlate with experimental measurements of the water binding (humectant) properties of the polyhydric alcohols.
7. The most general conclusion is that polyhydric alcohols bind water increasingly well as the number of hydroxyl groups increases. The efficiency of hydrogen bonding to hydroxyl groups increases as the OH-OH separation increases.
8. This work represents the first Monte Carlo simulation carried out on the aqueous solutions of ethylene glycol, 1,2-proplene glycol, 1,3-propylene glycol, and glycerol. In addition, it is the first work to detail the hydrogen bonding into acceptor and donor type for all of the above

and ethanol. It is also the first, to our knowledge, to calculate the properties of propane hydrate formation using an NPT-ensemble approach.

9. The next obvious step in simulations of this type is to increase the solute concentration. This requires the inclusion of solute-solute interactions into the calculation, with a large increase in the complexity and computation time of the simulation. Work is presently underway to assemble software which would allow the simulation of aqueous solutions of complex solutes over large concentration ranges.

REFERENCES

1. Bosart, L.W. and Snoddy, A.O., Ind. Eng. Chem., 19, 506 (1927).

2. Minor, C.S. and Dalton, N.N., "Glycerol," Reinhold Publishing Corp., (1953).

3. International Critical Tables, 3, 121 (1928).
International Critical Tables, 5, 157 (1928).

4. Gerlach, G. Th., Chem. Ind., 7, 277 (1884).

5. Ladyn, J, MS Thesis, Brooklyn Polytechnic Institute (Polytechnic U), (1948).

6. Lane, L.B., Ind. Eng. Chem., 17, 924 (1925).

7. Champeney, D.C. and Joarder, R.N., Mol. Phys., 58, 337 (1986).

8. Garawi, M., Dore, J.C. and Champeney, D.C., Mol. Phys., 62, 475 (1987).

9. Root, L.J. and Stillinger, F.H., J. Chem. Phys., 90, 1200 (1989).

10. Rajagopalan, S. and Verma, G.S., J. Phys. Soc. Japan, 25, 1204 (1968).

11. Solomon, J.E., J. Phys. Chem., 81, 1492 (1977).

12. Burnett, L.J. and Roeder, S.B.W., J. Chem. Phys., 60, 2420 (1974).

13. Murthy, N.M. and Subrahmanyam, S.V., Indian J. Pure and Applied Phys., 15, 485 (1977).

14. Murthy, N.M. and Subrahmanyam, S.V., J. Chem. Soc., Faraday Trans. I, 75, 2067 (1979).

15. Srivastava, A.P. and Tripathi, S.N., Current Sci., 55, 180 (1986).

16. Chidichimo, G., Imbardelli, D., Longer, M. and Saupe, A., Mol. Phys., 65, 1143 (1988).

17. Schwartz, M. and Colville, M.J., J. of Mag. Reson., 32, 377 (1984).

18. Pimentel, G.C. and McClellen, A.L., "Hydrogen Bond," W.H Freeman, SF, Calif., 53 (1960).

19. Jeffrey, G.A. and Takagi, S., Accounts of Chem. Res., Am. Chem. Soc., 264 (1978).

20. Terasawa, S., Itsuki, H. and Arakawa, S., J. Phys. Chem., 79, 2345 (1975).

21. Huot, J., Baltistel, E., Lumay, R, Villeneuve, G., Lavallee, J., Anusiem, A. and Jolicaeus, C., J. Solution Chem., 17, 601 (1988).

22. Metropolis, N.A., Rosenbluth, A.W., Rosenbluth, M.N., Teller, A.H. and Teller, E., J. Chem. Phys., 21, 1087 (1953).

23. Wood, W.W. and Parker, F.R., J. Chem. Phys., 27, 720 (1957).

24. McDonald, I.R., Mol. Phys., 23, 41 (1972).

25. Ben-Naim, A., "Water and Aqueous Solutions," Plenum Press, N.Y., (1974).

26. Wood, W.W., "Physics of Simple Liquids," edited by H.N.V. Temperley, J.S. Rowlinson, and G.S. Rushbrocke, (North-Holland Pub. Co.), Chap. 5, (1968).

27. Jorgensen, W.L. and Madura, J.D., J. Am. Chem. Soc., 105, 1407 (1983).

28. Jorgensen, W.L., J. Phys. Chem., 87, 5304 (1983).

29. Jorgensen, W.L., Madura, J.D., Swenson, C.J., J. Am. Chem. Soc., 106,2381 (1984).

30. Jorgensen, W.L., Chandrasekhar, J., Madura, J.D., Impey, R.W., Klein, M.L., J. Chem. Phys., 79, 926 (1983).

31. Jorgensen, W.L., Madura, J.D., Mol. Phys., 56, 1381 (1985).

32. Jorgensen, W.L., Swenson, C.J., J. Am. Chem. Soc., 107, 569 (1985).

33. Jorgensen, W.L., Gao, J., Ravimohan, C., J. Phys. Chem., 89, 3470 (1985).

34. Jorgensen, W.L., Swenson, C.J., J. Am. Chem. Soc., 107, 1489 (1985).

35. Jorgensen, W.L., J. Am. Chem. Soc., 102, 543 (1980).

36. Jorgensen, W.L., Ibrahim, M., J. Am. Chem. Soc., 104, 373 (1982).

37. Jorgensen, W.L., J. Am. Chem. Soc., 103, 345 (1981).

38. Jorgensen, W.L., J. Phys. Chem., 90, 1276 (1986).

39. Jorgensen, W.L., Buckner, J.K., Boudon, S. and Tirado-Rives, J., J. Chem. Phys., 89, 3742 (1988).

40. Gao, J. and Jorgensen, W.L., J. Phys. Chem., 92, 5813 (1988).

41. Jorgensen, W.L. and Tirado-Rives, J., J. Am. Chem. Soc., 110, 1657 (1988).

42. Mehrotra, P.K. and Beveridge, D.L., J. Am. Chem. Soc., 102, 4287 (1980).

43. Rossky, P.J. and Karplus, M., J. Am. Chem. Soc., 101, 1913 (1979).

44. Alagona, G. and Tani, A., Chem. Phys. Lett., 87, 337 (1982).

45. Alagona, G. and Tani, A., J. Mol. Structure, 106, 375 (1988).

46. Bernal, J.D. and Fowler, R.H., J. Chem. Phys., 1, 515 (1933).

47. Stillinger, F.H. and Rahman, A., J. Chem. Phys., 60, 1545 (1974).

48. Berendsen, H.J.C., Postma, J.P.M., Von Gunsteren, W.F. and Hermans, J., in "Intermolecular Forces," edited by B. Pullman (Reidel, Dordrecht, Holland) 331 (1981).

49. Matsuoka, O., Clementi, E. and Yoshimine, M., J. Chem. Phys., 64, 1351 (1976).

50. Madura, J.D., Pettitt, B.M. and Calef, D.F., Mol. Phys., 64, 325 (1988).

51. Neumann, M. J. Chem. Phys., 85, 1567 (1986).

52. Wilson, M.A., Pohorille, A. and Pratt, L.R., J. Phys. Chem., 91, 4873 (1987).

53. Wilson, M.A., Pohorille, A. and Pratt, L.R., J. Chem. Phys., 88, 3281 (1988).

54. Karin, O.A. and Haymet, A.D.J., Chem. Phys. Lett., 138, 537 (1987).

55. Mountain, R.D., J. Chem. Phys., 90, 1866 (1989).

56. Owicki, J.C. and Scheraga, A.A., J. Am. Chem. Soc., 99, 7403 (1977).

57. Owicki, J.C. and Scheraga, A.A., J. Am. Chem. Soc., 99, 7413 (1977).

58. Gupta, S., Yang, J. and Kestner, N.R., J. Chem. Phys., 89, 3733 (1988).

59. Lustig, R. and Steele, W.A., Mol. Physics, 65, 475 (1988).

60. Gelin, B.R. and Karplus, M., Biochemistry, 18, 1256 (1979).

61. Chao, J. and Hall, K.R., Inter. J. of Thermophysics, 7, 431 (1986).

62. Melberg, S. and Rasmussen, K., J. of Mol. Struct., 57, 215 (1979).

63. Burkert, U. and Allinger, N.L., Molecular Mechanics, ACS Monograph 177, American Chemical Society: Washington, D.C. (1982).

64. Kao, J., Private Communication.

65. Dewar, M.J.S. and Thiel, W., J. Am. Chem. Soc., 99, 4899 (1977).

66. Hehre, W.J., Radom, L., Schleyer, P.V.R. and Pople, J.A., Ab initio Molecular Orbital Theory, John Wiley and Sons, N.Y., 103 (1986).

67. Soper, A.K. and Phillips, M.G., Chem. Phys., 107, 47 (1986).

68. Englezos, P. and Bishvoi, P.R., AIChE J., 34, 1718 (1988).

69. Holder, G.D., Corbin, G. and Papadopoulos, K.D., Ind. Eng. Chem. Fundam., 19, 282 (1980).

70. John, V.T. and Holder, G.D., J. Phys. Chem., 85, 1811 (1981).

71. Holder, G.D. and Marganiello, D.J., Chem. Eng. Sci., 37, 9 (1982).

72. John, V.T., Papadopoulos, K.D. and Holder, G.D., AIChE J., 31, 252 (1985).

73. Mehrotra, P.K., Mezei, M. and Beveridge, D.L., J. Chem. Phys., 3166 (1983).

74. Sloan, A.E. and Labuza, T.P., Food Product Dev., 68, December (1975).

75. Swaninathan, S., Harrison, S.W. and Beveridge, D.L., J. Am. Chem. Soc., 100, 5705 (1978).

76. Christensen, C. Gmehling, J., Resmussen, P. and Weidlich, U., Heats of Mixing Data Collection - Binary Systems, Chemistry Data Series, Vol. III, Part I, Dechema Deutsche Gesellschaft für Chemisches Apparatewesen, Editors: Behrans, D. and Eckerman, R. (1984).

77. Redlich, O. and Kister, A.T., Ind. Eng. Chem., 40, 345 (1948).

78. Costigan, M.J., Hodges, L.J., Marsh, K.N. and Stokes, R.H., Aust. J. Chem., 33, 2103 (1980).

79. Matsumoto, Y., Touhara, H., Nakanishi, K. and Watanabe, N., J. Chem. Thermadyn., 9, 801 (1977).

80. DiPaola, G. and Belleau, B., Can. J. Chem., 55, 3825 (1977).

81. Chemical Engr. Handbook, Sixth Ed., McGraw-Hill, N.Y., Sec. 3, 89 (1984).

The two page vita has been removed from the scanned document. Page 1 of 2

The two page vita has been removed from the scanned document. Page 2 of 2